

# Disentangling influences of climate variability and lake-system evolution on climate proxies derived from isoprenoid and branched GDGTs: the 250-kyr Lake Chala record

Allix J. Baxter<sup>1</sup>, Francien Peterse<sup>1</sup>, Dirk Verschuren<sup>2</sup>, Aihemaiti Maitituerdi<sup>3</sup>, Nicolas Waldmann<sup>3</sup>, and Jaap S. Sinninghe Damsté<sup>1,4</sup>

<sup>1</sup>Utrecht University, Faculty of Geosciences, Department of Earth Sciences, Princetonlaan 8A, 3584 CB Utrecht, the Netherlands

<sup>2</sup>Ghent University, Department of Biology, Limnology Unit, K.L. Ledeganckstraat 35, B-9000 Gent, Belgium

<sup>3</sup>Dr. Moses Strauss Department of Marine Geosciences, Leon H. Charney School of Marine Sciences, University of Haifa, Mount Carmel 3498838, Israel

<sup>4</sup>NIOZ Royal Netherlands Institute for Sea Research, Department of Marine Microbiology and Biogeochemistry, PO Box 59, 1790 AB, Den Burg, the Netherlands

**Correspondence:** Allix J. Baxter (a.j.baxter@uu.nl)

**Abstract.** High-resolution paleoclimate records from tropical continental settings are greatly needed to advance understanding of global climate dynamics. The International Continental Scientific Drilling Program (ICDP) project DeepCHALLA recovered a 214.8-meter long sediment sequence from Lake Chala, a deep and permanently stratified (meromictic) crater lake in equatorial East-eastern equatorial Africa, covering the past c. 250,000 years (250 kyr) of continuous lacustrine deposition since the earliest phase of lake-basin development. Lipid biomarker analyses on the sediments of ~~this long-lived lake can provide much-needed~~ Lake Chala can provide quantitative records of past ~~climate variability from this currently variation in temperature and moisture balance from this~~ poorly documented region. However, the degree to which climate proxies derived from aquatically produced biomarkers are affected by aspects of lake developmental history is rarely considered, even though it may critically influence their ability to consistently register a particular climate variable through time. Modern-system studies ~~in of~~ Lake Chala revealed crucial information about the mechanisms underpinning relationships between proxies based on isoprenoid (iso-) and branched (br-) glycerol dialkyl glycerol tetraethers (GDGTs) and the targeted climate variables, but the persistence of these relationships in the past remains unclear. ~~To~~ Here we assess the reliability of long-term climate signals registered in the sediments of Lake Chala ~~, we compared by comparing~~ downcore variations in GDGT distributions with major phases in lake-system evolution as ~~indicated-reflected~~ by independent proxies of lake depth, mixing regime and nutrient dynamics: seismic reflection data, lithology and fossil diatom assemblages. Together, these records suggest that during early lake history (before c. 180-200 kyr ago, ka) the distinct mixing-related depth zones with which specific GDGT producers are associated in the modern-day lake were not yet formed, likely due to more open lake hydrology and absence of chemical water-column stratification. Consequently ~~during this early phase the~~ absolute GDGT concentrations ~~dating to this period~~ are relatively low, proxies sensitive to water-column stratification (e.g., BIT index) display highly irregular temporal variability, and correlations between proxies are dissimilar to expectations based on modern-system understanding. A sequence of lake-system

changes between c. 180-200 ka and c. 80 ka first established and then strengthened the chemical density gradient, promoting meromictic conditions despite the overall decrease in lake depth due to ~~sediment accumulation~~the basin gradually being filled up with sediments. From c. 180 ka onward some GDGTs and derived proxies (e.g., crenarchaeol concentration, BIT index and IR<sub>6Me</sub>) display strong ~23-kyr periodicity, likely reflecting the predominantly precession-driven insolation forcing of Quaternary climate variability in low-latitude regions. Our results suggest that GDGT-based temperature and moisture-balance proxies in Lake Chala sediments reflect the climate history of eastern equatorial Africa from at least c. 160 ka onwards, i.e., covering the complete last glacial-interglacial cycle and the penultimate glacial maximum. This work confirms the potential of lacustrine GDGTs for elucidating the climate history of tropical regions at Quaternary timescales, provided they are applied to suitably high-quality sediment archives. Additionally, their interpretation should incorporate a broader understanding of the extent to which lake-system evolution limits the extrapolation back in time of proxy-climate relationships established in the modern system.

## 1 Introduction

Reliable methods to ~~accurately~~ reconstruct past climate variability ~~on all of the world's continents are needed in order during both glacial and interglacial phases of the Quaternary are needed~~ to more precisely model global climate dynamics and to correctly ~~predict future climate changes~~project future climate change due to anthropogenic global warming at the regional scale. However, whereas mid- ~~and to~~ high-latitude ~~continents are relatively continental regions are~~ well represented by suitably long and high-quality climate reconstructions (e.g., Petit et al. 1999; Lisiecki and Raymo 2005; Barker et al. 2011b; Cheng et al. 2016), ~~high-resolution records of long-term~~ Petit et al. 1999; Barker et al. 2011b; Melles et al. 2012; Cheng et al. 2016; Wagner et al. 2019), long records of past climate variability from the tropics are still scarce. ~~Long-lived lakes on~~On the African continent, the largest landmass straddling the equator, ~~have proven to accumulate effective sedimentary archives of past climate states~~sediments accumulating without interruption in long-lived lakes are the principal natural archive of Quaternary climate history across its full range of variability (e.g., Lake Malawi: Powers et al. 2005; Scholz et al. 2007; Stone et al. 2011; Johnson et al. 2016; Woltering et al. 2011; ~~and~~ Scholz et al. 2007; Cohen et al. 2007; Stone et al. 2011; Johnson et al. 2016; Lake Tanganyika: Tierney et al. 2008, 2010e; Stager et al. 2009), ~~as lake sediments preserve an array of biological and geological~~ Scholz et al. 2007; Tierney et al. 2008; ?; Lake Bosumtwi: Scholz et al. (2007); Miller et al. (2016)), and provide a diverse array of climate information registered through various climate-controlled processes occurring within biological and geological processes in the lake and the surrounding terrestrial environments (Cohen, 2003). ~~Long-lived crater lakes, in particular, are valuable natural archives of past climatic conditions because their large depth relative to surface area promotes the formation of a permanently unmixing, oxygen-deprived bottom layer, which facilitates the continuous deposition and preservation of finely laminated sediments (e.g., varves) that are often rich in organic matter (Verschuren, 2003; Zolitschka, 2006). Additionally, crater lakes have restricted catchment areas without distinct stream inflows, so that their hydrology is relatively simple, and~~

~~past changes in lake water budget are more strongly tied to changes in the climate-controlled balance between precipitation and evaporation (e.g., Jones et al. 2001).~~

55 An increasingly important ~~biological~~ source of information on past climate change ~~preserved in lake sediments is derived from~~ extracted from lake sediments, both in Africa and elsewhere, are isoprenoid (iso-) and branched (br-) glycerol dialkyl glycerol tetraethers (GDGTs), membrane lipids produced by species of archaea and bacteria, respectively. These organic biomarkers are useful for paleoclimate ~~research~~ reconstruction owing to their ubiquitous presence in natural settings, resilience to degradation, and strong response to environmental parameters such as temperature and pH (Schouten et al., 2013).

60 IsoGDGTs consist of two ether-bound  $C_{40}$  isoprenoid alkyl chains that can have varying numbers (0 to 8) of cyclopentyl moieties (i.e., isoGDGT-0 to 8; see GDGT molecular structures in Fig. S1; De Rosa and Gambacorta 1988). Crenarchaeol (as well as its isomer cren'is), an isoGDGT with 4 cyclopentyl moieties and 1 cyclohexyl moiety (Sinninghe Damsté et al., 2002; Holzheimer et al., 2021), ~~which~~ is only known to be produced by chemolithotrophic, ammonia-oxidizing Thaumarchaeota (e.g., Sinninghe Damsté et al. 2002; Sinninghe Damsté et al. 2018; Schouten et al. 2013; Elling et al. 2017; Bale et al. 2019).

65 By contrast, isoGDGT-0 is synthesized ~~by many archaeal species, including Thaumarchaeota by Thaumarchaeota~~ (e.g., Sinninghe Damsté et al. 2012b; Schouten et al. 2013; Elling et al. 2017; Bale et al. 2019) ~~;~~ as well as anaerobic methane-oxidizing archaea (e.g., Pancost et al. 2001; Schouten et al. 2001) and methanogenic Euryarchaeota (Schouten et al. 2013, and references therein). ~~Synthesis of, and~~ isoGDGT-1 to -3 ~~has~~ have been demonstrated to occur in ~~Eury-, Cren- and Thaumarchaeota Thaum-, Eury- and Crenarchaeota~~ (Schouten et al. 2013, and references therein). ~~The Empirical observations from marine surface sediments suggesting that ring formation in isoGDGTs is controlled by (sub)surface temperature led to development of the~~ TetraEther indeX of 86 carbon atoms ( $TEX_{86}$ ; Table 1) paleothermometer ~~was developed~~ to reconstruct past sea surface temperature (SST) ~~based on empirical observations from marine surface sediments that suggest the ring formation of isoGDGTs is controlled by temperature (Schouten et al., 2002; Kim et al., 2010), further substantiated by incubation experiments (Wuechter et al., 2004; Schouten et al., 2007). This approach relies on the assumption that chemolithotrophic, ammonia-oxidizing Thaumarchaeota (specifically those belonging to Group I.1a) are the primary producers of isoGDGTs at the study site, as other archaea have not shown the same temperature dependency of ring formation as predicted by empirical (Schouten et al., 2002; Kim et al., 2010).  $TEX_{86}$  temperature models (e.g., Elling et al. 2017). The potential of  $TEX_{86}$  has also been used~~ to reconstruct lake surface temperature (LST) ~~has also been explored (Powers et al., 2004), albeit using a substantially smaller set of surface samples than the marine study, and resulted in temperature calibrations specific for lacustrine settings (Powers et al., 2004; Tierney et al., 2010a; Powers et al., 2010). There are now several LST reconstructions based on  $TEX_{86}$ , mainly from the sediment records of from isoGDGTs in the sediments of mainly~~ large lakes (e.g., Powers et al. 2005, 2011; Tierney et al. 2008, 2010a; Woltering et al. 2011; Blaga et al. 2013; Sun et al. 2020). However, use of  $TEX_{86}$  in lakes may be complicated by contributions of isoGDGTs from methanotrophs, methanogens and other archaea. Moreover, the position of the oxycline in the water column appears to strongly influence the niche available to Thaumarchaeota, and hence

80 the in situ  $TEX_{86}$  signal (e.g., Zhang et al. 2016; Cao et al. 2020; Baxter et al. 2021; Sinninghe Damsté et al. 2022). The strong influence of lake size and depth on oxycline formation may also imply that small and shallow lakes are less suited for application of the  $TEX_{86}$  proxy (Powers et al., 2010; Baxter et al., 2021; Sinninghe Damsté et al., 2022).

**Table 1.** Formulas of GDGT-based environmental proxies used-employed in this study, with 6-Me brGDGTs indicated by a prime symbol. GDGTs in GDGT identifiers within square brackets refer to the fractional abundances. The 6-Me within the respective group (iso- or brGDGTs are indicated with), the prime symbol, others refer to absolute abundances (i.e., integrated peak area)

Formula	Reference
$TEX_{86} = \frac{(GDGT-2+GDGT-3+cren')}{(GDGT-1+GDGT-2+GDGT-3+cren')}$	Schouten et al. (2002)
$BIT = \frac{(Ia+IIa+IIa'+IIIa+IIIa')}{(Ia+IIa+IIa'+IIIa+IIIa'+crenarchaeol)}$	Hopmans et al. (2004)
$f[CREN'] = \frac{cren'}{cren'+[crenarchaeol]}$	Baxter et al. (2021)
$\%GDGT-2 = \frac{100*isoGDGT-2}{isoGDGT-1+isoGDGT-2+isoGDGT-3+cren'}$	Sinninghe Damsté et al. (2012a)
$IR_{6Me} = \frac{IIa'+IIb'+IIc'+IIIa'+IIIb'+IIIc'}{IIa'+IIb'+IIc'+IIIa'+IIIb'+IIIc'+IIa+IIb+IIc+IIIa+IIIb+IIIc}$	De Jonge et al. (2015)
$MBT'_{5Me} = \frac{([Ia]+[Ib]+[Ic])}{([Ia]+[Ib]+[Ic]+[IIa]+[IIb]+[IIc]+[IIIa])}$	De Jonge et al. (2014)
$CBT' = \log \frac{([Ic]+[IIa'])}{([Ia]+[Ib]+[Ic]+[IIa]+[IIb]+[IIc]+[IIIa])}$	De Jonge et al. (2014)
$DC = \frac{([Ib]+2*[Ic]+[IIb]+[IIb'])}{([Ia]+[Ib]+[Ic]+[IIa]+[IIa']+[IIb]+[IIb'])}$	Sinninghe Damsté (2016); Baxter et al. (2019)
$MST = 20.9 + 98.1 * [Ib] - 12 * ([IIa] + [IIa']) - 20.5 * ([IIIa] + [IIIa'])$	Pearson et al. (2011)

BrGDGTs contain two linear C<sub>28</sub> alkyl chains methylated at C-13 and C-16 that most likely formed from the tail-to-tail linkage of two iso C15 fatty acids (Sinninghe Damsté et al. 2000; Fig. S1). ~~This~~ The basic tetramethylated brGDGT is usually accompanied by penta- or hexamethylated forms, where ~~the~~ additional methyl group(s) is/are placed-occur at the C-5 (Sinninghe Damsté et al., 2000; Weijers et al., 2006a) or C-6 (De Jonge et al., 2013, 2014) positions (i.e., the 5-Me and 6-Me brGDGT isomers) position. Cyclic brGDGTs contain 1–2 cyclopentane moieties, formed by cyclisation involving the mid-chain methyl groups (Weijers et al., 2006a). ~~The stereochemistry of the glycerol units is opposite that of the archaeal isoGDGTs, indicating a bacterial origin (Weijers et al., 2006a). Acidobacteria, which occur widespread in soil and peat, were initially identified as likely producers of these lipids in natural settings due to the correlation of their 16S rRNA gene copies with brGDGTs concentrations (Weijers et al., 2009). The biosynthesis of ester and ether-bound iso-diabolic acid (with a methyl group at C-5 or C-6), the precursor to brGDGTs, and the acyclic tetramethylated brGDGT by specific cultivated strains of this phylum (Sinninghe Damsté et al., 2011, 2014, 2018) confirmed this. Recently, two parallel studies~~

~~reported acyclic and cyclic tetra-~~ Combined lipid-16S rRNA and culture studies suggest that brGDGTs are likely produced by Acidobacteria (Weijers et al., 2009). (Sinninghe Damsté et al., 2011, 2014, 2018) (Chen et al., 2022; Halamka et al., 2023), penta- and hexamethylated (5-Me) brGDGTs in a culture of *Solibacter usitatus* (Chen et al., 2022; Halamka et al., 2023). However, besides Acidobacteria, ~~although~~ other bacterial phyla ~~likely also produce these lipids in nature~~ are likely also capable of producing these lipids (e.g., Sinninghe Damsté et al. 2011, 2018; Weber et al. 2018; De Jonge et al. 2019; van Bree et al. 2020; Sahonero-Canavesi et al. 2022; Halamka et al. 2023).

105 ~~BrGDGTs~~ As brGDGTs are particularly abundant in soils (Weijers et al., 2006b). ~~The~~, their abundance relative to that of aquatically produced crenarchaeol, quantified in the Branched versus Isoprenoid Tetraether (BIT) index (Hopmans et al. 2004; Table 1), a ratio expressing the relative abundance of presumed soil-derived brGDGTs and aquatically produced crenarchaeol, was initially used to assess the contribution of terrestrial material to the sedimentary GDGT pool in coastal marine settings. Consequently, in lacustrine settings, the BIT index was also thought to track terrestrial organic matter input into the lake system via soil erosion and runoff determine the input of soil material to coastal marine sediments as well as lakes (Sinninghe Damsté et al., 2009; Blaga et al., 2009). However, it is now established that *in-situ* also the production of brGDGTs in within lakes is significant and probably dominant in most systems, sometimes even dominant (Tierney and Russell, 2009; Sinninghe Damsté et al., 2009; Woltering et al., 2012; Weber et al., 2015, 2018; van Bree et al., 2020). More recently, it has been shown that in certain stratifying lakes In Lake Chala and possibly also other deep stratifying lakes, the BIT index may instead reflect long-term changes in lake depth, and therefore is rather than serve as a proxy for integrated climatic moisture balance than of rainfall amount rather than rainfall amount per se (Baxter et al., 2021).

Besides the BIT index, several other climate proxies based on brGDGT distributions have been developed. In essentially nearly all studied settings the distribution of these lipids displays a strong correlation to temperature, which following the discovery of 6-Me brGDGTs (De Jonge et al., 2014) is best reflected in the degree of methylation of 5-Me brGDGTs, as captured by the methylation of branched tetraether ( $MBT'_{5Me}$ ) index (Table 1; De Jonge et al. 2014). Warmer climates produce a generally higher relative abundance of less methylated brGDGTs (Weijers et al., 2007; Raberg et al., 2022) and, hence,  $MBT'_{5Me}$  may be used to reconstruct past continental temperatures. The potentially mixed soil and aquatic origin of brGDGTs in lakes (e.g., Niemann et al. 2012; Nacher et al. 2014; Miller et al. 2018) originally created uncertainty about which calibrations are most appropriate there, followed by clear support for the development of calibrations specifically applicable to lake sediments (Tierney et al., 2010b; Pearson et al., 2011; Russell et al., 2018; Martínez-Sosa et al., 2021; Raberg et al., 2021). Modern system studies continued to highlight the relative importance of lacustrine brGDGTs production (Sinninghe Damsté et al., 2009; Tierney and Russell, 2009; Bechtel et al., 2010) and application of a soil calibration to lake sediments produced temperature estimates differing  $\sim 10^{\circ}C$  from observations (Tierney et al., 2010b). Despite the 130 However, despite strong correlation between  $MBT'_{5Me}$  in lacustrine surface sediments and temperature (Russell et al., 2018; Martínez-Sosa et al., 2021; Raberg et al., 2021), only few downcore down-core applications of lake-based temperature calibrations since discovery of the 5-Me and 6-Me isomers have proved successful (Feakins et al., 2019; Stockhecke et al., 2021; Zhao et al., 2021; Zhang et al., 2021; Garelick et al., 2021; Ramos-Roman et al., 2022; Parish et al., 2023), partly due

to ~~uncertainties~~ continued uncertainty about the exact source(s) of brGDGTs in lakes. ~~Recommendations to select temperature~~  
135 ~~calibrations based on geographic region and/or mixing regime of the reconstruction site (Loomis et al., 2014b) are not strictly~~  
~~followed, and some studies use modified indices that seem better suited to the particular study site or reconstruction (e.g.,~~  
~~Bittner et al. 2022; Baxter et al. 2023).~~ Clearly, ~~application of brGDGT-based paleothermometers to lake-sediment archives~~  
~~shows great potential but is far from straightforward at present.~~

~~The influence of pH on the distribution of brGDGTs varies between environmental settings.~~  
140 ~~Studies of soil and peat carried out both before (Weijers et al., 2007; Peterse et al., 2010, 2012) and after~~  
~~(De Jonge et al., 2014; Xiao et al., 2015; Naafs et al., 2017a, b) the discovery of the 5-Me and 6-Me brGDGTs have~~  
~~shown that the degree of cyclisation of brGDGTs (represented by the cyclisation of branched tetraether index; CBT) and~~  
~~also the relative proportion of the 6-Me isomer (represented by the isomer ratio; IR<sub>6Me</sub>) are strongly related to pH. By~~  
~~contrast, the influence of pH on~~ In addition, several other environmental factors may influence brGDGT distributions  
145 ~~in lacustrine surface sediments is generally weaker than in other continental settings and sometimes reportedly absent~~  
~~(Loomis et al., 2014a; Russell et al., 2018; Martínez-Sosa et al., 2021; Raberg et al., 2022), possibly relating to the often large~~  
~~pH gradient with depth and unresolved origin of the brGDGTs in most lakes. Moreover, in lake-water microcosm experiments,~~  
~~no influence of pH on brGDGT distributions was found (Martínez-Sosa et al., 2020). Also, although culture studies found~~  
~~relationships between the methylation of the 5-Me brGDGTs and temperature mirroring those found in natural settings, the~~  
150 ~~same studies showed no response of brGDGT distributions to pH, indicating that community change may be the primary driver~~  
~~of the sensitivity to pH observed in nature (Chen et al., 2022; Halamka et al., 2023). This is also supported by simulations~~  
~~of membrane dynamics, which similarly did not find clear evidence that the cyclisation of brGDGTs is a means to control~~  
~~membrane fluidity in response to pH variation (Naafs et al., 2021). Moreover, due to the manner in which the commonly~~  
~~applied CBT<sup>2</sup> index is calculated (De Jonge et al., 2014), it does not only represent the degree of cyclisation, but is heavily~~  
155 ~~influenced by differences in the relative abundance of the 5-Me and 6-Me isomers. Hence, some studies apply another method~~  
~~for calculating the degree of cyclisation of the brGDGTs (DC; Sinninghe-Damsté 2016; Baxter et al. 2021).~~

~~Besides temperature and pH, several other environmental variables such as lake~~ lakes, such as the lake's depth (Tierney  
et al., 2010b; Loomis et al., 2014a), ~~nutrient-availability-trophic level~~ (Loomis et al., 2014b; Martínez-Sosa and Tierney, 2019),  
conductivity (Shanahan et al., 2013; Raberg et al., 2021), ~~and~~ dissolved oxygen content (Loomis et al., 2014a, b; Martínez-Sosa  
160 ~~and Tierney, 2019; van Bree et al., 2020; Yao et al., 2020; Wu et al., 2021) have been found to potentially impact brGDGT~~  
~~distributions in experimental and natural settings.~~ Redox conditions and redox conditions. The latter, in particular, have shown  
to exert a significant influence on has been shown to substantially influence the concentration and ~~distributions~~ distribution of  
brGDGTs in lacustrine ~~surface~~ sediments (Loomis et al., 2014a; Wu et al., 2021), as well as their ~~spatial pattern~~ distribution  
within the water column of ~~some~~ stratifying lakes (Weber et al., 2018; van Bree et al., 2020; Yao et al., 2020). ~~This sensitivity~~  
165 ~~to redox conditions has been further substantiated by micro- and mesocosm experiments (Martínez-Sosa and Tierney, 2019)~~ As  
a result, some studies use modified GDGT indices when these appear better suited to the particular study site or reconstruction  
(e.g., Bittner et al. 2022; Baxter et al. 2023).

In summary, most ~~Given that~~ GDGT-based climate reconstructions from ~~lake sediment records are supported only by~~ region-specific or global calibrations relating the distribution of GDGTs in recently deposited lacustrine sediments to targeted climate variables. To validate these ~~lake sediment records are based on space-for-time substitution of~~ empirical proxy-climate relationships among a suitably large number of present-day lakes situated along regional to global-scale climate gradients, investigation of the ~~modern-specific~~ lake system and depositional environment 'hosting' the reconstruction is crucial to identify the influence of confounding factors on the exact relationship of ~~specific GDGTs with~~ between specific GDGTs and temperature or moisture balance. However, ~~monitoring proxy variation in the modern system across seasonal to interannual time scales despite the substantial effort involved in such modern-system studies, monitoring of proxy variation during multiple seasons or even multiple years~~ does not necessarily suffice to explain proxy variation at the much longer time scale of climate reconstruction. ~~At this longer time scale, long-lived lakes are~~ from sedimentary GDGT distributions. Long-lived lakes are by nature dynamic systems experiencing large-scale physical, chemical and biological changes throughout their history related to the geological and tectonic evolution of the lake basin since its formation, its gradual infilling with sediments, and changes in the basin's hydrographic network and/or local tectonics lake's hydrology or connection to a regional hydrographic network. The influence of these long-term changes in the lake system on the lake-basin changes on local aquatic microbial communities may significantly impact the reliability of GDGT-based climate proxies, but regrettably climate reconstructions rarely take this important source of uncertainty in the reliability of climate reconstructions is rarely discussed consideration.

For almost two decades, Lake Chala near Mt. Kilimanjaro has been the focus of lake monitoring and climate proxy validation studies aimed at producing a long and robust paleoclimate reconstruction from ~~The present study aims to address this issue in context of GDGT-based climate reconstruction at Lake Chala in~~ eastern equatorial Africa with high temporal resolution. Particularly, a series of multi-year studies investigating the occurrence and climatic significance of various GDGTs (Sinninghe Damsté et al., 2009; Buckles et al., 2013, 2014; van Bree et al., 2020; Baxter et al., 2021) resulted in Lake Chala being ranked amongst the best studied lakes worldwide with regards to GDGTs. These modern-system investigations were carried out in preparation of the ~~a~~ 90-meter deep volcanic crater lake from where the International Continental Scientific Drilling Program (ICDP) project DeepCHALLA (Verschuren et al., 2013), which in 2016 extracted recovered a 214.8-m sediment sequence of continuously laminated, diatom and organic matter-rich sediments from Lake Chala covering the last ~~meter long sediment sequence covering~~ c. 250 ka (Verschuren et al., 2013; Martin-Jones et al., 2020). ~~At present, very few continuous climate records from tropical East Africa extend beyond the Last Glacial Maximum (LGM; c. 23,000 to 19,000 years ago), and even fewer cover the last glacial (MIS4-MIS2) or last interglacial (MIS5) periods (i.e., Tierney et al. 2008; Loomis et al. 2012; Johnson et al. 2016. While the long sediment sequence recovered by DeepCHALLA represents a unique opportunity to extend detailed knowledge of East African climate history back to the previous glacial-interglacial cycle (MIS6-MIS7), achieving this objective is contingent on confirmation that our understanding of the relationship between selected sedimentary proxies and climate is applicable throughout the record. To reach this objective, the present study aims to relate the kyr of continuous lacustrine deposition since shortly after lake-basin formation. This is done through detailed examination of the concentrations and~~ distributions of isoGDGTs, brGDGTs and the associated climate-proxy indices in 949 horizons throughout the c. 250-kyr DeepCHALLA sediment sequence associated proxies

in relation to major phases in the ~~basin evolution and aquatic ecology of Lake Chala~~ history of the lake's limnology, ecology and sedimentation dynamics as revealed by independent paleoenvironmental proxies derived from seismic reflection data, sediment lithology and fossil diatom assemblages). ~~We build on our~~ Lake Chala may provide a particularly valuable natural archive of regional climate history because its large relative depth, characteristic for crater lakes, has promoted the formation and persistence of a permanently stratified, oxygen-deprived lower water column allowing continuous undisturbed deposition of finely laminated sediments that are often rich in organic matter (Verschuren, 2003; Zolitschka, 2006). Situated in steep-sided basins, crater lakes also have a restricted catchment area lacking distinct stream inflows, so that ~~their hydrological setting is relatively simple, and past changes in lake water budget can be expected to be tied strongly to changes in the climate-controlled balance between precipitation and evaporation (e.g., Jones et al. 2001). Our interpretation of sedimentary GDGT data from Lake Chala also builds on good~~ understanding of GDGT proxy-climate relationships informed by diverse studies of the modern-system and more shallow sediment studies to examine the stability of these relationships throughout deposition of the entire DeepCHALLA record ~~modern-day lake system and less-ancient sediment records from~~ this location (Sinninghe Damsté et al., 2009; Buckles et al., 2013, 2014, 2016; van Bree et al., 2020; Baxter et al., 2021). This integrated analysis ~~enabled us to identify and allows us to~~ disentangle the influences of lake basin development and climate variability on the concentrations and distributions of GDGTs in the DeepCHALLA sedimentary archive ~~GDGT-based climate proxies extracted from the long and continuous sediment archive of Lake Chala, which may provide a unique view of climate and landscape history in eastern equatorial Africa spanning two complete glacial-interglacial cycles.~~

## 220 **2 Study site** ~~The modern system and results~~ history of previous work **Lake Chala**

### 221 **2.1 Site description** Setting of the study site

Lake Chala (~~also spelled 'Challa~~ 3°19' after the nearby village S, 37°42' E) is a relatively ~~small~~ large (4.2 km<sup>2</sup>), deep (c. 90 m in 2016) volcanic crater lake ~~bridging the border of Kenya and Tanzania in eastern equatorial Africa (3°19'S, 37°42'E)~~, situated at c. 880 m above sea level in the southeastern foothills of Mt. Kilimanjaro (~~Fig. 1~~). ~~Lake-surface evaporation (1735 mm yr<sup>-1</sup>; Payne (1970)) greatly exceeds~~ average mean annual rainfall (565 mm yr<sup>-1</sup>; De Wispelaere et al. 2017; Griepentrog et al. 2019). Therefore, besides rainfall on the lake and on the steep inner slopes of the crater basin, substantial subsurface inflow is required to balance the lake's water budget (Payne, 1970). This subsurface inflow is derived from ~~percolating rainfall on or above the forested slopes~~ rainfall on the forested and subalpine zones of Mt. Kilimanjaro (Hemp, 2006; Bodé et al., 2020) that reaches the lake 3–4 months later (Barker et al., 2011a). ~~Presently,~~ The modern-day Lake Chala is a fresh, slightly alkaline (surface- 230 water pH 8.4-9.3) and unproductive tropical lake with high concentrations of silica but low concentrations of phosphorus and nitrogen in the mixed surface layer, although these nutrients accumulate in the hypolimnion (Wolff et al., 2014). The lake ~~is topographically closed but occasionally after high rainfall a small creek is activated, which breaches the north-western crater rim (Buckles et al., 2014).~~ The lake has a typical crater-lake morphology, with steep crater walls ~~that reach~~ up to 170 m above the lake's surface and steep underwater slopes down to ~60–70 m which level off to form a flat central lake bottom (Moernaut et al., 2010). ~~It has a roughly triangular shape with a~~ and a total catchment area (of 5.6 km<sup>2</sup>) ~~that is~~ only 30% larger than the



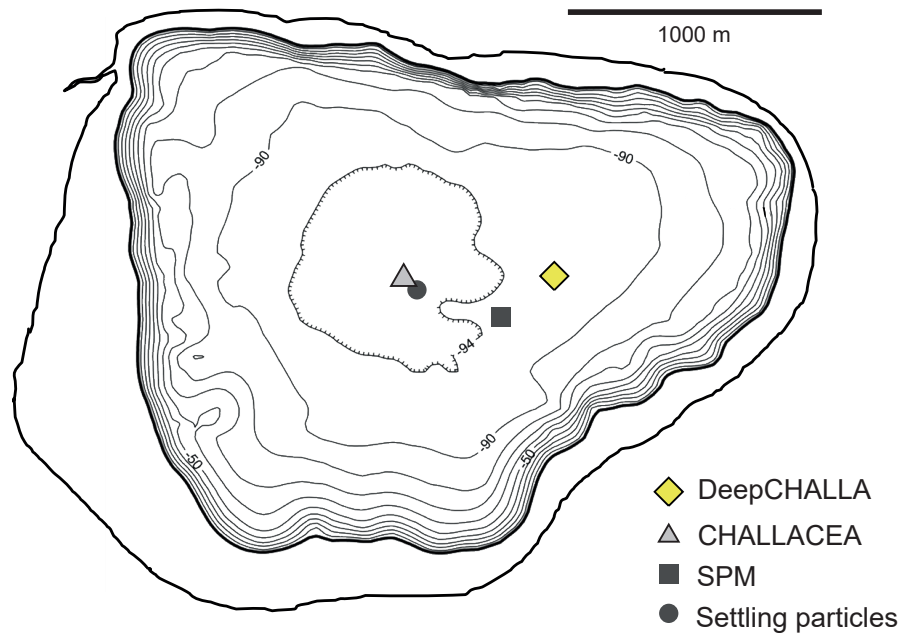


**Figure 1.** Bathymetry of Lake Chala (~~adapted from~~ Moernaut et al. (2010) ~~with~~; depth contours in meters) ~~surrounded by its steep-sided crater catchment, demarcated by the~~ outer-bold full line demarcating the crater catchment. The ~~drilling sites of the DeepCHALLA and 2005 CHALLACEA campaigns are indicated by a yellow diamond and (25 ka to present; grey triangle, respectively) and 2016 DeepCHALLA (c. Also shown 250 kyr to present; yellow diamond) drilling sites are indicated, as well as the fixed sampling locations of suspended particulate matter (SPM; dark grey square) and settling particles (dark grey circle) used in earlier~~ long-term monitoring studies of the modern system (Sinninghe Damsté et al., 2009; Buckles et al., 2014; van Bree et al., 2020; Baxter et al., 2021).

surface area of the lake itself ~~.From approximately~~ (Fig. 1). ~~From about~~ 10 m above the 2016 lake level, i.e. the upper limit of shallow caves formed by wave erosion during past high-stands, more significant outflow is possible through the porous upper crater walls.

In ~~this~~ the semi-arid tropical climate regime ~~, highest~~ characterizing eastern equatorial Africa, mean monthly  
 240 air temperatures are ~~reached~~ highest in February–March (night and daytime temperature of 21 and 33 °C), and lowest ~~temperatures~~ in July–August (~~night and daytime temperature of~~ 18 and 28 °C; Buckles et al. 2014). Orographically isolated from Atlantic- or Congo Basin-sourced moisture Sepulchre et al. (2006), Lake Chala is ~~located~~ situated east of the Congo Air Boundary (CAB) ~~and is therefore orographically isolated from Atlantic or Congo Basin-sourced moisture (Sepulchre et al., 2006; Verschuren et al., 2009; Tierney et al., 2013)~~. It is ~~located in~~ year-round  
 245 (Verschuren et al., 2009; Tierney et al., 2013) and thus part of the so-called greater Horn of Africa region which ~~is drier than more western parts of the continent at comparable latitude due to~~ depends entirely on relatively modest rainfall from the In-

dian Ocean [Wainwright et al. 2019](#). The region's climate is characterized by a [strongly](#) bimodal pattern of seasonal rainfall ([Wainwright et al. 2019 and references cited therein](#)) associated with the shifting latitudinal position of the intertropical convergence zone (ITCZ) ~~and tropical rain belt. Short and long rains.~~ [At the latitude of Lake Chala, rain seasons](#) occur from late  
250 October to December ([short rains](#)) and from March to May ~~, respectively. They are ('long rains')~~, separated by the main dry season from June to September, i.e. during ~~the~~ southern hemisphere (SH) winter, and a short dry season in January-February.

## 2.2 Water-column depth zones and mixing regime

Following Buckles et al. (2014), the water column of Lake Chala can be separated into 6 distinct zones (Fig. 2), differentiated by their frequency of mixing as reflected in physical and chemical properties. Zone 1 represents the daily mixed layer, and  
255 is fully oxygenated with uniform temperature and pH. Zone 2 is characterized by oxic to sub-oxic conditions and positioned from immediately below the principal thermocline to the oxycline which demarcates its base. Zone 3 is thus anoxic with pH falling to c. 7.2 and sharply increasing concentration of dissolved methane ~~which continues to increase through the lower water column~~ (Baxter et al., 2021). Zones 1–3 together constitute the mixolimnion, i.e., the portion of the water column that mixes at least once each year (Lewis, 1983; De Crop and Verschuren, 2021). Zones 4–6 together constitute the monimolimnion, and  
260 are defined by a stable temperature of 22.3 °C and permanent anoxia, except that rare deep-mixing events reaching into Zone 4 may occasionally inject oxygen that is however quickly consumed by bacterial activity. Across Zone 4, pH decreases further to c. 7.0 and the dissolved-ion concentration (measured as specific conductance) increases with depth from c. 350 µS/cm to c. 450 µS/cm (Barker et al., 2013; Wolff et al., 2014), creating a chemical density gradient across Zone 4 which largely prevents temperature-driven convective mixing (and oxygen injection) beyond the Zone 3-4 boundary (De Crop and Verschuren, 2021).  
265 Stable pH and dissolved-ion concentrations throughout Zone 5 indicate lack of mixing even on multi-annual time scales. This also applies to Zone 6, but being positioned directly above the profundal lake bottom the local water chemistry and redox conditions are affected by diffusion out of the uncompacted surficial sediments subject to diagenesis.

Lake Chala is characterized by a strong seasonal mixing pattern relating to the oscillation between windy dry and calm wet seasons, with substantial variability in the expression of these seasons between successive years. From September until  
270 May, i.e., the period encompassing the long and short rain seasons and the intervening warm dry season, high lake-surface temperatures and/or lower wind speeds result in reduced mixing of the upper water column, promoting stronger temperature and chemical stratification (Fig. 2a). Except for the daily mixed layer (Zone 1) oxygen renewal is diminished, and due to heterotrophic bacterial activity that is being promoted by high water temperatures, the depth range of sub-oxic transitional conditions (Zone 2) is greatly reduced or even eliminated, thereby shifting the oxycline (top of Zone 3) to a shallower position  
275 (~10 to 15 m), with most intensely stratified conditions occurring during SH summer (Wolff et al., 2014; van Bree et al., 2018; van Bree et al., 2020). This expansion of the anoxic (but seasonally mixing) Zone 3 increases the overall volume of anoxic water (Zones 3–6) relative to the oxygen-rich surface layers (Zones 1–2).

During the main dry season, lower air temperatures and higher wind speeds cause [deep](#) turbulent and convective [deep](#)-mixing of the upper water column [down](#) to 42–46 m (Wolff et al. 2014; Buckles et al. 2014; van Bree et al. 2020; Fig. 2b). During this  
280 deep-mixing period, which normally starts at the end of May and finishes by mid-September (Wolff et al., 2014; van Bree et al.,

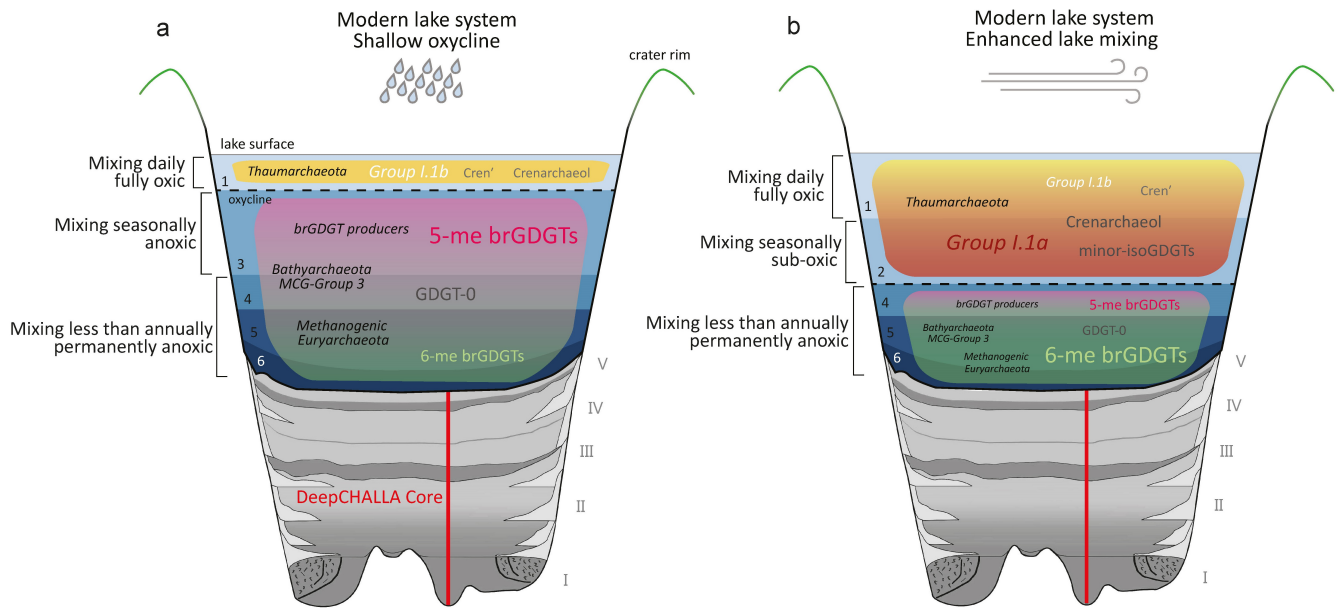


**Figure 2.** Schematic representation of the spatial ~~distributions~~ distribution of GDGT GDGTs and their producers in the ~~modern Lake Chala~~ modern-day Lake Chala water column of modern-day Lake Chala during the two seasonal extremes of (a) highly stratified (shallow oxycline) conditions associated with the rainy season and (b) enhanced upper water-column mixing associated with windy/dry conditions ~~based on distributions in, as shown by analysis of SPM and settling particles (Buckles et al., 2013, 2014; van Bree et al., 2020; Baxter et al., 2021) and seismic profiling of the underlying sediments with the five major depositional stages (I-V) indicated (Maitituerdi et al., 2022).~~ based on distributions in, as shown by analysis of SPM and settling particles (Buckles et al., 2013, 2014; van Bree et al., 2020; Baxter et al., 2021) and seismic profiling of the underlying sediments with the five major depositional stages (I-V) indicated (Maitituerdi et al., 2022). The lake water column is divided ~~into in~~ into in six distinct mixing zones with different mixing frequencies and chemical properties, following Buckles et al. (2014). Also shown is the location of DeepCHALLA drilling through the complete package of Quaternary sediments underlying Lake Chala, as documented by seismic profiling Moernaut et al. (2010), and defining five major depositional stages (I-V) in its c. 250-kyr history (Maitituerdi et al., 2022). See sections 2.1-2.4 and 2.2-2.4 for further description.

2018), ~~oxygen penetrates further into the water column causing the expansion of the oxygenated zones, most dramatically of Zone 2. Consequently, the depth range of Zone 3 is greatly reduced, and nutrient-rich deep water is brought up to the nutrient-starved epilimnion, promoting phytoplankton productivity (for example causing a pronounced diatom bloom; Wolff et al. 2014; van Bree et al. 2018). Hence, the oxygenated portion~~ Simultaneous replenishment of the upper water column with oxygen  
 285 causes a dramatic expansion of Zone 2 and shrinking of Zone 3, such that the oxygenated part of the water column (Zones 1–2) increases relative to the anoxic ~~portion part~~ portion part (Zones 3–6). ~~Also, A second period of deep mixing interrupts the long period of upper water-column stratification during the short dry season in January–February, a period of shallower mixing to c. 20–25 m interrupts the long period of stratification, driven by high wind speeds but hampered by high surface-water temperature it is limited to the uppermost 20–25 m (Wolff et al., 2014; van Bree et al., 2018; van Bree et al., 2020).~~  
 290 seasonal extremes of mixing states in Lake Chala associated with shallow or deep oxycline conditions, experienced during the mostly calm/wet and windy/dry seasons and associated with shallow or deep oxycline conditions, respectively. The permanent

anoxia of the lower water column of Lake Chala leads to the deposition of organic-rich, diatomaceous and often seasonally laminated sediments (i.e., varves; Wolff et al. 2011).

### 2.3 Depositional history of Lake Chala inferred from seismic stratigraphy

295 Seismic profiling of the ~~erater basin of Lake Chala~~ Chala crater basin revealed that the lake overlies at least c. 210 m of near-continuous lacustrine sedimentation (Moernaut et al., 2010). ~~Based on the extrapolation of long-term mean sedimentation rates from the~~ Extrapolation of mean sedimentation rate in the previously cored and dated upper portion of the ~~seismic sequence (Moernaut et al., 2010) to the lowermost section~~ sequence Blaauw and Christen (2011) to the base of the seismic ~~stratigraphy,~~ it was inferred that the sediments may reflect 250-kyr ~~profiles indicated that the complete sequence may encompass 250 kyr~~ of deposition, i.e., the entirety of the two most recent last two glacial-interglacial cycles (Verschuren et al., 2013). ~~Detailed analysis of high-resolution seismic profiles of the Chala crater basin has permitted reconstruction of the complete depositional history of the lake back to 250 ka, beginning with the initial lacustrine sediment infill after the collapse of the caldera (Maitituerdi et al., 2022). Building on the earlier analysis of the upper half of the seismic profiles (Moernaut et al., 2010), the stratigraphic~~ The seismic-stratigraphic sequence is characterized by ~~either undisturbed and uniform a sequence of either~~ basin-wide ('draped') sedimentation deposited under mostly high lake-level conditions, or basin-focused ('ponded') sedimentation reflecting periods of low lake level. ~~The seismic record is hence separated into five depositional stages (Stages V–I),~~ Moernaut et al. (2010), defining five successive phases in the basin's evolution (depositional stages V–I) characterized by pronounced changes in lake depth. Importantly, because i) ponded sedimentation reflects the greater sediment focusing which ~~results occurs~~ when turbulent mixing extends to reaches the profundal lake bottom (Maitituerdi et al., 2022), and ii) the steep-sided ~~morphology of Chala crater~~ basin entails constancy through time in the minimum water depth allowing undisturbed accumulation of soft organic sediments (Håkanson and Jansson, 1983), seismic stratigraphy serves as a lake-level proxy tied ~~more strictly~~ rather to absolute water-column depth ~~and or~~ mixing regime. ~~On this long-time scale, lake level~~ Also, over the complete 250-kyr history of Lake Chala, the surface level of the lake is a reflection of both climate-driven ~~moisture variability~~ variability in lake water balance and changes in basin hydrology as the crater ~~progressively fills basin progressively filled~~ with sediments. During Stage I (c. 248–207 ka), ~~the oldest depositional phase, represents the initial lacustrine sedimentation which lacustrine sedimentation~~ was limited to a ring-shaped depositional area surrounding the ~~then still exposed at that time still exposed~~ cones of volcanic tuff in the center of the basin, and further characterized by thick mass-wasting deposits ~~at the in the steeply sloping~~ basin periphery (Maitituerdi et al., 2022). Lake ~~level during Stage I is estimated to be depth was probably~~ low, but this could either be due to ~~relatively dry regional dry~~ climate conditions or to the still leaky nature of the crater basin during the period ~~following caldera collapse shortly after lake formation~~. Stage II (c. 207–113 ka) is defined by the complete burial of the central tuff cones and the start of basin-wide sedimentation. During the first half of ~~Stage II this stage~~ (c. 207–147 ka) a gradual transition to more draped sedimentation takes place, indicating that the water column became progressively taller; ~~due to the still relatively thin underlying sediment package, the greatest overall depth of the lake during~~ . During the second half (c. 147–113 ka) Lake Chala may have attained the greatest depth of its entire 250-kyr history ~~was likely reached during the second half of this stage, albeit partly due to the still relatively thin~~

underlying sediment package. Stage III (c. 113–99 ka) represents a ~~distinct~~ period of significantly reduced lake level implying severe climatic drought, ~~as indicated by strongly basin-focused sedimentation in the seismic profiles. During Stage III,~~ During this stage Lake Chala developed the flat central lake floor which still exists today, ~~and~~ consequently from this stage onwards the total depositional area of the crater basin has remained fairly constant through time. Stage IV (c. 99–19 ka) was a period of mostly high lake-level conditions, ~~as implied by continuity of draped sedimentation,~~ except for a short-lived low-stand c. 60 ka ago. Lastly, Stage V (19 ka to present) represents a period of fluctuating lake level, as inferred from a succession of ponded lenses reflecting ~~sediment focusing under reduced lake level~~ intermittent sediment focusing sandwiched between units of draped sediments (Maitituerdi et al., 2022).

## 2.4 Ecological history ~~of Lake Chala~~ inferred from fossil diatom assemblages

~~Lake Chala sediments contain abundant fossil diatoms (Wolff et al., 2011, 2014), and consequently the analysis of diatom assemblages in the DeepCHALLA sequence has provided insights into upper water-column mixing, water chemistry, and nutrient dynamics throughout the lake's 250-kyr history (Tanttu, 2021). The pelagic (open-water)~~ The diatom community of modern-day Lake Chala ~~is relatively poor in species, consisting mainly of *Afrocybella barkeri* (Coeqyt and Ryken, 2016)~~ consists mainly of the open-water (pelagic) planktonic species *Afrocybella barkeri* and *Nitzschia fabiennejansseniana* (Coeqyt and Ryken, 2017). ~~The more common presence of diatom.~~ Analysis of fossil diatom assemblages indicate that Lake Chala has been a true freshwater lake throughout its 250-kyr history (Tanttu, 2021). Diatom species associated with littoral (near-shore) and benthic (bottom) habitats ~~during the early history of the lake are common only during early lake history (c. 248–221 ka)~~ suggests, indicating that Lake Chala was at that time ~~was a relatively a fairly~~ shallow and well-mixed lake ~~environment with greater~~ with adequate nutrient availability. ~~Fossil diatom assemblages deposited after c. 221 ka~~ After that time ~~fossil diatom assemblages~~ are entirely dominated by *N. fabiennejansseniana* and other needle-shaped *Nitzschia* species, indicating a ~~change to a~~ purely pelagic environment with deep water column, weak upper water-column turbulence, and ~~strongly nutrient-limited~~ nutrient-starved conditions. *A. barkeri* makes its first appearance c. 144 ka, and from then on the diatom community had a composition similar to that of the modern-day lake, except for ~~major temporal variability in dominance of~~ variation in the dominance of *A. barkeri* versus one or more needle-like *Nitzschia* spp. ~~aversus the more heavily silicified *A. barkeri*.~~ Dominance of the ~~latter~~ former is interpreted to reflect episodes with greater mixed-layer turbulence and more efficient nutrient ~~recycling, whereas the former cycling, whereas dominance of the latter~~ reflects a shallower ~~or weaker~~ mixed upper layer and therefore more extreme nutrient depletion. To the extent that alternation between these conditions was climate-controlled, *A. barkeri* dominance ~~may therefore be associated with reduced lake depth (lower lake level) during periods of drier climate conditions (Tanttu, 2021).~~ *A. barkeri* dominated the diatom community of Lake Chala during the periods dated to ~~during the periods c. 108–96 ka and 28–13 ka .~~ From 94 ka to 48 ka, reappearance of *Nitzschia* suggests a transition towards greater lake depth and more stable upper water column. Importantly, the fossil diatom data indicate that Lake Chala has been a true freshwater lake throughout its 250-kyr history may therefore indicate reduced lake depth under a drier climate regime (Tanttu, 2021).

## 2.5 GDGTs in the modern Lake Chala system, and climate-proxy relationships GDGT biogeochemistry

360 The aim to better understand the producers, sources, and climatic sensitivity of GDGTs extracted from the DeepCHALLA sediment record, and thus to validate the climate-proxy relationships used for paleoclimate reconstruction, has stimulated extensive investigations into the occurrence and distribution of distribution and sources of specific GDGTs in Lake Chala and its surrounding catchment (Sinninghe Damsté et al., 2009; Buckles et al., 2013, 2014, 2016; van Bree et al., 2020; Baxter et al., 2021). To determine  
365 seasonal to interannual-scale variation in GDGT distributions, some of these studies involved in surrounding catchment soils and in recent sediments has been the focus of extensive modern-system studies, including monthly monitoring of lake conditions and measurement of GDGT variation spanning multiple years. Namely, brGDGTs (van Bree et al., 2020) and isoGDGTs (Baxter et al., 2021) were analyzed in settling particles collected at 35 m water depth during 98 consecutive months, and in suspended particulate matter (SPM) collected at 13 discrete water  
370 depths during 17 consecutive months (Fig. 1). This section provides an overview of the outcome physical limnology, SPM and settling particles over multiple years, and analysis of GDGT distributions in profundal surface sediments throughout the basin and in the mid-lake sediment record of the last 25 kyr drilled by the CHALLACEA project (Sinninghe Damsté et al., 2009; Buckles et al., 2013, 2014, 2016; van Bree et al., 2020; Baxter et al., 2021). The results of these studies ~~for the~~ provide important context for interpretation of GDGT proxies, ~~to later be applied in the context of the~~  
375 distributions in the complete, c. 250-kyr DeepCHALLA sedimentary record sediment record recovered by the DeepCHALLA project.

### 2.5.1 The BIT index

~~In the 25-kyr record from the CHALLACEA site in Lake Chala (Fig. 1), the BIT index~~

The BIT index record of Lake Chala over the last 25 kyr showed good agreement with a first-order lake-level reconstruction based on seismic stratigraphy (Verschuren et al., 2009). ~~It was also recognized that~~ As soils in the hills surrounding Mt. Kilimanjaro contain high amounts of brGDGTs (Sinninghe Damsté et al., 2008). ~~Hence, based on the then-current understanding of brGDGT sources in lakes, the~~ temporal variation in the sedimentary BIT index was ~~inferred initially interpreted~~ to reflect varying transport input of soil-derived brGDGTs to the lake ~~associated with~~ due to varying precipitation and consequent soil erosion. Following the discovery that brGDGTs in Lake Chala are abundantly produced within the  
385 lake itself (Buckles et al., 2013, 2014), additional modern-system studies ~~elucidated aimed to elucidate~~ the exact nature of the relationship between the Chala BIT index and hydroclimate (van Bree et al., 2020; Baxter et al., 2021). ~~Namely, These established that~~ brGDGTs are primarily produced in the anoxic zone of the water column (Zones 4–6), and ~~that~~ their depth range follows the seasonal cycle of lake mixing and stratification ~~such that~~. Specifically, during the deep-mixing season between June and September they are restricted deeper in the water column, while under conditions of strong upper water-column  
390 stratification during the rest of the year, the oxycline moves upwards, thereby expanding the brGDGT production zone (Fig. 2; van Bree et al. 2020). On the other hand, ~~the niche of~~ Group I.1a Thaumarchaeota, generally which are the main producers

of crenarchaeol in Lake Chala (with secondary contributions from Group I.1b; Buckles et al. 2013; Baxter et al. 2021), ~~is-are~~ primarily restricted to the (sub-)oxic zone between the principal thermocline and the oxycline (Zone 2), where the degree of sunlight is much less intense than in the uppermost layer and ~~ongoing-or-recent-deep-mixing-provides-deep-mixing-events~~ provide nitrogen in the form of ammonium (Buckles et al. 2013; Baxter et al. 2021; Fig. 2a). During periods of prolonged shallow oxycline conditions, ~~this-the~~ depth niche of Group I.1a Thaumarchaeota (Zone 2) is eliminated, and their annual “bloom” is suppressed (Buckles et al. 2013, 2014; Baxter et al. 2021; Fig. 2b). ~~In-a-study-of~~ SPM sampled throughout the water column during a year when exceptionally shallow oxycline conditions prevailed, ~~yielded~~ only gene copies of Group I.1b Thaumarchaeota ~~were-detected-and-~~, while crenarchaeol concentrations were several orders of magnitude lower than recorded previously (Buckles et al., 2016; Baxter et al., 2021). With substantially lower amounts of crenarchaeol settling on the lake bottom during such intervals, the accumulating sediments attain higher BIT-index values (Baxter et al., 2021). During periods of sustained deep mixing, the reverse situation of prolonged oxygenation of the upper water column (Zones 1–2) promotes development of Thaumarchaeota, thus increasing crenarchaeol production and lowering BIT-index values.

Therefore, the BIT index ~~effectively~~ tracks changes in the relative size of the anoxic and oxygenated zones in the water column ~~in Lake Chala~~. Within a single year, the oxycline position is controlled by the timing and duration of seasonal deep mixing ~~related-to-monsoon-variability, such that when the intertropical convergence zone (ITCZ) is overhead, heavy-~~ Heavy rainfall and low wind speeds ~~cause-when the ITCZ is overhead cause stratification of the upper water column and hence~~ shallow oxycline conditions, ~~and-while high wind speeds~~ when the ITCZ is located ~~to the North/South, high wind speeds and lack of rainfall enhance lake mixing~~ North or South of the Lake Chala region promote deep mixing, which pushes the oxycline down (van Bree et al., 2020; Baxter et al., 2021). On the long time scales of paleoclimate reconstruction, the relative proportion of the anoxic and oxic zones ~~will-also-be-strongly-is-also~~ influenced by changes in overall lake depth ~~(De Crop and Verschuren, 2021)~~. High-stand episodes of greater lake depth will be associated with an overall taller anoxic zone, whereas during low-stands the anoxic zone will shrink, increasing the relative volume of the upper mixed layer (Verschuren, 1999, 2001). Hence, on the long time scales registered in Lake Chala sediments, the BIT index ~~is-a-reflection-of-reflects~~ temporal variation in hydrological moisture balance (Baxter et al., 2021), which in ~~this-relatively-the-rather~~ dry tropical region of eastern equatorial Africa is chiefly determined by changes in the strength of the Indian Monsoon and temperature effects on continental evaporation (Baxter et al., 2021, 2023).

### 2.5.1 ~~IsoGDGT distribution and TEX<sub>86</sub>~~

The ephemeral nature of Zone 2 in the water column of Lake Chala, where Group I.1a Thaumarchaeota are most abundant, has a major influence on sedimentary proxies based on isoGDGTs (Baxter et al., 2021). During periods of exceptionally shallow oxycline and thus Thaumarchaeotal bloom suppression, greater contributions to the isoGDGT pool from methanotrophs, methanogens and other anaerobic archaea ~~to the isoGDGT pool-render the temperature signal derived from-render~~ TEX<sub>86</sub>-based temperature estimates untrustworthy (Sinninghe Damsté et al., 2012a; Baxter et al., 2021). ~~In-this-way,-Hence, in line with the results of other modern system studies~~ (e.g., Zhang et al. 2016; Cao et al. 2020; Dang et al. 2016; Sinninghe Damsté et al. 2022), temporal variation in ~~mean-annual~~

water-column stratification is a crucial factor controlling the sedimentary TEX<sub>86</sub> signal in Lake Chala, potentially equally important as temperature variation (Baxter et al., 2021), ~~in line with the results of other modern system studies (e.g., Zhang et al. 2016; Cao et al. 2020; Dang et al. 2016; Sinninghe Damsté et al. 2022)~~ itself (Baxter et al., 2021). As methanogens produce relatively high amounts of isoGDGT-0, the ratio between isoGDGT-0 and crenarchaeol (isoGDGT-0/cren) ~~has been~~ can be used to assess the contribution of methanogens to the sedimentary isoGDGT pool (e.g., Blaga et al. 2009; Bechtel et al. 2010). ~~Similar to brGDGTs, also Like brGDGTs,~~ isoGDGT-0 is produced most abundantly in the anoxic lower water column of Lake Chala (Buckles et al., 2013; Baxter et al., 2021). Therefore, the isoGDGT-0/cren ratio likewise reflects changes in the relative volume of the anoxic and oxic portions of the water column, and is relatively higher during highly stratified lake conditions and lower during periods of deep mixing (Fig. 2). A greater relative abundance of the crenarchaeol isomer may reflect periods during which the contribution of Group I.1b Thaumarchaeota to the isoGDGT pool is increased, as these archaea produce a greater amount (typically 14–29%) of the isomer than Group I.1a Thaumarchaeota (typically only 0–3%; Pitcher et al. 2010, 2011; Kim et al. 2012; Sinninghe Damsté et al. 2012b; Elling et al. 2017; Bale et al. 2019). ~~Significantly~~ Notably, Group I.1b Thaumarchaeota do not produce isoGDGTs with the same temperature dependency of ring formation as Group I.1a (e.g., Elling et al. 2017). In Lake Chala, ~~similarly to crenarchaeol itself, the crenarchaeol isomer is most abundant in the oxygenated~~ both crenarchaeol and its isomer most abundantly occur in Zones 1–2 (Fig. 2). In the 98-month data set of settling particles, higher than average f[CREN'] values (a measure of the contribution of the crenarchaeol isomer; Table 5.1) were recorded during a ~~sustained~~ period in 2013 when only Group I.1b Thaumarchaeota gene copies were detected (Baxter et al., 2021). Hence, it appears that the two groups of Thaumarchaeota are ~~differentially~~ differently impacted by lake stratification, with Group I.1a being severely diminished when the (sub-) oxic Zone 2 is eliminated or reduced (Fig. 2b). The f[CREN'] proxy can therefore be used as an indicator of prolonged shallow-oxycline conditions in Lake Chala (Baxter et al., 2021).

### 2.5.1 ~~BrGDGT distribution and associated proxies~~

~~The 17-month time series of SPM data from Lake Chala revealed that the~~ The 5-Me and 6-Me ~~brGDGT isomers appear to isomers of brGDGTs, from their side,~~ occupy spatially distinct zones within the anoxic lower water column (van Bree et al., 2020). ~~Namely, of lake Chala (van Bree et al., 2020):~~ the 5-Me brGDGTs are produced mainly in the anoxic but seasonally variable Zone 3, whereas 6-Me brGDGTs are produced most abundantly in the equally anoxic but permanently stratified Zones 4–6 (Fig. 2). ~~As presented above, Zone 3 is greatly reduced during~~ During periods of deep lake mixing Zone 3 is greatly reduced, hence limiting the growth of 5-Me brGDGT producers and increasing the relative contribution of 6-Me brGDGT producers. The isomer ratio (IR<sub>6Me</sub>; Table 5.1) captures this relative contribution of 6-Me to 5-Me ~~GDGTs~~ brGDGTs. Indeed, low IR<sub>6Me</sub> values in settling particle data (van Bree et al., 2020) correspond to trends in other proxies (BIT index, isoGDGT-0/cren) indicative of an unusually shallow oxycline ~~conditions (Baxter et al., 2021). Just as (Baxter et al., 2021). Like~~ in the case of the BIT index, on the long timescales ~~reflected in~~ registered by sedimentary records, changes in the IR<sub>6Me</sub> ratio will be predominantly controlled by changes in lake depth, because the increased inputs of fresh water which cause lake level to rise lead to the expansion of Zone 3 where 5-Me brGDGT producers proliferate, hence causing



460 lower IR<sub>6Me</sub> values in the sediment (Baxter et al., 2023). ~~The latter study concluded, supported by findings from detailed water column studies in Lake Chala (van Bree et al., 2020; Baxter et al., 2021), that temperature calibrations based on MBT'<sub>5Me</sub> are not suitable for local paleotemperature reconstruction because past episodes of low lake level likely resulted in strong reduction of Zone 3 where the 5-Me brGDGT isomers are produced. Instead it was shown that 6-Me brGDGTs need to be included in the transfer function to properly capture the temperature sensitivity of the local brGDGT producers.~~

## 465 3 Materials and Methods

### 3.1 Construction of the sediment sequence, lithofacies description and age model

~~In 2016 the International Continental Scientific Drilling Program (ICDP) project 'DeepCHALLA' recovered a sedimentary sequence of c. The 214.8 m below the lake floor by hydraulic piston coring (Fig. 1). Drilling occurred in five main long sediment sequence from Lake Chala was recovered from five drill holes (A–E) at a single location in the eastern depocenter of Lake Chala (Fig. 1), with overlapping 3-m sections achieving complete (100%) recovery in the upper 123 m (c. 160 ka to present) of the sediment sequence and near-complete (~85%) recovery of the lower 92 m.~~

~~The Core splitting, imaging, non-destructive scanning, and preliminary lithological description, and cross-correlation of the DeepCHALLA cores were carried out at the U. S. National Lacustrine Core Facility (LacCore) hosted by the University of Minnesota (Minneapolis, in Minneapolis (USA), as previously described by Baxter et al. (2023) with respect to the upper 475 68.39 m of the composite part of the sediment sequence. The entire drilled sequence of these matrix sediments consists of fine-grained and diatom-rich organic muds with visually clear mm-scale lamination or cm-scale banding. This allowed overlapping, allowing cross-correlation of core sections from different drill holes to be precisely cross-correlated at the with mm-scale while viewing the high-resolution digital line-scan images in Corelyzer software, and identifying either shared lamination features or the base and top of turbidites as robust stratigraphic tie points precision. Before extraction of sediment samples for analysis of 480 bulk sediment composition, organic biomarkers and fossil diatom assemblages, among others, other proxy analyses, all event deposits (turbidites) with thickness >2 cm were excluded from the continuous composite depth scale, to obtain a provisional 'event-free' depth scale and to ensure that samples mostly reflect genuine reflect so-called 'matrix' sediments of primary lacustrine deposition at the drill site. Sets of samples Samples were extracted from the work halves of core sections represented in the composite sequence, at predetermined constant depth intervals on the event-free depth scale such that proxy time series 485 have a more or less uniform temporal resolution throughout the sediment record. Following detailed inventory of all turbidites (Swai, 2018) the event-free depth scale was updated to also exclude turbidites of 0.5–2.0 cm thickness, prompting exclusion of some already analysed samples from the final proxy time series (see below).~~

Absolute dating efforts of the DeepCHALLA sequence are ongoing. Considering the focus of the present study on long-term lake-basin development rather than paleoclimate reconstruction, we use a preliminary sediment chronology based on transfer 490 of the high-resolution <sup>14</sup>C-based age model for the last 25 ka kyr at the CHALLACEA site (Blaauw and Christen, 2011) to the DeepCHALLA site; links between the seismic stratigraphy of Chala basin at both sites and known near-global climate events back to 140 ka (Moernaut et al., 2010; Maitituerdi et al., 2022) (Moernaut et al., 2010); and linear extrapolation of the average

sedimentation rate over this 140-ka interval to the base of the DeepCHALLA core sequence at 215-214.8 m below the lake floor (Martin-Jones et al., 2020).

495 During sampling of the DeepCHALLA sequence in June 2017 the general appearance of the sediment at-in each 2-cm thick sampled depth interval was noted, with reference to the preliminary lithological description executed-at doneat LacCore. Matrix sediments were classified into one of two primary lithofacies, namely mm-scale (varve-like) laminations and cm-scale (banded) sediments. A third lithofacies type is used to describe core sections characterized-by-rapid-alternation-between-where these two facies at-the-cm-scale alternate frequently (Baxter et al., 2023). Mm-scale laminated sediments are interpreted to have been  
500 deposited under stable stratification and a permanently anoxic lower water column as exists in-the-lake today, whereas cm-scale banding reflects post-depositional disturbance of the uppermost few cm of originally mm-scale laminated muds, due to bottom currents associated with occasional complete water-column mixing. Although such events may have injected some oxygen to the near-bottom environment, almost certainly this must have been consumed rapidly (in days rather than weeks) by bacterial activity (Lewis, 1987; De Crop and Verschuren, 2019) such that for all practical purposes the lower water column would still  
505 have been permanently anoxic. Nevertheless, sections of mm-scale lamination can be considered to represent periods of stable meromixis, whereas cm-banded sections represent periods when complete water-column mixing occurred at least occasionally at-the-scale-of-decades on a decadal time scale.

### 3.2 Sample preparation and GDGT analysis and calculation of GDGTs derived proxies

The present study involved In the present study a total of 949 sediment horizons from throughout the DeepCHALLA sequence  
510 are analysed, each 2 cm thick and extracted at a regular interval of 16 cm in matrix sediments (i.e., skipping turbidites >2 cm thick). Detailed inventory of all turbidites (Swai, 2018) revealed that 73 sediment horizons extracted and analyzed for GDGTs (7.5% of the total) partly consist of thin turbidites (< 2 cm thick). Here only the 33 samples containing >25% of turbidite material (3.3% of the total) were excluded from the final proxy time series, which hence consist of 916 sediment horizons spanning the past c. 250 ,000-years kyr. Methods of sample preparation and GDGT analysis on-DeepCHALLA-sediments have  
515 been described previously (Baxter et al., 2023). In short, freeze-dried and powdered sediments (0.3–1.2 g dry weight) were extracted with a Dionex accelerated solvent extraction (ASE) system using a 9:1 v/v mixture of dichloromethane (DCM) and methanol and 1  $\mu$ g of internal standard (synthetic C46 glycerol trialkyl glycerol tetraether; GTGT) was added to the total lipid abstract (TLE) (Huguet et al., 2006). TLEs were dissolved in DCM, passed through a  $\text{Na}_2\text{SO}_4$  column and dried under  $\text{N}_2$  gas before being separated into apolar, ketone and polar fractions using eluents of hexane/DCM (9:1, v/v), hexane/DCM (1:1,  
520 v/v), and DCM/methanol (1:1, v/v), respectively, and passing through an  $\text{Al}_2\text{O}_3$  column. The fractions were dried under  $\text{N}_2$  gas and the polar fractions, containing the GDGTs, were redissolved in hexane/isopropanol (99:1, v/v) prior to being filtered using a PTFE 0.45  $\mu$ m filter. Measurement of GDGTs was carried out using an Agilent 1260 Infinity ultrahigh performance liquid chromatography (UHPLC) system coupled to an Agilent 6130 single quadrupole mass detector following the method of  
(Hopmans et al., 2016) Hopmans et al. (2016). GDGTs were identified by  $[\text{M} + \text{H}]^+$  ion detection in selected ion monitoring  
525 (SIM) mode for m/z 1018.0, 1020.0, 1022.0, 1032.0, 1034.0, 1036.0, 1046.0, 1048.0, 1050.0 (brGDGTs), m/z 1292.3, 1294.3, 1296.3, 1298.3, 1300.3 and 1302.3 (isoGDGTs), and m/z 743.8 (internal standard) with a mass window of 1.0. Peak area

integration of the peaks representing GDGTs in the  $[M + H]^+$  mass chromatograms was done using Agilent Masshunter software. A peak area of  $3 \times 10^3$  units was used as the detection threshold, with peaks below this threshold being excluded for proxy calculation.

### 530 3.3 Calculation of GDGT concentrations and derived climate proxies

Absolute concentrations of isoGDGTs and brGDGTs were normalized to the organic carbon ( $C_{org}$ ) content of the sampled intervals and hence expressed in  $\mu\text{g g}^{-1} C_{org}$ . ~~Determination of  $C_{org}$  was based on samples of determination, c. 1.0 g of wet sediment representing wet sediment from~~ the same 2-cm core increments as the ~~samples extracted for GDGT samples. They were GDGT samples was~~ weighted immediately after extraction and again after freeze-drying to measure the loss in mass as estimate of water content ( $\%H_2O$ ). The freeze-dried samples were homogenized, split in two and analyzed using a Primacs Carbon Analyzer at the University of Haifa (Israel), which determines total carbon content by combusting the sample at 1050 °C and measuring the evolved carbon dioxide. One subsample was first treated with phosphoric acid ~~before the measurement~~, to remove any inorganic carbon present and thus measure  $C_{org}$  only (Maitituerdi, 2023). The GDGT concentration time series comprises 909 sediment horizons ~~(as opposed n = 916 for the full biomarker proxy series)~~ due to missing dry sample weight or  $\%C_{org}$  values for ~~a handful of samples~~ seven GDGT samples. The  $TEX_{86}$  index was calculated according to Schouten et al. (2002) (Table 4.3.2). The BIT index was calculated according to Hopmans et al. (2004) ~~and~~, modified to explicitly show the inclusion of both the 5- and 6-Me brGDGTs (De Jonge et al., 2014). ~~In addition, isoGDGT-0~~ IsoGDGT-0/crenarchaeol,  $f[\text{CREN}]'$ , and  $\%isoGDGT-2$  were calculated to investigate the producers contributing to the isoGDGT pool ~~in Lake Chala (Sinninghe Damsté et al., 2012a; Baxter et al., 2021). IR<sub>6Me</sub> captures (Sinninghe Damsté et al., 2012a; Baxter et al., 2021). In addition,~~ the relative abundance of 6-Me versus 5-Me isomers ~~, with the 6-Me isomers indicated by the prime symbol, and (IR<sub>6Me</sub>)~~ was calculated according to ~~(De Jonge et al., 2015). The De Jonge et al. (2015), the~~ methylation of 5-Me branched tetraether index ( $MBT'_{5Me}$ ) and cyclisation of branched tetraether index (CBT') ~~were calculated~~ according to De Jonge et al. (2014). ~~Additionally also, and~~ the degree of cyclisation (DC) of ~~brGDGT was calculated~~ brGDGTs according to (Sinninghe Damsté, 2016; Baxter et al., 2021). For temperature reconstruction we applied the global lake calibration of Pearson et al. (2011), which ~~calculates~~ represents mean summer temperature (MST) and was determined by Baxter et al. (2023) to be the brGDGT-based paleotemperature-inference model best suited ~~for application to Lake Chala sediments to the setting of Lake Chala~~ at the intended time scale. In Table 4.3.2, the original calibration is rewritten to highlight the inclusion of both 5-Me and 6-Me isomers, with GDGTs in square brackets referring to the fractional abundances. The resulting 250-kyr MST record was then rescaled to the mean temperature range of an ensemble temperature reconstruction for the last 25 kyr based on ~~seven independent GDGT-based temperature reconstructions from other East African lakes, according to Baxter et al. (2023).~~

### 545 3.3 Numerical ~~and~~, statistical and periodicity analysis

The relationships between temporal variation in individual GDGT compounds and selected proxies throughout the DeepCHALLA sediment sequence were explored using univariate and multivariate analyses, mostly in the R statistical package FactoMineR (Lê et al., 2008). Univariate analyses were performed on organic-matter normalized absolute concentrations,

560 whereas multivariate principal component analyses (PCAs) were performed on the fractional abundances of individual GDGTs, relative to either the full suite of iso- and brGDGTs (22 compounds) or only the brGDGTs (15 compounds), isoGDGTs (7 compounds) or the sub-set of four isoGDGTs used in  $TEX_{86}$  calculation (isoGDGT-1,-2,-3 and cren'). To assess the influence of lake-basin development and water-column mixing regime on GDGT distributions, and by extension their sensitivity to climate variability, the 916 ~~analysed sediment horizons~~ sediment horizons (or 909, in case of GDGT concentrations) were grouped according to seismic lake-history stage or lithofacies to explore trends in GDGT concentrations, PCA scores, proxies, and possible relationships to changes in lake properties through time. Tukey multiple comparison of means with a 95% family-wise confidence interval was used to test if the GDGT concentrations and proxy values of these groups are significantly different; means are considered significantly different ~~according~~ at the 5% level of significance.

### 3.4 Periodicity analysis

570 The time series of GDGT concentrations and derived proxies were subjected to periodicity analysis using Acycle 2.3.1 software (Li et al., 2019), after standardization (mean = 0, standard deviation = 1) and 3rd-order detrending. For wavelet (morlet) analysis, the standardized and detrended GDGT time series were first resampled at the median temporal resolution (between 206 and 200 years depending on the selected time interval). Gaussian band pass filtering was also performed on select GDGT proxies using bandwidths that targeted periodicities compatible with obliquity (41-kyr) and precession (23-kyr) orbital insolation forcing, as revealed by wavelet analysis.

## 4 Results

### 4.1 Trends in isoGDGT and brGDGT concentrations

The overall composition of GDGTs in the drilled Lake Chala sediments is dominated by crenarchaeol and isoGDGT-0, with mean fractional abundances of 0.30 and 0.28 respectively, followed by tetramethylated (0.14), 6-Me (0.10) and 5-Me brGDGTs (0.07). GDGT concentrations display a high degree of high-frequency variability with major swings between adjacent samples (Fig. 3). Smoothing of the time series (black curves indicate a 10-point rolling mean) reveals that substantial changes also occurred with regard to longer-term trends. The concentrations of crenarchaeol (Fig. 3c; range = 0–2740  $\mu\text{g g}^{-1} C_{\text{org}}$ , average = 201  $\mu\text{g g}^{-1} C_{\text{org}}$ ) and the less abundant isoGDGTs used to calculate  $TEX_{86}$  (“minor” isoGDGTs) (Fig. 3d; range = 0.2–900  $\mu\text{g g}^{-1} C_{\text{org}}$ , average = 62  $\mu\text{g g}^{-1} C_{\text{org}}$ ) are highly correlated ( $R = 0.99$ ,  $p < 0.001$ ; Fig. S3), as they both fluctuate in the same semi-regular pattern throughout the record with the exception of two longer periods ~~withing Stages IV from within Stage IV~~ (c. 80–70 ka and c. 50–30 ka) during which these compounds are often nearly absent. Concentrations of isoGDGT-0 (Fig. 3e; range = 11–740  $\mu\text{g g}^{-1} C_{\text{org}}$ ; average = 142  $\mu\text{g g}^{-1} C_{\text{org}}$ ) and the summed brGDGTs (Fig. 3f; range = 6–810  $\mu\text{g g}^{-1} C_{\text{org}}$ ; average = 164  $\mu\text{g g}^{-1} C_{\text{org}}$ ) are also highly correlated with one another ( $R = 0.83$ ,  $p < 0.001$ ; Fig. S3). The concentrations of all ~~GDGT-GDGTs~~ are notably lower in the lowermost, oldest portion of the record compared to later stages (Fig. 3). For example, average summed concentrations of iso- and brGDGTs during ~~depositional~~ Stage I are respectively 149 and 60  $\mu\text{g}$

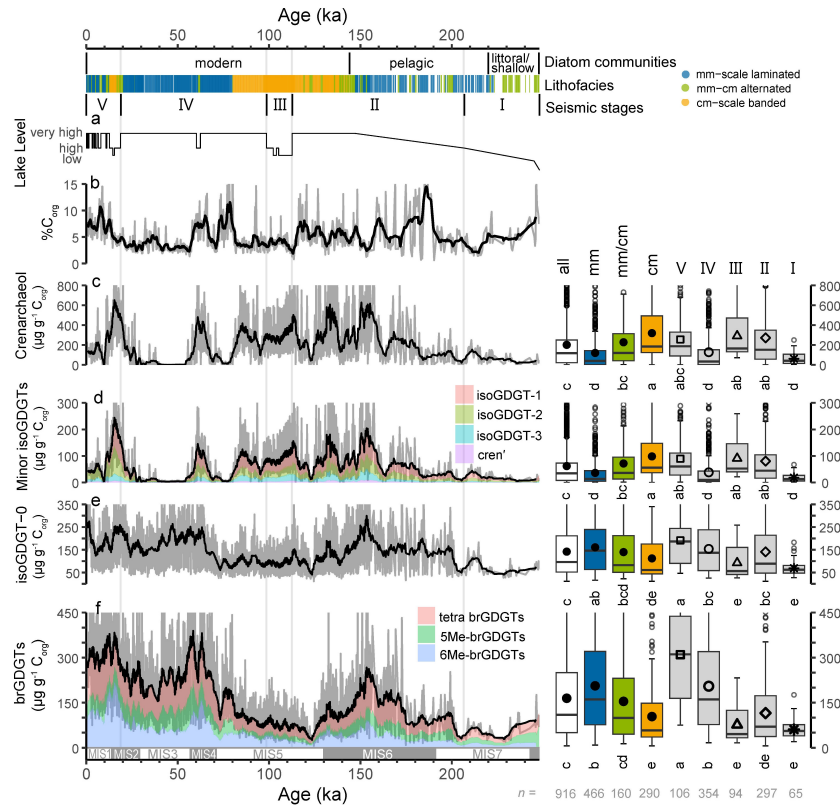


**Figure 3.** Down-core profiles of the organic-specific concentration of selected (groups of) GDGTs in the DeepCHALLA sediment sequence, in relation to Lake Chala lake-system evolution over the past 250 kyr. Indicated on top is-are the timing of three major phases in the diatom communities lake ecology as registered in the DeepCHALLA sequence (after Tanttufossil diatom assemblages Tantu (2021), 2021); the lithofacies category of each sediment horizon (colored bar) -and- the depositional stages (V-I) based on the seismic stratigraphy of Lake Chala (Maitituerdi et al., 2022). Subsequent panels show (a) the lake level reconstruction based on the seismic reflection data stratigraphy (Maitituerdi et al., 2022), (b) the percentage of sedimentary organic carbon content (%TOC) content, and TOC-normalized concentrations of (c) crenarchaeol, (d) the minor isoGDGTs (isoGDGT-1, -2, -3, and the crenarchaeol isomer), (e) isoGDGT-0, and (df) the brGDGTs. Black curves represent the 10-point rolling averages of the full data series, shown in grey. The boxplots associated with the box plots compare GDGT concentration profiles are values in samples grouped by the lithofacies category or depositional stage (using the same colour legend n = number of samples), and by depositional stage. The boxplots indicate the with median (black line) and average (solid or open shapesymbol) values, and the first and third quartiles (lower and upper hinges) -Whiskers-, whiskers (thin lines) extend extending to 1.5 × the interquartile range (IQR) from the hinges, with and data points beyond this range treated as outliers (open black circles) defined as data points beyond this range. Letters in a-d near the box plots indicate statistically significant groups of data determined using Tukey multiple comparison of means with a 95% family-wise confidence interval; means which. Means that do not share letters are significantly different according at the 5% level of significance. Note that in both the depth profiles In panels (b-f) and associated boxplots the y-axis has been stretched such that many high datapoints, and boxplot outliers fall off scale, in order to improve readability of the 10-point rolling average trends, but such that many individual data points with very high values, and corresponding box plot outliers, are off scale. At the bottom the timing of the marine isotope stages (MIS) as defined by; Lisiecki and Raymo (2005) is shown for reference.

$g^{-1} C_{org}$ : ~~in both cases~~, only 27% of their average concentrations in the full record (405 and 164  $\mu g g^{-1} C_{org}$ ). All GDGT concentrations generally increase from the oldest horizon until a pronounced maximum halfway through Stage II (dated to c. 153 ka ~~(i.e., halfway through Stage II)~~), and ~~notably display highly similar trends during this interval, which continues until c. 125 ka~~ display notably similar trends until near the end of Stage II when all GDGT concentrations experience a pronounced minimum. ~~Using the diatom-guided~~ dated to c. 125 ka. Using the diatom-based lake phases as reference, correlations between the concentrations of crenarchaeol, minor isoGDGTs (isoGDGT-1, -2, -3, and cren'), isoGDGT-0 and brGDGTs are universally ~~quite high~~ high in the period before establishment of the modern diatom community c. 144 ka ( $R = 0.69-0.99$ ,  $p < 0.001$ ; Fig. S5) ~~in the period preceding the appearance of the modern diatom community (c. 250-144 ka), whereas during c. 144-0 ka~~ , while since then (Fig. S7) the concentrations of crenarchaeol and minor isoGDGTs are strongly correlated ( $R = 0.99$ ,  $p < 0.001$ ), and likewise those of isoGDGT-0 and the brGDGTs ( $R = 0.84$ ,  $p < 0.001$ ) but correlations across these two groups are severely reduced ( $R = 0.25-0.52$ ) and ~~not statistically no longer~~ significant ( $p > 0.05$ ), as is also the case in the present-day lake (see section 2.3.2.5). The broad interval of c. 125-75 ka is characterized by lower-than-average isoGDGT-0 and brGDGT concentrations, after which concentrations increase again and generally remain high throughout the upper part of the record.

Samples extracted from mm-scale laminated ~~or~~ and cm-scale banded sediments ~~are characterized by~~ contain significantly different GDGT concentrations (boxplots in Fig. 3). Mm-scale laminated sediments contain higher amounts of isoGDGT-0 (~~average =~~ on average 146  $\mu g g^{-1} C_{org}$ ) and brGDGTs (~~average =~~ 206  $\mu g g^{-1} C_{org}$ ), and lower amounts of crenarchaeol (~~average =~~ 120  $\mu g g^{-1} C_{org}$ ) and minor isoGDGTs (~~average =~~ 36  $\mu g g^{-1} C_{org}$ ) compared to cm-scale banded sediments (~~which have~~ averages of respectively 112, 103, 319 and 98  $\mu g g^{-1} C_{org}$ , ~~all differences being statistically significant at the 5% level of significance. Sediments described as consisting of an alternation between these two lithofacies contain intermediate concentrations of these~~  $p < 0.05$  on all differences). Concentrations of these four classes of GDGTs ~~in samples containing a mixture of the two lithofacies are intermediate, with differences also being statistically different from these categories~~ significant.

## 4.2 Trends in the distribution of individual GDGTs

Principal component analysis (PCA) was performed on the fractional abundances of all 22 measured GDGTs together, and separately on the brGDGTs, isoGDGTs and minor isoGDGTs (~~Fig~~ Figs. 4 and S8). First considering the full suite of GDGTs, the first principal component (PC1) accounts for 91.3% of the variance, and is chiefly related to the strongly opposing behavior of crenarchaeol versus isoGDGT-0 and the brGDGTs, in particular brGDGTs Ia, IIa' and IIa (Fig. 4a). PC2 accounts for only 6.9% of the variance and mainly separates the isoGDGTs from the brGDGTs. In the PCA of only the isoGDGTs (Fig. 4b), PC1 accounts for a remarkable 99.7% of the variance, and as seen in the PCA on the full suite of GDGTs, relates overwhelmingly to the opposing behavior of crenarchaeol and isoGDGT-0. PC2 accounts for only 0.2% of the variance, and mainly separates isoGDGT-1 from isoGDGT-2 and -3. In the PCA of only the minor isoGDGTs contributing to the TEX<sub>86</sub> proxy (i.e., isoGDGT-1, -2, -3, and cren'; Fig. 4d), PC1 accounts for 74.3% of the variance and is mainly controlled by the ~~differing~~ different loadings of isoGDGT-1 and isoGDGT-2. PC2 accounts for 24.3% of the variance, with isoGDGT-3 plotting strongly on the negative side along with the weak negative position of cren', versus the positive position of isoGDGT-1 and -3. Finally, in the PCA

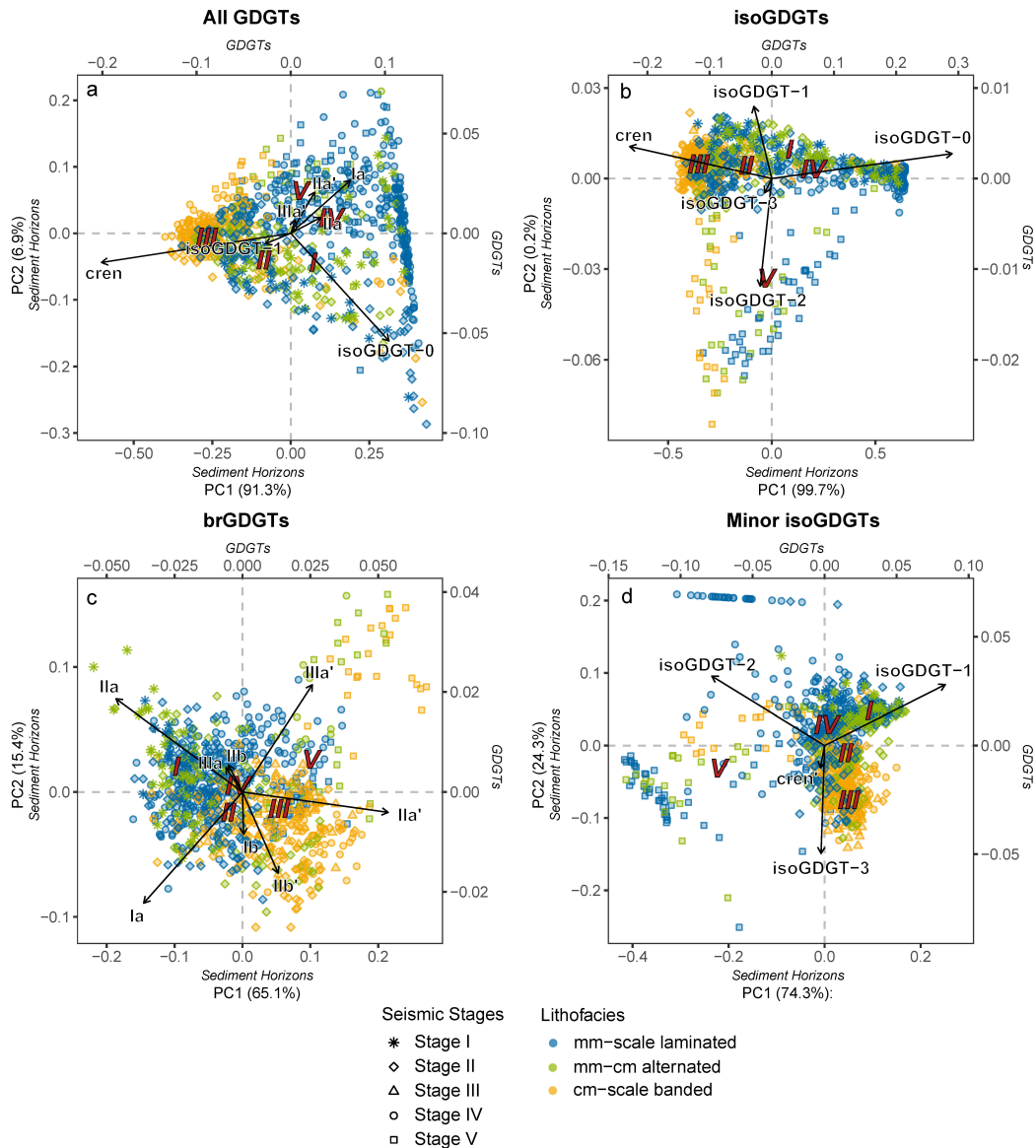


**Figure 4.** Principal component analyses (PCAs) biplots of the fractional abundances of (a) all GDGTs, (b) the isoGDGTs, (c) brGDGTs, and (d) the minor isoGDGTs (i.e., isoGDGT-1, -2, -3 and the crenarchaeol isomer) in the 250-kyr DeepCHALLA sediment sequence. The loadings of individual GDGTs is shown in the plot with arrows. In cases where GDGTs contributed at least 1% of the variability of the data among samples on both either PC1 and/or PC2, they were removed to improve readability (but their fractional abundances were still included during analysis or both shown as arrows). Individual scores of DeepCHALLA sediment horizons from depositional stages I-V are presented by different symbols, and colored according to lithofacies, with seismic stage indicated by different symbols. Red numerals I-V represent the centroid values (i.e., average PC scores) of the sequence separated according to the samples from those respective depositional stages. Note that separate PC axes indicate the position of the individual PC axes for individual samples (sediment horizons) and variables (GDGT vectors) and that the amount of variability within the dataset predicted by PC1 and PC2 is provided as a percentage (in brackets).

625 highlighting the differing distributions of individual brGDGTs (Fig. 4c), PC1 accounts for 65.1% of the variance, mainly separating the 6-Me brGDGTs (in order of contribution: IIa', IIIa' and IIb'), which plot on the positive side, from the acyclic tetramethylated brGDGT Ia and the pentamethylated 5-Me brGDGT IIa, which plot on the negative side. PC2 accounts for 15.4% of the variance, with as largest contributors the opposing groups of IIIa' and IIa versus Ia and IIb'.

In all PCAs described above ~~there are noticeable differences between~~ the PC scores of samples originating from each of the three lithofacies as defined above are noticeable different (colour codes in Fig. 4). Generally, samples from cm-scale banded sediments show greater contributions of crenarchaeol, the crenarchaeol isomer, 6-Me brGDGTs and isoGDGT-3, whereas samples from mm-scale laminated sediments have a greater contribution of isoGDGT-0 and the 5-Me brGDGTs. ~~In~~ Further, in the PCA of the brGDGTs, ~30 samples from cm-scale banded and cm-mm alternating sediments deposited during Stage V are ~~notably~~ separated from all other samples (Fig. 4c; upper right hand corner) by ~~their~~ unusually high fractional abundances of IIIa'.

### 4.3 Trends in GDGT-based proxies

#### 4.3.1 The BIT index

As presented above, PCA on the full suite of GDGTs strongly separates the brGDGTs from crenarchaeol along PC1. ~~Consequently~~ Moreover, variation in the BIT index (Fig. 5b) is highly correlated ( $R = 0.99$ ,  $p < 0.001$ ) to the PC1 scores of the respective sediment horizons ~~in this PCA~~ (Fig. 6a; Fig. S3). ~~This result demonstrates that this long-defined proxy (Hopmans et al., 2004), demonstrating that this proxy captures the most significant variability in GDGT distributions throughout the DeepCHALLA-250-kyr sediment sequence. Lake Chala sediments cover nearly the full range of possible BIT-index values (range = 0.06–1; Fig S2) with an overall average value of 0.5. From the oldest sediments up to c. 160 ka, variation in the BIT index is erratic, switching rapidly between high (> 0.8) and low (< 0.3) values without discernable discernible long-term trends. From c. 160 ka onwards changes in the BIT index become less erratic, and from c. 138 ka to c. 84 ka sustained periods of very low values (< 0.2) are interrupted by periods with predominantly high BIT values. In particular, the BIT index is BIT-index values are consistently low (< 0.2) during c. 114–96 ka, largely overlapping with Stage III which is identified as a pronounced lake low-stand episode based on seismic reflection data (Maitituerdi et al. 2022; Fig. 5a-b). The lowest BIT index BIT-index values of the entire record (0.06) occur at the very start of this interval. From c. 80 ka onward, corresponding almost exactly with a sustained lithofacies shift from cm-scale banded to mm-scale laminated sediments, a major change is observed in the nature of BIT-index variability, with values approaching unity that are sustained for longer periods. BIT-index values are continuously high until c. 24 ka (roughly corresponding to the Stage IV to V at the Stage IV-V transition), except for a ~10-kyr long episode c. 62-52 ka and a brief interruption dated to c. 37 ka. Sustained low BIT-index values between 20 ka and 14 ka again correspond to a sustained period of cm-scale banded sedimentation interpreted as a pronounced lake low-stand (Maitituerdi et al., 2022). Thereafter, BIT-index values rise steadily before experiencing a brief reversal to low BIT values 13–11 ka, followed by a period with values close to unity during 11–9 ka. Over the last 6 kyr, the Chala BIT index has fluctuated around 0.6.~~



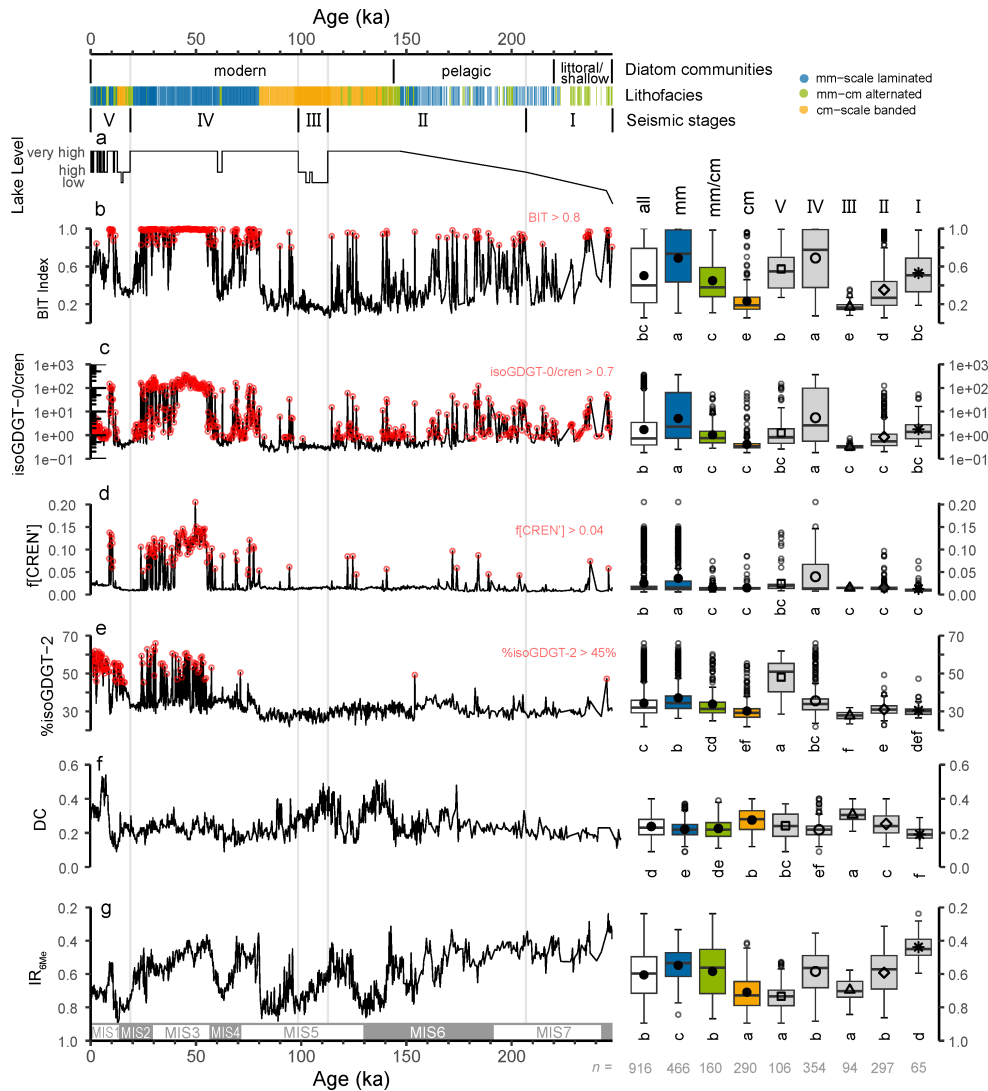


**Figure 5.** Down-core profiles of selected GDGT-derived proxies in the DeepCHALLA sediment sequence, in relation to [Lake Chala lake-system-system](#) evolution over the past 250 kyr. Indicated [from on top to bottom, are](#) the timing of three major phases in [the diatom communities-lake ecology as registered in the DeepCHALLA sequence-fossil diatom assemblages](#) (Tanttu, 2021), the lithofacies category of each sediment horizon (colored bar) [and](#) the depositional stages (V-I) based on [the seismic stratigraphy of Lake Chala, as well as Maitituerdi et al. \(2022\)](#). [Subsequent panels show](#) (a) [the lake level reconstruction based on the seismic reflection data stratigraphy](#) (Maitituerdi et al., 2022). [GDGT-based ratios and proxies from the DeepCHALLA sediment sequence are shown:](#) (b) The BIT Index, (c) isoGDGT-0/crenarchaeol ratio, (d) f[CREN'], (e) %isoGDGT-2, (f) degree of cyclisation (DC), and (g) IR<sub>6Me</sub>. [Red Data points with a red highlight](#) indicate values [for which of](#) BIT index > 0.8, isoGDGT-0/cren > 0.7, f[CREN'] > 0.04 [and](#) %isoGDGT-2 > 45% (see methods). The associated [boxplots-box plots](#) are as described in Fig. 3. Also shown is the timing of the marine isotope stages (MIS) [as defined by Lisiecki and Raymo \(2005\)](#), [for reference](#).

Comparison of the ~~BIT index~~ BIT index time series with those of the absolute concentrations of crenarchaeol and the summed brGDGTs reveal that ~~variation in the BIT index~~ BIT index variation is predominantly influenced by ~~the abundance of crenarchaeol and~~ crenarchaeol abundance, considerably less by the contribution of brGDGTs (Fig. 7a–b), ~~in agreement with as is also the case in~~ settling particle data (Baxter et al., 2021). However, sediment horizons with BIT-index values < 0.2 generally have brGDGT concentrations < 300  $\mu\text{g g}^{-1} \text{C}_{\text{org}}$ , suggesting that brGDGT variability ~~may also does~~ affect BIT-index variation ~~at least~~ to a small extent. ~~Once again,~~ Also the average BIT index of the three lithofacies ~~categories~~ differs significantly (boxplots in Fig. 5b), with cm-scale banded sediments ~~being characterized by~~ most often showing low values (average = 0.2, including a handful of distinct outliers), whereas mm-scale laminated sediments ~~generally~~ have much higher values (average = 0.7), and samples from the mm-cm scale alternating lithofacies ~~most often display~~ intermediate values (average = 0.4).

### 4.3.2 IsoGDGT-derived proxies

~~Three additional proxies based on ratios between isoGDGTs that have been used to investigate changes in Thaumarchaeotal production (Sinninghe Damsté et al., 2012a; Baxter et al., 2021) are the~~ The isoGDGT-derived proxies isoGDGT-0/crenratio, f[CREN'] ~~,~~ and %isoGDGT-2 (Table ) ~~allow to investigate changes through time in Thaumarchaeotal production (Sinninghe Damsté et al., 2012a; Baxter et al., 2021). In the 250-kyr record of Lake Chala (Fig. 5c–e).~~ ~~The,~~ the isoGDGT-0/cren ratio is strongly correlated to PC1 of the PCA on all GDGTs ( $R = 0.59$ ,  $p < 0.001$ ;  $\rho = 0.99$ ,  $p < 0.001$ ; Fig. S3) and PC1 of the isoGDGTs ( $\rho = 1.0$ ,  $p < 0.001$ ; Fig. 6d; Fig. S3). Hence ~~also the~~ isoGDGT-0/cren ~~ratio and is also strongly correlated~~ with the BIT index ~~are highly correlated~~ ( $R = 0.61$ ,  $p < 0.001$ ;  $\rho = 0.95$ ,  $p < 0.001$ ; Fig. 7f), as expected ~~owing to because~~ both of them ~~being controlled are controlled~~ by crenarchaeol abundance, and ~~the isoGDGT-0 and brGDGTs have~~ overlapping ecological niches ~~of brGDGTs and isoGDGT-0~~ in the anoxic lower water column of Lake Chala (Baxter et al., 2021). ~~Variability in the isoGDGT-0 (Fig. 2). IsoGDGT-0/cren ratio variability~~ is highly erratic in the lower part of the DeepCHALLA sequence (c. 250–160 ka) and becomes more structured thereafter, mirroring the trends displayed by the BIT index. f[CREN'] is moderately correlated with PC1 scores of all GDGTs ( $R = 0.51$ ,  $p < 0.001$ ) and of the isoGDGTs separately ( $R = 0.58$ ,  $p < 0.001$ ), and more strongly correlated to isoGDGT-0/cren ( $R = 0.70$ ,  $p < 0.001$ ; Fig. 7g; Fig. S3). Through most of the DeepCHALLA sequence values of f[CREN'] ~~attains considerably low values are low~~ ( $< 0.025$ ) ~~in most of the DeepCHALLA sequence~~ (Fig. 5d), presumably ~~indicating an reflecting the~~ often limited presence of Group I.1b Thaumarchaeota (Baxter et al., 2021). The very few instances of higher f[CREN'] values before 60 ka mostly consist of single sediment horizons. Sustained periods of high f[CREN'] values ( $> 0.04$ ) occurred from c. 60 ka to 25 ka ~~,~~ mostly in mm-scale laminated sediments deposited during the middle and latter part of Stage IV, ~~in Stage IV~~ and from 11 ka to 9 ka ~~,~~ also in Stage V, ~~mostly~~ in mm-scale laminated sediments. The %isoGDGT-2 proxy (Fig. 5e) is strongly inversely correlated to PC1 of the minor isoGDGTs ( $R = -0.93$ ,  $p < 0.001$ ). Before c. 80 ka its value hovers ~~remarkably~~ stably around 30%, with only two instances of more elevated values. After this time its baseline shifts to higher percentages. From c. 55 to 24 ka ~~within in~~ Stage IV, %isoGDGT-2 is highly variable, ~~and frequently exceeds~~ frequently exceeding 50%. Two other periods of ~~generally~~ high %isoGDGT-2 values occurred between 20–11 ka and 9–0 ka.

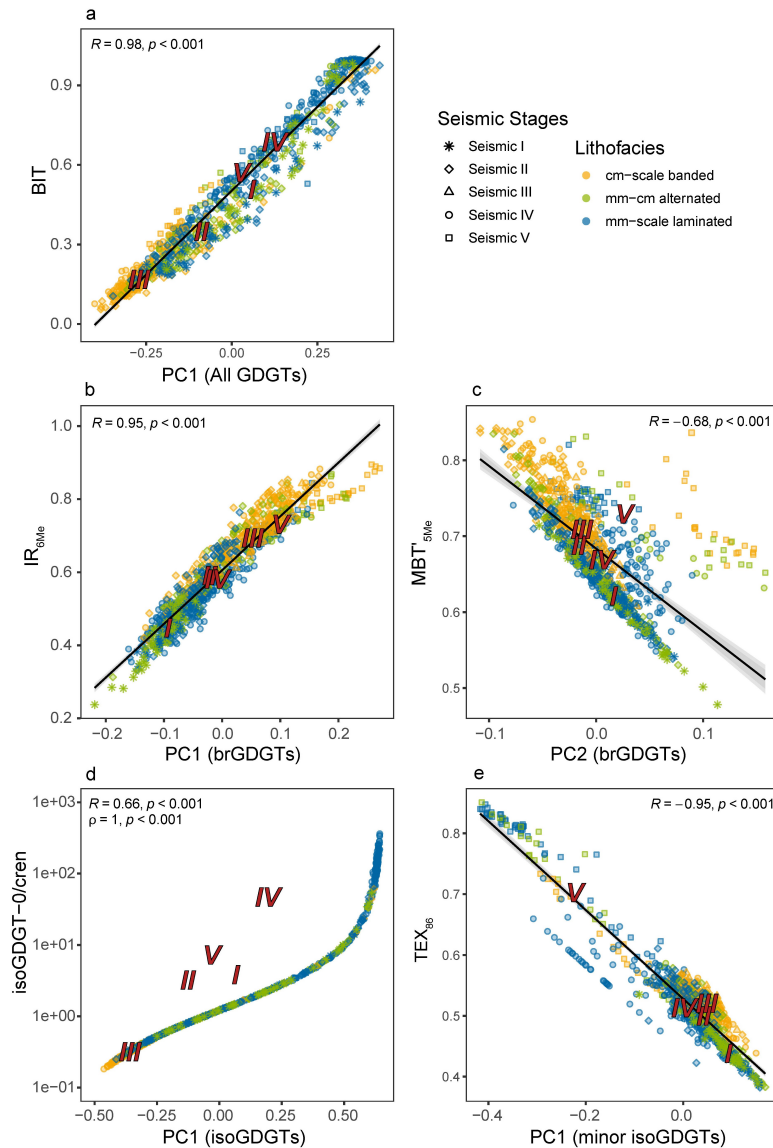


**Figure 6.** Scatter plots comparing GDGT-based proxies with the PC scores and GDGT ratios of individual sediment horizons in the 250-kyr DeepCHALLA sequence. (a) BIT index versus PC1 scores from the PCA of on all the GDGTs compared to the BIT index. From PCA of the brGDGTs, (b) PC1 scores are compared to  $IR_{6Me}$  and versus PC1 from the PCA on brGDGTs. (c) PC2 scores are compared to  $MBT'_{5Me}$  versus PC2 from the PCA on brGDGTs. (d)  $isoGDGT-0/cren$  versus PC1 scores from PCA of the PCA on isoGDGTs compared to the  $isoGDGT-0/cren$  archaeol ratio. (e)  $PC2-TEX_{86}$  versus PC1 scores from PCA of the PCA on minor isoGDGTs (isoGDGT-1 to -3, and cren') compared to  $TEX_{86}$ . Data points Sediment horizons from depositional stages I-V are presented by different symbols, and colored according to lithofacies, and the depositional stage is indicated by the point shape colored according to lithofacies. Red numerals (V-I) I-V represent the average values PC scores of the sequence grouped according to the samples from those respective depositional stages.

TEX<sub>86</sub> is strongly correlated to PC1 of the minor isoGDGTs ( $R = -0.95$ ,  $p < 0.001$ ; Figs. 6e and S3). From the oldest sediment horizon until c. 180 ka, the index is relatively stable around 0.45, after which it increases to  $\sim 0.55$  by c. 165 ka, remaining at that level until c. 80 ka (Fig. 8b). The period c. 80–20 ka is characterized by highly variable TEX<sub>86</sub> values ranging between 0.43 and 0.77. At 20 ka the index rises dramatically, reaching peak values of 0.85 at  $\sim 5$  ka and remaining high until the top of the sequence.

~~Average Mm-scale laminated and cm-scale banded sediments again differ significantly in average~~ isoGDGT-0/cren ratio, f[CREN'] and %isoGDGT-2 values ~~of mm-scale laminated and cm-scale banded sediments differ significantly~~ (boxplots in Figs. 5c–d), with mm-scale laminated sediments having higher average values (39.6, 0.04, and 37.1%) than cm-scaled banded sediments (1.1, 0.01, and 30.2%) ~~for all three proxies, values in~~, and mm-cm scale alternating sediments ~~being having values~~ intermediate (isoGDGT-0/cren ratio, %isoGDGT-2) or near-identical to cm-scale banded sediments (f[CREN']). In contrast, average TEX<sub>86</sub> values of the three lithofacies are not significantly different from one another (boxplots in Fig. 8b).

### 4.3.3 BrGDGT-derived proxies

The IR<sub>6Me</sub> of penta- and hexa-methylated brGDGTs varies substantially throughout the DeepCHALLA sequence (0.24–0.89, average = 0.61) (Fig. 5g, note the reversed y-axis). There is strong correlation between IR<sub>6Me</sub> and PC1 of the PCA on brGDGTs ( $R = 0.95$ ,  $p < 0.001$ ; Fig. 6b), meaning that this ratio reflects an important aspect of variability in the distribution of brGDGTs in Lake Chala sediments. IR<sub>6Me</sub> values are relatively low and stable in the early part of the time series, becoming more variable from c. 170 ka onwards. Temporal variability in IR<sub>6Me</sub> shows ~~some similarities to that of~~ moderately negative correlation with the BIT index ( $R = -0.49$ ,  $p < 0.001$ ; Fig. 7c) and isoGDGT-0/cren ~~ratio~~ ( $R = -0.33$ ,  $p < 0.001$ ) ~~reflected in moderate negative~~ correlations with those proxies over the full time series. At c. 142 ka a sharp transition occurs from low to high IR<sub>6Me</sub> values, almost coeval with the sustained transition to cm-scaled banded sedimentation ~~at that level~~ and establishment of the modern-day diatom community. From this time onwards similarity between trends in IR<sub>6Me</sub> and BIT index (and also isoGDGT-0/cren) is enhanced, resulting in stronger negative correlation between IR<sub>6Me</sub> and the BIT index after 144 ka ( $R = -0.64$ ,  $p < 0.001$ ; Fig. S7). Comparing variation in IR<sub>6Me</sub> to the concentrations of 5-Me and 6-Me brGDGTs indicates that both groups of brGDGTs have a comparable influence on the IR<sub>6Me</sub> signal (Fig. 7d–e). For example, sediments with the highest IR<sub>6Me</sub> values ( $> 0.7$ ) also have the highest concentrations of 6-Me brGDGTs, while those with IR<sub>6Me</sub> below 0.7 generally have greater amounts of 5-Me brGDGTs.

The CBT' index ~~, typically used in pH reconstruction,~~ is partly affected by the degree of cyclisation of the brGDGTs, but as shown by its strong positive correlation with IR<sub>6Me</sub> throughout the DeepCHALLA sequence ( $R = 0.95$ ,  $p < 0.001$ ; Fig. S3), in Lake Chala this index is mainly controlled by variation in the relative abundance of 5-Me and 6-Me brGDGTs. Accordingly, the CBT' index also shows strong correlation with PC1 of the PCA on the brGDGTs, which separates the 5-Me and 6-Me brGDGTs ( $R = 0.99$ ,  $p < 0.001$ ; Fig. S3). On the other hand, the degree of cyclisation of the brGDGTs (expressed with the DC ratio) shows only ~~a~~ weak positive correlation with IR<sub>6Me</sub> ( $R = 0.35$ ,  $p < 0.001$ ; Fig. S3), and is also only weakly correlated with either PC1 and PC2 of brGDGT distribution ( $R = 0.31$ ,  $p < 0.001$ ;  $R = -0.30$ ,  $p < 0.001$ ). This suggests that DC is not a strong measure of the variance in the distribution of brGDGTs in Lake Chala sediments. Accordingly, its time series does not

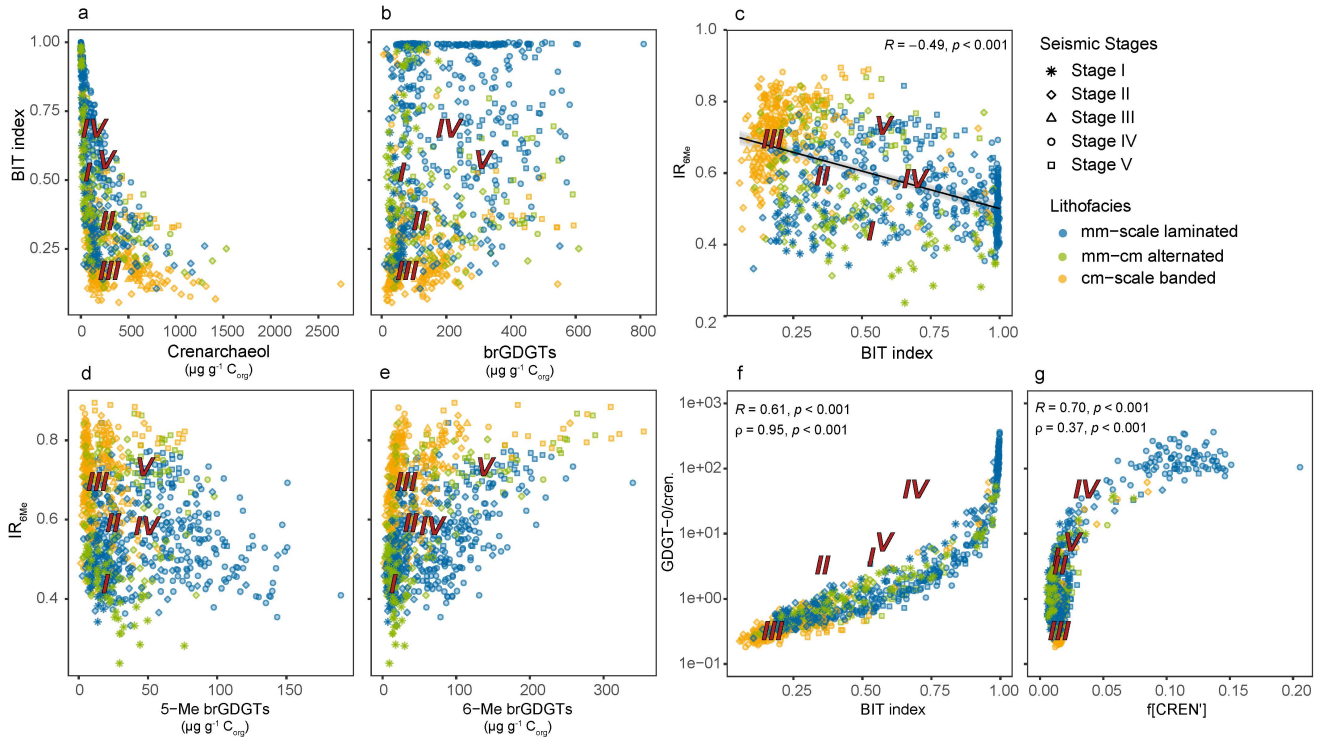


**Figure 7.** Scatter plots comparing the variation in selected GDGTs and GDGT-based proxies. (a) BIT index versus the crenarchaeol concentration of, (a) crenarchaeol and (b) brGDGTs,  $IR_{6Me}$  BIT index versus summed brGDGT concentration; (c)  $IR_{6Me}$  versus BIT index, and the summed concentration of; (d) the  $IR_{6Me}$  versus summed 5-Me brGDGTs brGDGT concentration, and (e) the  $IR_{6Me}$  versus summed 6-Me brGDGTs brGDGT concentration, (f) the BIT index versus the isoGDGT-0/cren ratio versus BIT index, and (g) isoGDGT-0/cren versus f[CREN'] versus the isoGDGT-0/cren ratio. The sediment horizons from depositional stages I-V are indicated by different symbols, and colored according to lithofacies, and the depositional stage is indicated by the point shape. Red numerals (I-V) represent the average values PC scores of the sequence grouped according to the samples from those respective depositional stages.

show large changes, remaining mostly around 0.2, except during the period between c. 140 ka and c. 100 ka and in the last 10 kyr when larger temporal variability is observed (Fig. 5f).

The 250-kyr time series of  $MBT'_{5Me}$  shows strong correlations is strongly correlated to both PC1 ( $R = 0.66$ ,  $p < 0.001$ ; Fig. 6c; Fig. S3) and PC2 ( $R = -0.68$ ,  $p < 0.001$ ) of the brGDGTs, and hence, naturally also to  $IR_{6Me}$  ( $R = 0.84$ ,  $p < 0.001$ ) and CBT' ( $R = 0.68$ ,  $p < 0.001$ ). This index ranges from 0.48–0.85, and besides a sharp rise at the base of the record, is relatively stable in sediments deposited before c. 175 ka (Fig. 8c). Thereafter,  $MBT'_{5Me}$  first increases to near-maximum values ( $\sim 0.8$ ) at c. 160 ka and then drops abruptly to a sustained minimum ( $\sim 0.6$ ) dated to c. 150–140 ka which terminates as sharply as it started. The period from c. 140 ka until c. 80 ka is characterized by variable but generally high  $MBT'_{5Me}$  values (frequently above 0.8), again ending in an abrupt drop to values below 0.7.  $MBT'_{5Me}$  reaches its lowest values just after c. 60 ka, then

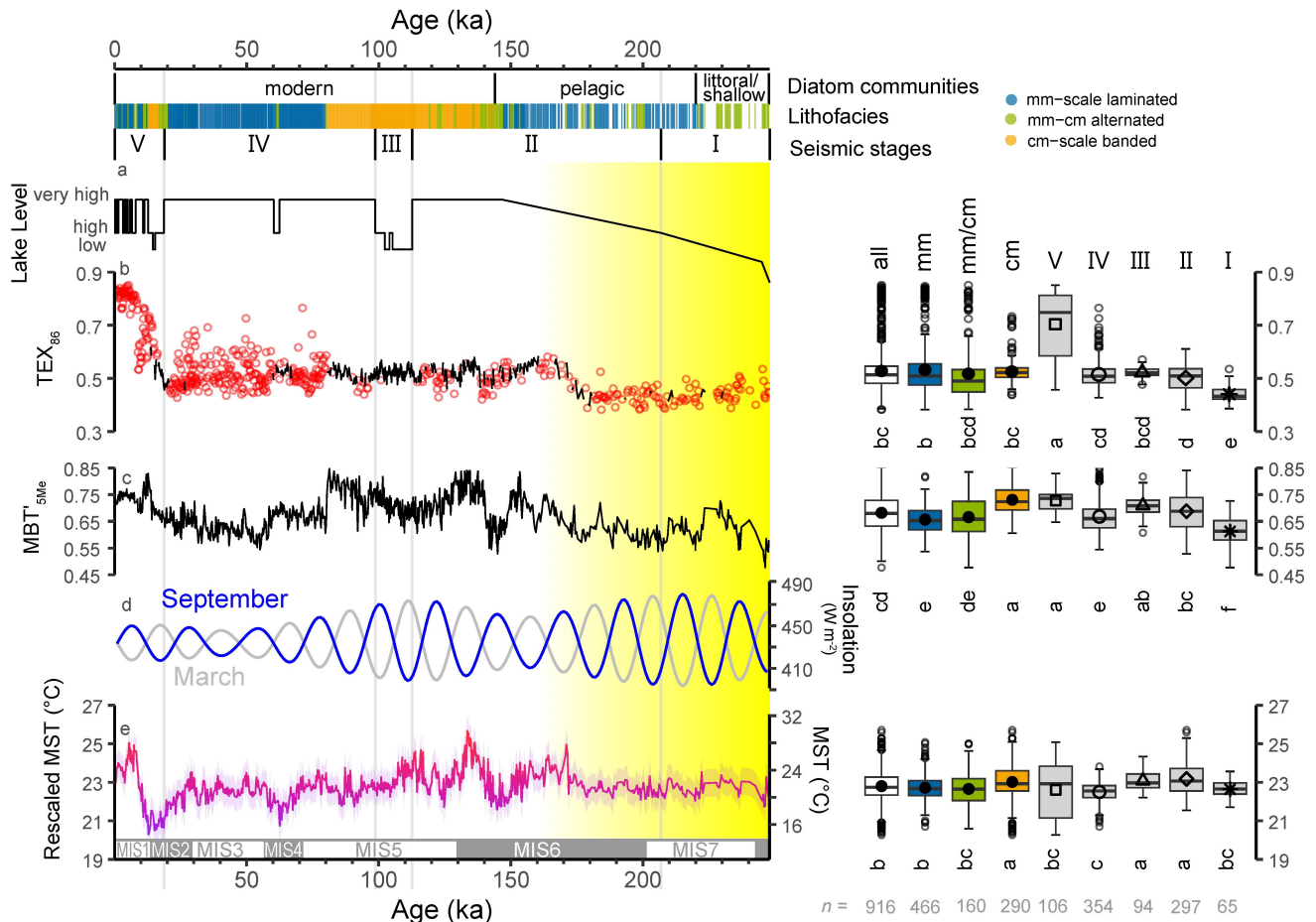


**Figure 8.** Down-core profiles of select-selected GDGT-based paleotemperature proxies in the DeepCHALLA sediment sequence, in relation to Lake Chala lake-system-system evolution over the past 250 kyr. Indicated from-on top to-bottom, are the timing of three major phases in the diatom communities-lake ecology as registered in the DeepCHALLA-sequence fossil diatom assemblages (Tanttu, 2021), the lithofacies category of each sediment horizon (colored bar) and the depositional stages (V-I) based on the seismic stratigraphy of Lake Chala, as well as Maitituerdi et al. (2022). Subsequent panels show (a) the lake level reconstruction based on the seismic reflection data stratigraphy (Maitituerdi et al., 2022) and, (b) TEX<sub>86</sub> values for the DeepCHALLA sediment sequence with red circles reflecting indicating samples which are excluded according to from the time series using the filtering method of Baxter et al. (2021). Black line connects those sediment horizons which remain after the filtering, (c) MBT'<sub>5Me</sub> index and, (d) mean daily insolation for at the months of equator in September (blue line) and March (grey line) at the equator, and (e) Mean Summer Temperature (MST), calculated according to Pearson et al. (2011) and rescaled using an ensemble reconstruction of post-glacial (20-0 ka) temperature records-history from seven other East African lakes following Baxter et al. (2023). The associated boxplots-box plots are represented as described in Fig. 3. Also shown is the timing of the marine isotope stages (MIS; Lisiecki and Raymo (2005)) as defined by Lisiecki and Raymo (2005), for reference.

735 gradually increases until 14 ka when a short-lived spike occurs, lasting until 11 ka and followed by a gently rising then falling trend over the last 10 kyr.

The time series of MST ~~reconstructed using the global lake calibration of Pearson et al. (2011) (see Methods)~~ spanning the complete DeepCHALLA sequence is strongly correlated to PC2 of the brGDGTs ( $R = -0.65$ ,  $p < 0.001$ , Fig. S3) and to the DC ( $R = 0.76$ ,  $p < 0.001$ ). Rescaled MST values (Baxter et al., 2023) range between 20.3 °C and 25.6 °C. As reconstructed, 740 rescaled MST is rather stable (generally 22–23 °C) from c. 250 ka until 180 ka, at which time it gently increases to  $\sim 24$  °C then again decreases to a pronounced minimum ( $\sim 21.5$  °C) dated to c. 145 ka (Fig. 8e). After this, MST ~~increases rapidly, reaching attains~~ peak values at c. 134 ka. ~~Following another and 121–108 ka, separated by a~~ minimum bottoming out c. 126 ka, ~~another period of frequently above-average MST occurs at c. 121–108 ka.~~ From c. 108 to 24 ka, rescaled MST generally hovers between 22 and 23.5 °C, with the exception of an inferred cooler episode ( $\sim 21.5$  °C) centered at c. 60 ka. Sustained low 745 MST values also occur from 21 to 14 ka. Thereafter, MST rises sharply ~~and the period to a mid-Holocene maximum (8.5–4.5 ka is inferred to have been marked by higher than average temperatures, occasionally reaching  $\sim 25$  °C. In )~~ followed by slightly lower values in sediments deposited during the last 4 kyr, ~~MST is mostly between 23 and 24 °C.~~

As is the case with most GDGTs, also average values of the proxies  $IR_{6Me}$ , DC,  $MBT'_{5Me}$  and rescaled MST (°C) are significantly different between samples extracted from mm-scale laminated and cm-scale banded sediments, now with cm- 750 scale banded sediments producing higher values on average (respectively 0.71, 0.30, 0.72 and 23.0; see boxplots in Figs. 5 and 7) than mm-scale laminated sediments (0.54, 0.32, 0.66 and 22.7).

#### 4.4 Periodicities in GDGT concentrations and proxies

Periodicity analysis ~~performed on selected on~~ down-core profiles of ~~selected~~ GDGT concentrations and proxies (Fig. 9; Figs. S9–S11) ~~revealed show~~ strong cyclicities likely related to orbital precession (23 kyr) and perhaps obliquity (41 kyr). ~~For~~ 755 ~~example~~ ~~However~~, periodicities of 22.2 and 44.4 kyr ~~occur~~ in the concentration of crenarchaeol, ~~which become apparent from respectively become apparent only from~~ c. 180 ka and c. 110 ka onwards, ~~respectively~~ (see wavelet analysis; Fig. 9c). The ~~absence lack~~ (or weakness) of these cycles in the older portion of the ~~erenarchaeol time series sediment record~~ is also evident in the varying amplitude of band-pass filters with those periodicities (Fig. 9b): ~~the amplitude of the precession and obliquity period filters, which~~ is very modest in ~~the oldest Stage I~~ sediments and increases ~~steadily~~ in the course of ~~lake-basin~~ 760 ~~Stages I and Stage II~~. Moreover, in the global wavelet spectrum restricted to the period 180–0 ka, the signatures of precession- and obliquity-scale cycles are enhanced compared to ~~the wavelet spectrum covering the complete time series that covering the complete record~~, and the cycle lengths shift closer to the astronomical solutions (Figs. 9d and 9e). Also the ~~time series of the BIT index and~~  $IR_{6Me}$  ~~and BIT index time series~~ display periodicities close to ~~the 23-kyr and 41-kyr cycles of precession and obliquity 23 and 41 kyr~~ (Figs. S9–S10). ~~Likewise, although Although~~ less clear as in the case of crenarchaeol, also the wavelet 765 spectra and band-pass filtered time series of these two proxies indicate weak expression of the astronomical cycles during Stage I and the first half of Stage II, becoming more pronounced when analysis is restricted to the last 180 kyr.

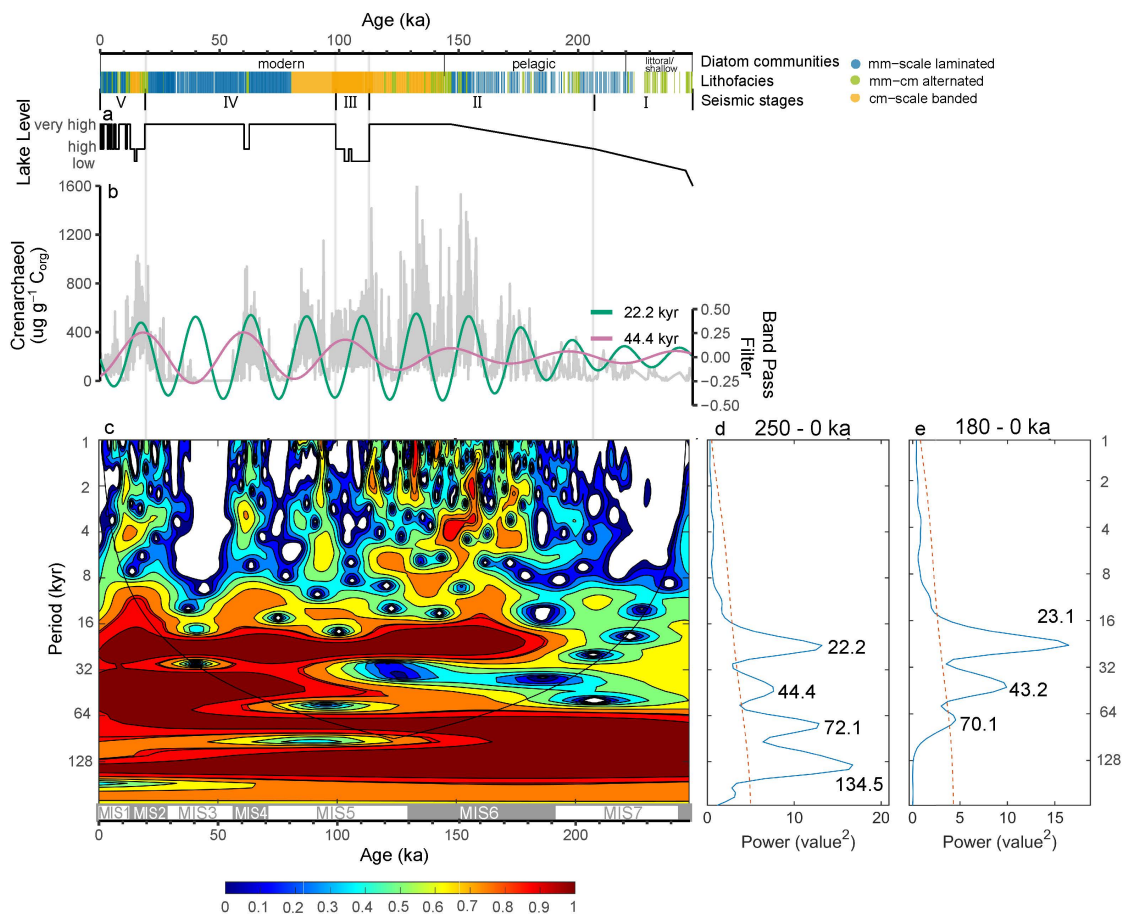


**Figure 9.** Periodicity analysis of the concentration of crenarchaeol concentration in the 250-kyr DeepCHALLA sediment sequence. Indicated from on top to bottom, are the timing of three major phases in the diatom communities lake ecology as registered in the DeepCHALLA sequence fossil diatom assemblages (Tanttu, 2021), the lithofacies category of each sediment horizon (colored bar) and the depositional stages (V-I) based on the seismic stratigraphy of Lake Chala, as well as Maitituerdi et al. (2022). Subsequent panels show (a) the lake level reconstruction based on the seismic reflection data stratigraphy (Maitituerdi et al., 2022), (b) The concentration of variation in crenarchaeol concentration in light grey with green and pink curves representing the band-pass filtered time series after band-pass filtering with periods reflected by wavelet analysis which are comparable similar to the periods those of orbital precession and obliquity, respectively, as revealed by wavelet analysis, and (c) Wavelet visual representation of wavelet analysis using a morlet function, with the corresponding (d) wavelet spectrum resulting from analysis of the full sequence DeepCHALLA sequence. Warm warm and cold colors reflect reflecting high and low values of the power spectrum. Also shown is the timing of the marine isotope stages (MIS; Lisiecki and Raymo (2005)), respectively for reference. Panels (d) and (e) Wavelet spectrum from spectral analysis summarize the wavelet spectra of crenarchaeol concentration in the sedimentary complete DeepCHALLA sequence representing (250-0 ka) and in the section 180-0 ka only, showing the to highlight more pronounced precession and obliquity cycles in the latter. The red stippled line in (d) and (e) represents the 95% confidence interval; the dominant frequencies are labelled at the top of the maxima. Also shown is the timing of the marine isotope stages (MIS) as defined by Lisiecki and Raymo (2005).



## 5 Discussion

### 5.1 Influence of lake basin evolution on GDGT niches

The low concentrations of all GDGTs during the first c. 50–70 kyr of lacustrine deposition in the Lake Chala basin (Fig. 3) ~~could suggest might be interpreted to indicate~~ poorer preservation of ~~GDGTs the aquatically produced GDGTs~~, due to longer exposure to oxygen while settling through the water column and/or in ~~the surface sediments unconsolidated surficial sediments after settling but~~ prior to permanent burial, ~~or their apparent dilution because of greater amounts of organic carbon~~. However, GDGTs are ~~found abundantly in well-oxygenated environments such as aerated soils, and are generally~~ considered to be resilient to degradation at least on the timescale of this study, ~~and found abundantly in well-oxygenated environments including aerated soils (Schouten et al., 2013). Moreover, the sedimentary~~ (Schouten et al., 2013). Alternatively, the GDGT concentrations may only appear low because of normalisation against higher  $C_{org}$  ~~content~~ values. However, the  $C_{org}$  content of Lake Chala sediments deposited during this early period is ~~comparable to that of not~~ systematically higher than in later stages (Fig. 3b). ~~Therefore, we~~ ~~We therefore~~ interpret the low concentrations of all GDGTs ~~during the first c. 50–70 kyr in this section of the record~~ (Fig. 3) to reflect ~~the prevalence of a shallower lower GDGT production, because a shallow~~ and/or ~~better mixed water column than today during Stage I and the early part of Stage II, which well-mixed and oxygenated water column~~ was less favorable to either brGDGT producers or Thaumarcheota ~~due to lack of well-developed anoxic and sub-oxic zones~~ (Fig. 10a). ~~In agreement with the low GDGT concentrations, seismic analysis also suggests that lake level was markedly lower than today~~ Seismic stratigraphy does indicate that lake depth during Stage I (c. 248–207 ka) ~~was markedly lower than today~~ (Maitituerdi et al., 2022), and also the ~~high relative abundance common occurrence~~ of benthic diatoms in ~~the~~ first c. 30 kyr of ~~the DeepCHALLA sequence confirm the lake history (Tanttu, 2021) confirms the~~ proximity of shallow-water habitat ~~(Tanttu, 2021). The to the drill site. The first meaningful rise in GDGT concentrations c. 215 ka (Fig. 3) is broadly coeval with the~~ disappearance of benthic diatomse. ~~220 ka (Tanttu, 2021) suggests that water level rose strongly from at least this period onwards, and is concurrent, indicative of a substantial increase in water depth; and~~ with the first ~~meaningful rise in GDGT concentrations. The first prolonged consistent~~ deposition of mm-scale laminated ~~sediments (varve-like) sediments around this~~ time (Fig. 3) ~~suggests, suggesting~~ that this deepening ~~of the water column also~~ promoted greater persistence of bottom water anoxia. ~~The sharp increase in GDGT concentrations at c. 210 kyr may suggest a rise in lake level, and corresponds to the boundary between Stage I and II (Maitituerdi et al., 2022), and thus of the sub-oxic and anoxic niches required by aquatic GDGT producers.~~

Besides ~~the lower-than-average GDGT concentrations before c. 200–180 ka~~, several other aspects of GDGT variability were ~~different during this early depositional phase from before c. 200–180 ka compared to~~ later on. First, ~~the GDGT concentrations concentrations of all GDGTs~~ (crenarchaeol, isoGDGT-0, minor isoGDGTs, and summed brGDGTs) ~~universally show moderate to strong positive correlations during this period (e.g., 250–~~ are positively correlated with each other (see Fig. S4 in comparison ~~to correlations during~~ 180 ka; Fig. S4), ~~contradicting our current understanding of ~ 0 ka in Fig. S6), in conflict with~~ their niche partitioning in the modern system, ~~which predicts distinct behavior of temporal trends in~~ the two groups of GDGTs associated with either the upper mixed layer ~~or the anoxic zones (respectively, (crenarchaeol and minor isoGDGTs versus-)~~

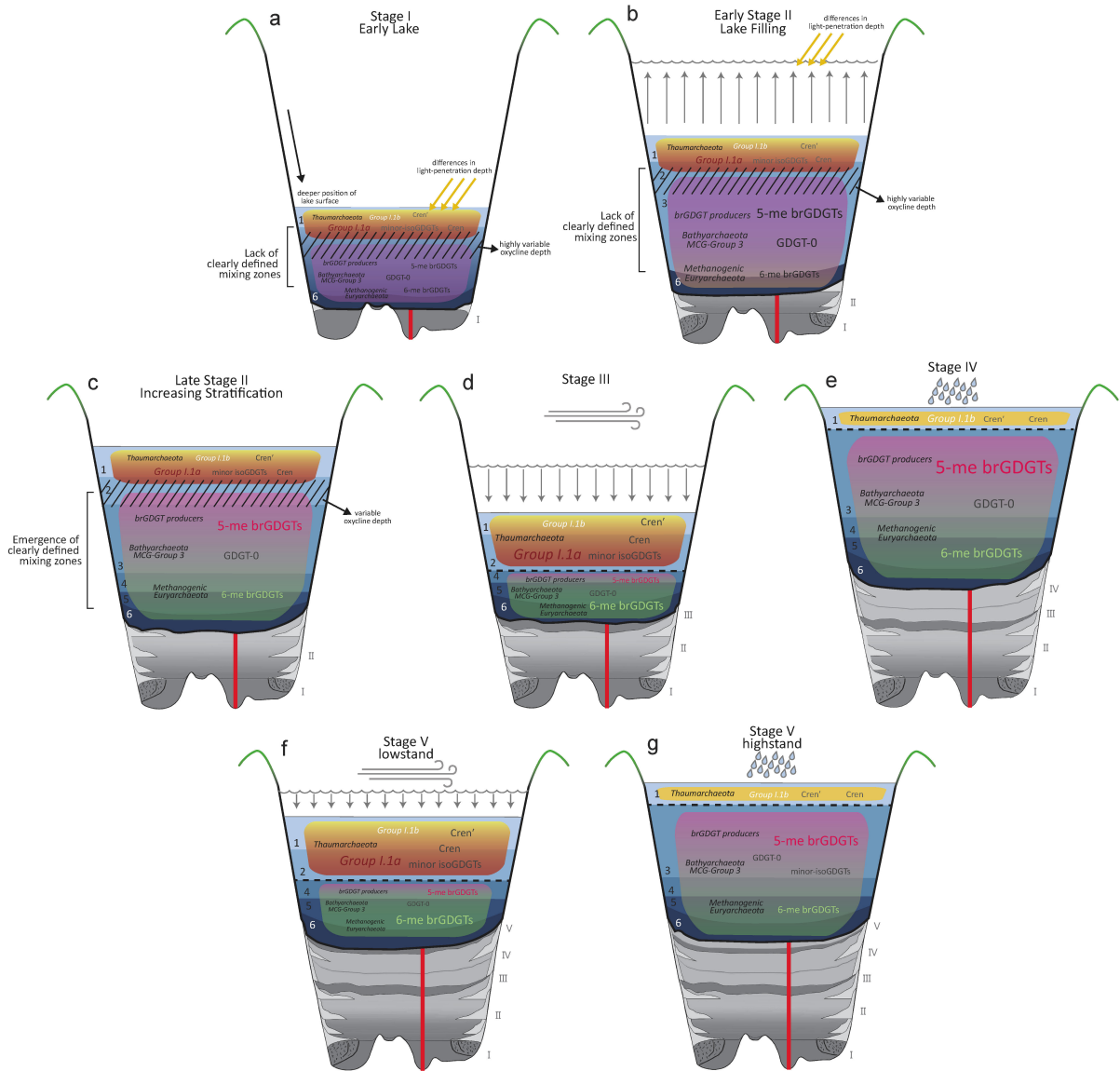


**Figure 10.** Schematic representation of ~~our current understanding~~ the ecological niches and distribution of GDGTs and their producers in the ~~development water column~~ of Lake Chala (both water column and sediment infill) during major successive stages of lake basin history over the ~~last past 250 ka-kyr.~~ based on GDGT time series in the DeepCHALLA sediment sequence (red line; this study) and inferences from SPM and settling particle and sediment trap data (Sinninghe-Damsté et al., 2009; Buckles et al., 2014; van Bree et al., 2020; Baxter et al., 2021) and seismic profiling of in the Chala basin (Maitituferdi et al., 2022) modern system (Sinninghe Damsté et al., 2009; Buckles et al., 2014; van Bree et al., 2020; Baxter et al., 2021). The ecological niches and distribution gradual infill of GDGTs and their producers are shown for the five major depositional stages. Lake bottom crater basin with sediments are shown in is based on seismic stratigraphy (Maitituferdi et al., 2022), with darker grey shading reflecting low-stand conditions.

or the anoxic zones (isoGDGT-0 and brGDGTs). Correlations among these GDGTs reflect the known associations of these biomarkers with the different water column zones (for example, isoGDGT-0 and the brGDGTs being strongly correlated to one another but not to crenarchaeol) only when they brGDGTs). Only when the GDGT time series are limited to the last c. 144 ka, i.e., the period during which kyr do correlations between these GDGTs reflect their different association with distinct water column zones in the modern lake. Notably, the last c. 144 kyr is the period for which fossil diatom assemblages attest that the water column structure (and hence, dominant mode of nutrient recycling) nutrient budgets and cycling in Lake Chalahas been comparable to, and thus presumably also its water column structure, have resembled the present-day situation. Similar temporal differences can be seen shifts occur in the correlations between the GDGT-derived GDGT-based proxies. For example, the inverse correlation between the BIT index and IR<sub>6Me</sub> improves from R = -0.31 (p < 0.001) in the section before c. 144 ka to R = -0.64 (p < 0.001) after c. 144 ka, reflecting the stronger connection between these proxies based on our understanding of GDGT niches strong connection between them based on the niches of GDGT producers identified in the modern system. Secondly, the variation in GDGT proxies associated with Also, temporal variation in some GDGT proxies influenced by water-column mixing and stratification (e.g., the BIT index, isoGDGT-0/cren) is highly erratic before c. 170 ka, while other proxies are seemingly unresponsive before c. 200 ka (e.g., and others (IR<sub>6Me</sub>, and f[CREN']) -Hence, at face value seem largely unresponsive before c. 200 ka. In summary, these proxies do not paint a cohesive history appear to provide a cohesive account of changes in lake depth and mixing regime during this period the early part of lake history. During Stage II (c. 207–113 ka), seismic stratigraphy reveals a gradual transition from predominantly ponded to draped sedimentation, indicating indicates that total water depth increased steadily, meaning that throughout this period i.e. the surface level of Lake Chala must have risen rose faster than the rate of sediment accumulation filling the basin. However, due to the near-vertically sloping crater walls this lake deepening resulted in was accompanied by only a very modest increase in lake surface area, due to the near-vertically sloping crater walls (Maitituerdi et al., 2022). Comparative morphometric analysis and water-column profiling in analysis of 60 volcanic crater lakes in western Uganda found showed that the depth of water-column mixing in these systems is most strongly related to lake surface area, not the relative height of the crater rim that might be thought to provide wind shelter (De Crop and Verschuren, 2021). This means that Therefore in Lake Chala, where lake surface area is more or less nearly constant across a large range of lake depths (Maitituerdi et al., 2022), changes in lake surface level depth alone cannot be responsible for changes in the depth of the mixed layer. In the absence of >100 m of sediments deposited later on, the lake crater basin during Stage II was substantially deeper than today, and likely the water column of Lake Chala may have attained its overall maximum height greatest height ever (>200 m) during this stage. Under such. Under these conditions, mixing of the entire water column might be expected to have been much less likely than today. However, given the thinner sediment infill at this that time, the crater bottom and lower side walls were probably still relatively side walls probably were still fairly porous, allowing greater subsurface outflow and thus removal of any the dissolved solids that might otherwise accumulate in the lower water column by decomposition of organic matter, or following the dissolution of photosynthetically precipitated calcite. This more 'leaky' nature of the crater basin would have prevented development of the endogenic chemical density gradient that might promote which promotes permanent stratification (biogenic meromixis sensu; sensu Hutchinson 1937), and thus allowed at least occasional mixing of the deeper water column at multi-annual time scales, despite great lake depth. Lacking

chemical stratification, it was more likely that under the right weather conditions (for example, exceptional strong lake-surface cooling during an extremely windy dry season episode) this deep exceptionally windy dry season, this deep but chemically dilute water column could fully turn over experience complete turnover, allowing oxygen to penetrate to the water-sediment interface. As such profundal lake bottom. Therefore, not only Stage I but also the deep early phase of Stage II were likely characterized by sporadic short-lived events of complete mixing, contrasting with the present-day lake state of situation of a permanently stratified, and permanently anoxic, lower water column. We suggest that the highly erratic behaviour of erratic variation in GDGT-based stratification proxies such as the BIT index, isoGDGT-0/erenarchaeol, cren and f[CREN'] prior to c. 170 ka may be explained by the occasional occurrence of these such deep-mixing events, with intermittent peak values indicating that episodes of multi-annual stratification did occur during this interval multi-annual episodes of stratification and deep-water anoxia did occur, but inconsistently (Fig. 5). In line with this, although the mostly support of this inference, frequent interruption of the mm-scale laminated sediments deposited during Stages II imply that bottom-water anoxia prevailed, their frequent interruption by alternated by alternating mm-cm scale lamination confirms that erratic imply that events of complete mixing did indeed occur. Most importantly, lack of chemical stratification in the deep-lake environment of during Stage II meant that meromictic conditions were maintained (at least most of the time) by the temperature gradient alone (thermogenic meromixis sensu; sensu Katsev et al. 2010), and thus that the water column of Lake Chala was not separated into the did not comprise today's six well-defined depth zones as it is today (Buckles et al. 2014; (Fig. 10a). Specifically, the equivalent to Zones 4–5 as recognized in the modern system, which presently form, which at present constitute the permanent anoxic zone and are characterized by higher conductivity have higher dissolved ion content and lower pH compared to the upper mixed layers (than the mixing Zones 1–3), most, probably did not yet exist (Fig. 10b). Hence Consequently the depth of oxygen penetration during seasonal deep-mixing events must have been highly variable as between years, because it was not restricted by a static chemocline (De Crop and Verschuren, 2021). Moreover, due to the more dilute water mass and the lower primary productivity typically associated with in addition to low biological productivity typical of deep lakes, perhaps also the average depth of visible light and UV penetration depths differed from was greater than today (Secchi disk depth seasonally varying varies seasonally between 1 and 8 m; van Bree et al. 2018; Fig. 10a–b). As Thaumarchaeota are known to be photosensitive (Merbt et al., 2012; Horak et al., 2018)) this may also have influenced their ability to grow in the upper water column and, hence, their presence and/or maximum production. Given these marked differences in the ambient aquatic environment, it therefore seems unsurprising that relationships between distributional relationships among different GDGTs and the derived proxies in this time interval do not mirror GDGT-based proxies from before c. 170 ka do not match those observed in the modern system. As the and younger sediments. As association of the different GDGTs with particular niches in the water column underpins the modern-day water column of Lake Chala underpins understanding of climate-proxy relationships, simple extrapolation of this understanding to the earliest phases of lake basin evolution is not valid history is unwarranted.

Further support for a diminished influence of climate on the GDGT proxies measured in the older sediments can be gleaned from the periodicity analysis. Namely, the apparent influence of orbital insolation forcing on certain GDGT concentrations (e.g., crenarchaeol) and proxies (i.e., crenarchaeol concentration, BIT index, e.g., BIT index and IR<sub>6Me</sub>) is strong in the younger portion of the time series but weak before c. 180 ka in the case of precession and before as recently as c. 90 ka in the

case of obliquity (Fig. 9, Figs. S9-S10). Precession is known to strongly influence ~~the monsoon system and terrestrial monsoon dynamics and~~ hydroclimate in tropical Africa, as it controls the amount and distribution of solar radiation received there (Singarayer and Burrough, 2015). Due to ~~varying variation in orbital~~ eccentricity modulating the amplitude of precessional insolation forcing ~~the strength of the~~ (Scholz et al., 2007; Blome et al., 2012), ~~the prominence of a~~ precession signature in ~~tropical~~ African climate history can be expected to vary through time (Blome et al., 2012). However the amplitude of precession was ~~markedly larger~~ larger, on average, during c. 250-180 ka (late MIS8 to early MIS6) than during the last glacial period (MIS4–MIS2) (Fig. 8d). ~~Delayed~~, arguing against this being a feasible explanation for our data. Also, delayed expression of the obliquity cycle relative to precession ~~may could~~ partly relate to the ~~growth of the~~ polar ice sheets reaching greatest extent during the last glacial period (MIS4–MIS2), enhancing as this enhanced the influence of high-latitude climate dynamics on the tropics (Tjallingii et al., 2008). ~~However, this does not~~, but this fails to explain the lack of an obliquity signature during the penultimate glacial period (MIS6). Moreover the timing of when ~~this cyclicity appeared~~ an apparent orbital period appears in the GDGT time series is not consistent among proxies and ~~in most cases began before the start of~~ most often began before MIS4 (Fig. 9, Figs. S9-S10). ~~Regardless, the absence of a strong signature of either obliquity or precession from the start of the DeepCHALLA record~~ In conclusion, lack of orbital insolation signatures in GDGT time series from the older part of the sequence confirms that climate variability was probably not the dominant mechanism driving variability in sedimentary GDGT distributions during this period, unlike during ~~the more recent lake~~ basin stages history.

Continuous Progressive accumulation of fine-grained sediments in the ~~deep crater basin of Lake Chala~~ Lake Chala basin (in total ~70 m by c. 180 ka; Maitituerdi et al. 2022; Fig. 10b) gradually diminished the leaky nature of the basin floor. ~~As a result,~~ , such that more dissolved solids were retained, ~~in turn promoting~~ the development of development of the chemical density stratification supporting that could maintain biogenic meromixis. Thus ~~the distinct~~ mixing Zones 4 and 5 probably developed during the later portion phase of Stage II (~~not shown in~~ Fig. 10b). Based on Judging from our GDGT data, ~~this first time~~ the water column of Lake Chala attained its modern-day structure of six mixing zones ~~occurred from~~ c. 180-170 ka. ~~Then around~~ onward. Nevertheless, establishment of the modern-day diatom community c. 144 ka the fossil diatom assemblages indicate ka (Tanttu, 2021) implies a dramatic change in ~~lake conditions and internal nutrient cycling~~ (Tanttu, 2021). ~~Both dominant diatom species in Lake Chala must be well-adapted to the nutrient-limited environment that is typical of deep lakes with small catchments, but as the more open-water nutrient budgets or cycling ~30 kyr later. As the~~ heavily silicified *A. barkeri* presumably requires more nutrients for population persistence than *Nitzschia* species (Tanttu, 2021), appearance establishment of the former taxon in ~~the DeepCHALLA sequence~~ Lake Chala c. 144 kyr ago testifies to improved upcycling of nutrients from the hypolimnion. Notably, the coincident Coincident transition to mainly cm-scale banded sedimentation ~~at c. 145 ka~~ (Fig. 3a) indicates that deep mixing at least must indeed have occasionally reached the lake bottom, causing modest sediment disturbance. ~~This~~ The occurrence of such events would have been promoted if ~~a trend towards an episode of~~ drier climatic conditions reduced lake depth by lowering its surface elevation level. However, as ~~clear evidence of such an event~~ evidence of lake-level lowering at this time is lacking in ~~the~~ seismic stratigraphy (Fig. 3a), ~~this facies transition may be explained solely by we surmise that both the facies transition and the improved nutrient budget may have resulted from~~ shallowing of the water column due to the progressive infilling accumulation of sediments (~100 m by that time; Maitituerdi et al. 2022). ~~Together the~~

~~The combined~~ evidence suggests that despite development of the six-zone ~~'modern'~~ ~~water column~~ ~~water column~~ structure, the ~~magnitude stability~~ of chemical stratification ~~at this time~~ was still relatively ~~modest, such low, so~~ that it could be overcome by the ~~lake surface cooling~~ ~~deep convective mixing~~ occurring during an exceptionally cool or windy ~~deep mixing season~~. ~~During Stage III, a period of strongly basin-focused sedimentation implying a dry season. Another ~30 kyr later, Stage III started with~~  
910 ~~a major drop in lake surface level (Moernaut et al., 2010; Maitituerdi et al., 2022), the reduction in lake volume due to prolonged negative water budget (indicating that water loss by lake surface evaporation exceeding the sum of markedly exceeded water inputs from catchment precipitation and sub-surface inflow) increased the overall. The consequent reduction in lake volume must have led to an overall increase in~~ dissolved-ion concentrations ~~such that the resistance of chemical stratification to, such that by the end of Stage III the resistance to deep~~ mixing approached conditions similar to today (Fig. 10c). Presumably, the  
915 transition to a more positive water ~~budget ending this low stand period c. 99 ka also acted to strengthen balance which ended Stage III also strengthened~~ chemical stratification across the Zone 3/4 boundary by adding dilute water to the ~~at least~~ annually mixed surface layer (Zones 1-3), such that by c. 80 ~~ka kyr ago~~ Lake Chala enjoyed stable meromixis, as evidenced by the almost uninterrupted deposition of mm-scale laminated sediments throughout the remainder of Stage IV. ~~Hence~~ ~~In summary,~~ the sequence of events which first created the ~~different six~~ depth zones in the water column ~~of Lake Chala~~ and then enhanced  
920 their distinctness in terms of ambient physical and chemical conditions, allowed the niches of GDGT producers to become increasingly relatable to those observed in the modern-day ~~lake system. As such, system. Consequently~~ between c. 180 ka and c. 80 ka there is ~~a progressively~~ increasing consistency between lake conditions as inferred from the ~~GDGT concentrations and indices distributions of GDGTs~~ based on modern-system understanding, and the ~~lithofacies evidence from lithostratigraphy, fossil diatom assemblages~~ and seismic reflection data which reflect the long-term history of changes in respectively water-  
925 column mixing and lake depth.

~~From~~ ~~Between~~ c. 140 ~~to and~~ c. 80 ka, a period when ~~lithostratigraphy indicates meromixis to have been predominantly cm-scale banded sediments indicate that permanent stratification (meromixis) in Lake Chala was~~ less stable than before and after, ~~there were several prolonged periods several long sections~~ of low BIT-index ~~values, low and~~ isoGDGT-0/cren ~~ratios, and values occur in combination with~~ high IR<sub>6Me</sub> values, suggesting a relatively thicker oxygenated layer (Zones 1–2) and  
930 greatly reduced or absent anoxic lower mixed layer (Zone 3). This is also indicated by lower-than-average concentrations of the anoxically produced brGDGTs and isoGDGT-0. ~~The combined evidence suggests~~ ~~These data indicate~~ that deep mixing was frequent but most often halted by the chemocline at the top of Zone 4, which in turn suggests that also total lake depth was lower during this broad period than before and after. In particular, ~~there is near-perfect agreement between~~ the longest period of consistently low BIT-index and isoGDGT-0/cren values c. 113–99 ka ~~match near-perfectly~~ with the timing of the major  
935 Stage III ~~lowstand evidenced by seismic stratigraphy low stand~~ (Fig. 5; Fig. 10d). ~~Essentially~~ ~~Concentrations of~~ all GDGTs and ~~indices derived proxies~~ point to an unprecedented change in the structure of the water column ~~of Lake Chala~~ c. 80 ~~ka, when a loss of Thaumarchaeota kyr ago, when inferred loss of Thaumarchaeota~~ and increasing absolute and relative ~~proportion proportions~~ of all GDGTs produced in anoxic waters suggest ~~persistence a rather abrupt establishment~~ of strongly stratified conditions, as also indicated by the equally abrupt ~~lithofacies transition ifrom transition from~~ cm-scale banded to mm-scale  
940 laminated sediments. The seismic record ~~shows suggests~~ that lake level was consistently high ~~during the period c. 80-25 ka~~

(the entire Stage IV; throughout Stage IV (Fig. 10e), except for a brief interlude of ponded sedimentation (i.e., an inferred lake low-stand) centered at c. 60–62 ka, also registered as a brief interruption of mm-scale laminated sedimentation (Fig. 3a). During this interval (c. 80–25), the Between c. 80 ka and 25 ka, GDGT concentrations and proxies predominantly mostly suggest an expanded anoxic zone under tall water column conditions and more limited upper water column mixing; reduced amounts of crenarchaeol and the minor isoGDGTs in comparison relative to isoGDGT-0 and the brGDGTs are reflected in the translate to mostly high BIT-index and isoGDGT/cren values and further correspond, and generally low IR<sub>6Me</sub>. Similarly to the lithofacies and seismic profiling, the These patterns in stratification-associated GDGTs and proxies responded to the brief lowstand at c. reversed during a ~10-kyr period dated to between c. 69 ka and c. 60 ka. From 24 to 14 ka the GDGT proxies (e.g., BIT index, isoGDGT-0/cren and IR<sub>6Me</sub>) are also, in agreement with the seismic and lithofacies evidence for a low-stand at c. 62 ka. Also at the end of Stage IV and after transition to Stage V, patterns in these GDGT proxies remain consistent with the seismic and lithofacies data (Fig. 5) which suggest, which indicate another period of reduced lake level and deep mixing between 24 ka and 14 ka (Fig. 10f), apparently second in amplitude only to the Stage III lowstand. However it should be noted that by that time, the additional deposition low-stand (Fig. 5). However by the onset of Stage V the additional accumulation of ~55 m of sediments had markedly reduced the magnitude of lake-level drop required to generate bottom disturbance, at a comparable position of the lake's surface level. After a period of very wet high-stand conditions between 12 ka and 9 ka indicated by the GDGTs (Fig. 10g), the ensuing period until the present is in the last 9000 years Lake Chala has been characterized by a moderately deep water column, with certain GDGT proxies (e.g., the BIT index) suggesting a somewhat fluctuating lake level. The generally wet conditions suggested by the GDGT proxies are matched by a return to but high stability of water-column stratification inferred from GDGT proxies matching the predominantly mm-scale laminated sedimentation.

## 960 5.2 Environmental control of controls on the Lake Chala IR<sub>6Me</sub> proxy in the Lake Chala record

In soils and peats (Weijers et al., 2007; Peterse et al., 2012; De Jonge et al., 2014; Xiao et al., 2015; Naafs et al., 2017a, b) strong correlations have been found occur between pH and the degree of cyclisation of brGDGTs (e.g., expressed in CBT' index), or the relative contribution of 6-Me brGDGTs (e.g., expressed in the IR<sub>6Me</sub>). By contrast, although these relationships are sometimes reported for lake. Although similar relationships have been reported in surface sediment datasets from lakes (e.g., Raberg et al. 2021; Dang et al. 2016), they are not unambiguous (e.g., Russell et al. 2018; Martínez-Sosa et al. 2021), possibly relating to the highly variable due to unaccounted variability in pH conditions with depth and season in lakes. In the DeepCHALLA sequence, it appears that the relative contribution of the 5-Me and 6-Me isomers has a strong influence on the CBT' index and that the degree-of-cyclisation index (DC) DC is not an obviously important measure for understanding variability in brGDGT distributions. Notably, whereas SPM data from Lake Chala (van Bree et al., 2020) do not clearly reveal the environmental significance of the DC and CBT' indices, clear understanding emerged of in modern-day Lake Chala, they revealed that IR<sub>6Me</sub> being a reflection of reflects variation in the spatially distinct niches of 5-Me and 6-Me brGDGT producers in the water column (see section 2.5.32.5; van Bree et al. 2020). However the ambient Notably, the pH range in their respective niches (~7.2–8 in Zone 3 and ~6.9–7.1 in Zones 4–5; Buckles et al. 2014; Baxter et al. 2021) opposes the trend found in

soils, where the 6-Me isomers dominate in high pH conditions (De Jonge et al., 2014). This ambiguity suggests that IR<sub>6Me</sub> variability-variation in the Lake Chala sediment sequence is likely related to another factor than pH.

Our mechanistic-Mechanistic understanding of the modern-system-of-Lake-Chala-modern-day Lake Chala system strongly couples variation in the BIT index and IR<sub>6Me</sub> on the seasonal-timescale-and-longer-seasonal and longer timescales with BIT-index variation. An increase in IR<sub>6Me</sub> can be linked to either enhanced mixing or a-lower-lake-level-reducing-the-extent-of-reduced lake depth shrinking Zone 3, which-is-compensated-by-an-increase-in-the-relative-proportion-compensated-by relative expansion of Zone 2 where Group I.1a Thaumarchaeota are produced, thus lowering the BIT index(see-section-2.2). The opposing trends in the-records-of these two proxies is clearly apparent in the last c. 160 kyr (R = -0.61, p < 0.001), and imply that both the BIT index and IR<sub>6Me</sub> register changes in lake-hydrology-the lake's water balance through its influence on the relative size of the different mixing zones. Although-these-two-moisture-balance-proxies-are-highly-comparable,-However, as hydrological proxies they also display important differences, such as the sharpness of recorded transitions in water-column structure. For example, during the Stage III lowstand period c. 113–99 ka(i.e., the Stage III lowstand), the-, the BIT index displays sustained low values (most often <0.2), suggesting that the strong reduction in lake depth and enhanced upper water column mixing started and ended abruptly (Fig. 5ab). The IR<sub>6Me</sub> during this period begins at relatively-low values but steadily increases, indicating-inferring a similarly dramatic -,but more gradual decrease in lake depth (Fig. 5e).-As-the-BIT-index-is controlled-by-the-g). BIT-index shifts through time may be rather abrupt because it depends on the proliferation of Thaumarchaeota, which appear highly sensitive to changes in the upper mixed layer (i.e., they either bloom or fail to bloom depending on ambient conditions) -,BIT-index shifts through time can be expected to be more abrupt (Baxter et al., 2021). By contrast, the brGDGTs on-which-the-controlling variation in IR<sub>6Me</sub> is-based are produced in the anoxic zone-of-the-lake-lower water column, which makes their abundance less sensitive to environmental changes impacting the upper water column and thus generating displaying a more paced response to gradual expansion/shrinking of the anoxic zones during phases of lake level rise or decline. The-Consequently the BIT index may thus-be more sensitive and/or respond quicker to changes-in-monsoon-strength than-the-IR<sub>6Me</sub>-climate-driven changes in lake water balance (as attested by its truthful registration of relatively modest drought events in the last 200 years: Buckles et al. 2016), although-even-though overall lake depth is likely the most important factor controlling the BIT index on long time scales. Events-Episodes when both the BIT index and IR<sub>6Me</sub> infer abrupt changes in lake depth, for example, at c. 140 ka and 80 ka, thus likely do represent drastic changes in regional-climatic moisture balance within a relatively brief period of only a few hundreds-of-years.-Also, hundred years. Additionally, under extreme shallow oxycline conditions (i.e., strong upper water-column stratification) the BIT index has a sensitivity threshold defined by the near absence of Thaumarchaeota (BIT index values approaching 1)under-extreme-shallow-oxycline-conditions, beyond which further-changes-to-inferred-wetter-elimatic-variation in inferred wet climate conditions are no longer registered (Baxter et al., 2021). In the DeepCHALLA time-series-record the BIT index is-near-approaches 1 for-a-sustained-period-dated-to-during several sustained periods between c. 80 -ka and 24 ka, largely overlapping with seismic Stage IV and suggesting persistent high lake level and extremely stratified water column conditions -(Fig. 5b). The IR<sub>6Me</sub> varies-continuously-proxy continues to vary in this section (Fig. 5g), and therefore provides valuable additional information on lake-level-changes in lake depth or water-column changes-structure during such intervals. Notably,-the-Certainly, the exact relationship between the relative-pro-



1010 portion of 5Me- and 6Me-brGDGTs and lake depth ~~documented~~ in Lake Chala is not ~~universal across all~~ likely universal across  
different lake systems. Even in the similarly meromictic Lake Lugano (Switzerland) markedly different brGDGT distributions  
with depth occur (Weber et al., 2018), ~~meaning implying~~ that comprehensive local ~~water column~~ water-column profiling of  
GDGT distributions is necessary prior to interpretation of down-core BIT index or IR<sub>6Me</sub> records.

### 5.3 Reliability of GDGT-based ~~paleotemperature~~ temperature proxies in Lake Chala

1015 Multiple lines of evidence presented above (see section ~~5.1~~ suggest 5.1) indicate that GDGT variability in the deepest, old-  
est portion of the DeepCHALLA sediment sequence is not predominantly controlled by past climate variation. ~~Therefore,~~  
~~discussion of the~~, prompting restriction of GDGT-based ~~paleotemperature proxies~~ (temperature inference (using TEX<sub>86</sub>,  
MBT'<sub>5Me</sub>, ~~MST) is conservatively constrained or MST)~~ to the last 180 kyr of the record.

#### 5.3.1 ~~TEX<sub>86</sub>-based temperature reconstruction~~

1020 ~~Previous studies~~ Previous studies (Sinninghe Damsté et al., 2012a; Buckles et al., 2013; Baxter et al., 2021) already  
showed that the TEX<sub>86</sub> index of Lake Chala sediments is highly sensitive to contributions from non-  
Thaumarchaeotal sources to the sedimentary isoGDGTs, leading to incorrect ~~palaeotemperature reconstructions~~  
~~(Sinninghe Damsté et al., 2012a; Buckles et al., 2013; Baxter et al., 2021)~~ temperature reconstruction. To distinguish be-  
tween trustworthy and ~~erroneous measurements, problematic temperature estimates, the~~ isoGDGT-0/cren, f[CREN'] ~~,~~ and  
%isoGDGT-2 ~~were applied proxies have been used~~ to detect TEX<sub>86</sub> values which are likely influenced by mixed isoGDGT  
1025 sources and therefore do not accurately reflect past temperature (Sinninghe Damsté et al., 2012a). ~~Specific to Lake Chala~~  
~~, the importance of such~~ In Lake Chala the non-Thaumarchaeotal ~~sources contribution~~ can be assessed using threshold  
values informed by GDGT distributions in multi-year SPM and settling particle data ~~and SPM profiles~~ (Baxter et al., 2021).  
Accordingly, sediment horizons ~~in the 180–0 ka section of the DeepCHALLA sequence with either BIT index~~ with either  
BIT index > 0.8, isoGDGT-0/cren > 0.7, f[CREN'] > 0.04 or %isoGDGT-2 > 45% (407 out of 798 in the 180–0 ka section,  
1030 or 51% of the total) indicate that the ~~isoGDGT pool is~~ sedimentary isoGDGTs are not largely derived from (Group I.1a)  
Thaumarchaeota and, hence, that ~~the associated~~ TEX<sub>86</sub> temperature estimates from these horizons should be rejected. ~~In~~  
~~particular,~~ The consequent rejection of the overwhelming majority of ~~sediments deposited during seismic Stage IV must~~  
~~be excluded, preventing reconstruction of past temperature measurements on Stage IV sediments prevents~~ TEX<sub>86</sub>-based  
temperature reconstruction over most of the ~~period c. 85–20 ka glacial period (MIS4 to MIS2) between c. 85 ka and 20 ka~~ (Fig.  
1035 8b). ~~With~~ Moreover, with exception of a TEX<sub>86</sub> increase from ~0.45 to 0.6 after 20 ka (translating to a warming of > 10 °C  
using the calibration of Tierney et al. 2010a), presumed trustworthy TEX<sub>86</sub> values ~~are~~ remain relatively stable at ~0.45–0.55  
throughout the last c. 180 kyr. ~~This would imply a comparable temperature regime during glacial and interglacial periods,~~  
which can be considered unrealistic as global available climate records indicate that ~~large temperature variation occurred over~~  
~~these intervals, also at low latitudes~~ (Blome et al., 2012). ~~Although the discussed thresholds offer some guidelines for omitting~~  
1040 ~~untrustworthy values, the need to exclude over~~ also low-latitude regions including tropical Africa experienced significant  
temperature variation at glacial-interglacial time scales (Blome et al., 2012; Johnson et al., 2016). Thus even though the named

thresholds provide some guidance for identifying trustworthy values, exclusion of more than half of the measured sediment horizons and apparent lack of response of the remnant time series to global temperature trends compromises the reliability of the TEX<sub>86</sub> index as paleothermometer in Lake Chala.

### 1045 **5.3.1 BrGDGT-based temperature reconstruction**

Variation in the MBT'<sub>5Me</sub> index throughout the 180-0 ka section of the DeepCHALLA sequence ~~infers~~ implies a temporal pattern of temperature change which is likewise incompatible with global temperature ~~variations reflected in the marine benthic foraminiferal oxygen isotope stack (Lisiecki and Raymo, 2005) or with variations in atmospheric CO<sub>2</sub> concentration as principal greenhouse-gas forcing (Petit et al., 1999)~~ variation at glacial-interglacial time scales. For example, ~~although while~~ MBT'<sub>5Me</sub> correctly ~~infers~~ estimates regional temperature to have been ~~higher than average above-average~~ during the last interglacial period (MIS5), ~~the it shows no clear~~ pattern of alternating warmer and cooler ~~isotope substages MIS5a-conditions during interstadials MIS5e, with highest temperatures recorded during MIS5e, is not clear. Moreover, -MIS5a. Also~~ the inferred coldest interval ~~during the of the~~ last glacial cycle is ~~inferred-reconstructed~~ to have occurred around 50 ka ~~near the MIS3-MIS2 transition within MIS3, rather than around-during~~ the Last Glacial Maximum (~~in MIS2; Baxter et al. 2023~~). ~~The abrupt-~~ Notably the abrupt shifts increase and decrease in MBT'<sub>5Me</sub> at respectively c. 140 ka and c. 80 ka occur simultaneously with major hydrological changes in Lake Chala as recorded by the BIT index and IR<sub>6Me</sub> (Figs. 5 and 8). This suggests ~~that the a strong~~ imprint of climate-driven hydrological ~~changes in Lake Chala change~~ on MBT'<sub>5Me</sub> ~~is strong~~, and reason to disqualify its use for temperature reconstruction at this site. Periodicity analysis of MBT'<sub>5Me</sub> over the last 180 kyr does reveal ~~periodicities-cycles~~ of 24.8 kyr and 37.6 kyr ~~, which may be linked to variation in solar insolation due to orbital~~ potentially reflecting response to insolation variation due to precession and obliquity, ~~although only the obliquity-related periodicity can be considered-but only the obliquity-band signal is~~ significant using the 95% confidence interval. ~~As similar periodicities~~ However, as similar cyclicities occur in the hydrological proxies (~~i.e., concentration of~~ crenarchaeol, BIT index and IR<sub>6Me</sub> ; (Fig. 9, Figs. S9-S10), and as especially precession ~~has a strong influence on~~ strongly influences tropical monsoon dynamics, this does not suffice to ~~support its applicability as temperature proxy for use~~ MBT'<sub>5Me</sub> as paleotemperature proxy at Lake Chala.

Recent ~~paleoclimate studies in African lakes~~ GDGT-based climate studies on African lake records (e.g., Bittner et al. 2022) ~~, including Lake Chala (Baxter et al., 2023) indicate that (some)~~ indicate that in order to achieve more consistent temperature reconstructions 6-Me brGDGTs should be included in the calibration of brGDGT-based temperature proxies ~~in order to achieve more consistent temperature reconstructions. Application in DeepCHALLA of an earlier~~ Baxter et al. (2023). Application of the global lake calibration by Pearson et al. (2011), which estimates MST mean summer temperature (MST) based on the combined abundance of 5-Me and 6-Me brGDGTs (~~Pearson et al., 2011~~), ~~results in-~~ to the DeepCHALLA sequence produces a temperature reconstruction ~~that displays~~ displaying peak temperatures of 25 °C ~~being~~ reached during the current interglacial period (the ~~last 11.7 ka~~ Holocene) and between c. 140 and c. 130 ka, ~~which~~ likely (i.e., ~~taking into consideration the chronological uncertainty~~) representing the globally-accounting for chronological uncertainty in the present age model represents MIS5e, ~~the known~~ warmest episode of the last interglacial period (~~MIS5e~~) (Fig. 8e). Conversely, ~~inferred~~ cool episodes centered at c.

150 ka, c. 60 ka and 15 ka correspond to known periods of ~~extreme-extensive high-latitude~~ glaciation during the penultimate ~~ice age~~ (MIS6) and ~~last glacial periods~~ ~~the last glacial period~~ (MIS4 and MIS2). Importantly, the MST time series does not ~~include-show~~ large shifts at c. 140 and c. 80 ka ~~in-conjunction-with-those-of-together-with-those-in~~ the BIT index and IR<sub>6Me</sub>, ~~suggesting-indicating~~ that this temperature proxy is not affected by reorganization of water column structure related to changes in lake depth, and thus likely ~~is-a~~ more trustworthy tracer of changes in ~~regional-air-temperature-local air temperature than MBT'~~<sub>5Me</sub>. The MST ~~record-time series~~ also does not display clear changes ~~coincident-with-the-sequence-of-associated-with~~ low BIT-index and isoGDGT-0/cren values during the ~~severe-Stage-III-lowstand, further-Stage III low-stand~~, supporting the notion that the GDGT drivers of the MST proxy ~~function-independently-from-vary independently from changes in~~ lake mixing. ~~Therefore, it appears fair to-We therefore~~ suggest that the MST time series covering the last 180 ka of the DeepCHALLA sequence may constitute a reliable record of past ~~regional-temperature-variation-temperature variation in the Lake Chala region~~ covering almost two glacial-interglacial cycles. This suggestion appears to be supported by clear periodicities of 23.0 kyr and 40.1 kyr in this data over the last 160 kyr, presumably reflecting the influences of orbital precession and obliquity on tropical African paleoclimate (Fig. S11e).

## 6 Conclusions

1090 Analysis of iso- and brGDGTs in the 250-kyr DeepCHALLA sediment sequence from Lake Chala shows that the first c. 70 kyr of sedimentation are characterized by relatively low GDGT concentrations, and erratic variation in the BIT index and isoGDGT-0/cren ratio, suggesting a poorly stratified water column with highly unstable oxycline position. Comparison with independent measures of lake-basin evolution ~~, lake-mixing-and-chemistry indicates that the structure of the water column indicates that~~ water column structure during this early period was dissimilar to the present-day situation, because the lake had a leaky hydrology which prevented the accumulation of dissolved solids, thereby hampering chemical stratification and the formation of distinct mixing zones. Hence the differentiated niches of various GDGT producers as occurring in the water column today were not yet established, resulting in GDGT proxy values that ~~are-were~~ not predominantly controlled by climate variability. In line with this, time series of crenarchaeol concentration, the BIT index and IR<sub>6Me</sub> only start to display periodicities reflecting orbital ~~insolaion-insolation~~ forcing of the ~~local-region's~~ climate from c. 180 ka onwards, suggesting that ~~from-around-from~~ around this time climate rather than lake basin evolution exerted the primary control on niches of GDGT producers and hence GDGT-derived proxies in the lake. The connection between GDGT proxies and ~~regional-climate~~ as understood on the basis of modern-system studies ~~gradually~~ solidified between c. 180 ka and c. 80 ka as the lake gradually developed the strong chemical gradient in the lower water column characterising modern-day conditions, permitting increasingly more trustworthy quantitative inferences of past climate ~~regimes-variability~~ during those more recent periods.

1105 The IR<sub>6Me</sub>, which captures the relative proportion of 6Me-brGDGTs and 5Me-brGDGTs, is in Lake Chala related to past changes in lake depth ~~,as-this-alters-altering~~ the relative size of the distinct niches ~~were-where~~ these lipids are most abundantly produced. Hence ~~,it-could-IR<sub>6Me</sub>-can~~ be an important method-proxy for investigating past changes in ~~regional-climatic~~ moisture balance changes in this system, alongside the BIT index. Detailed consideration of ~~available-alternative~~ GDGT-based

paleothermometers resulted in rejection of the  $\text{TEX}_{86}$  temperature proxy, as previously set filtering criteria (Baxter et al., 2021) indicate that ~~51% half~~ of the sediment horizons younger than c. 180 ka ~~likely contain large contributions~~ contain a significant fraction of non-Thaumarchaeotal isoGDGTs. In particular, the strong influence of upper water-column mixing on Thaumarchaeota niche space casts doubt on the application of this temperature proxy in Lake Chala, and likely also other (tropical) lakes experiencing shallow oxycline conditions. The  $\text{MBT}'_{5\text{Me}}$  index, ~~which is~~ commonly assumed to best capture the temperature dependence of brGDGTs (Russell et al., 2018; Martínez-Sosa et al., 2021), results in a reconstruction that lacks a clear glacial-interglacial pattern and shows evidence for an overprint of lake mixing influences. ~~Following research that shows~~ Consistent with indications of the importance of ~~including~~ 6-Me brGDGTs in temperature proxies applied to Lake Chala (Baxter et al., 2023), we find that MST reconstruction using the global lake calibration of Pearson et al. (2011) ~~is found to display~~ displays a strong and temporally feasible alternation between ~~glacial and interglacial periods and major stadials~~ inferred warm and cool episodes over the last glacial-interglacial cycle, and contains clear periodicities related to the long-term variation in solar insolation due to orbital precession and obliquity.

Importantly, the types of chemical and physical changes that characterize ~~the~~ lake-system evolution ~~of~~ at Lake Chala are not altogether unique, and similar processes are certainly involved in the history of most lake basins. To date these potential confounding factors are generally not considered when interpreting biomarker-based climate records from lakes. This work shows the necessity of applying a comprehensive approach which incorporates lake-basin information when interpreting down-core trends in sedimentary GDGT proxies to reconstruct past climate history, in particular when ~~using biomarkers, like GDGTs~~ involving GDGTs that are produced *in situ* in the water column or sediments. Based on our findings, particular caution is recommended when interpreting proxy records that extend to the initial filling stage of lakes or include episodes when lake-system functioning and sedimentation were clearly different from today, regardless of the apparent continuity of lacustrine deposition.

1130 *Data availability.* Data from this manuscript will be made available online upon publication.

*Author contributions.* Project administration was done by DV. Project conceptualization was done by DV, JSSD, FP and AJB. Funding acquisition, data curation and resource procurement were done by DV and JSSD. FP, DV, JSSD and NW were responsible for supervision. Investigation was performed by AJB and AM. Formal analysis, visualization and writing of the original draft was done by AJB. All authors reviewed and edited the manuscript.

1135 *Competing interests.* The author has declared that there are no competing interests.

*Disclaimer.* Publisher's note: Copernicus Publications remains neutral with regard to jurisdictional claims in published maps and institutional affiliations.

*Acknowledgements.* This research was co-financed by NESSC Gravitation Grant 024.002.001 from the Dutch Ministry of Education, Culture and Science (OCW) to JSSD; by Ghent University Collaborative Research Operation grant BOF13/GOA/023, BRAIN-be ~~project grant~~ BR-1140 121-A2 from the Belgian Science Policy Office (BelSPO), Hercules infrastructure grant AUGÉ/15/14-G0H2916N from the Research Foundation of Flanders, and a Francqui research professor mandate to DV; and by ~~ICDP~~ the International Continental Scientific Drilling Program through the DeepCHALLA project (<https://www.icdp-online.org/projects/world/africa/lake-challa/>). Recovery of the Lake Chala sediment record was facilitated by the government of Kenya through permit P/16/7890/10400 from the National Commission for Science, Technology and Innovation (NACOSTI), license EIA/PSL/3851 from the National Environmental Management Authority (NEMA), and research passes 1145 for foreign nationals issued by the Department of Immigration; and by the government of Tanzania through permits NA-2016-67 (270-285) and NA-2016-201 (277-292) from the Tanzania Commission for Science and Technology (COSTECH), permit EIA/10/0143/V.I/04 from the National Environmental Management Council, and resident permits issued by the Immigration Department. The lake-drilling operation was subject to environmental impact assessments conducted by Kamfor (Nairobi, Kenya) and Tansheq (Dar es Salaam, Tanzania), and permission from the Lands and Settlement Office of Taita-Taveta County (Kenya) to use government land as staging area.

1150 The authors ~~especially~~ wish to thank ~~our DeepCHALLA partners and the institutions of their affiliation~~ DeepCHALLA partners in Kenya and Tanzania for project facilitation; ~~Caxton Mukhwana~~ C. M. Oluseno, the 'Air Force One' team, the Kamba and Taveta communities of Lake Chala area (villages of Challa, Kasokoni, Kidong and Nakuruto), and the DeepCHALLA team of field scientists for assistance in recovering the complete sediment record of Lake Chala; and the National Lacustrine Core Facility (LacCore) at the University of Minnesota (USA) for organizing the splitting, logging and initial processing of core samples. We are further grateful to F. Hilgen for assistance with 1155 periodicity analysis-, and to C. De Jonge and two anonymous reviewers whose feedback has substantially improved this manuscript.

## References

- Bale, N. J., Palatinszky, M., Rijpstra, W. I. C., Herbold, C. W., Wagner, M., and Damsté, J. S.: Membrane lipid composition of the moderately thermophilic ammonia-oxidizing archaeon "Candidatus Nitrosotenuis uzonensis" at different growth temperatures, *Applied and Environmental Microbiology*, 85, <https://doi.org/10.1128/AEM.01332-19>, 2019.
- 1160 Barker, P. A., Hurrell, E. R., Leng, M. J., Wolff, C., Cocquyt, C., Sloane, H. J., and Verschuren, D.: Seasonality in equatorial climate over the past 25 k.y. Revealed by oxygen isotope records from Kilimanjaro, *Geology*, 39, <https://doi.org/10.1130/G32419.1>, 2011a.
- Barker, P. A., Hurrell, E. R., Leng, M. J., Plessen, B., Wolff, C., Conley, D. J., Keppens, E., Milne, I., Cumming, B. F., Laird, K. R., Kendrick, C. P., Wynn, P. M., and Verschuren, D.: Carbon cycling within an East African lake revealed by the carbon isotope composition of diatom silica: A 25-ka record from Lake Challa, Mt. Kilimanjaro, *Quaternary Science Reviews*, 66, <https://doi.org/10.1016/j.quascirev.2012.07.016>, 2013.
- 1165 Barker, S., Knorr, G., Edwards, R. L., Parrenin, F., Putnam, A. E., Skinner, L. C., Wolff, E., and Ziegler, M.: 800,000 Years of abrupt climate variability, *Science*, 334, <https://doi.org/10.1126/science.1203580>, 2011b.
- Baxter, A. J., Hopmans, E. C., Russell, J. M., and Damsté, J. S. S.: Bacterial GMGTs in East African lake sediments: Their potential as palaeotemperature indicators, *Geochimica et Cosmochimica Acta*, 259, 155–169, <https://doi.org/10.1016/j.gca.2019.05.039>, 2019.
- 1170 Baxter, A. J., van Bree, L., Peterse, F., Hopmans, E. C., Villanueva, L., Verschuren, D., and Sinninghe Damsté, J. S.: Seasonal and multi-annual variation in the abundance of isoprenoid GDGT membrane lipids and their producers in the water column of a meromictic equatorial crater lake (Lake Chala, East Africa), *Quaternary Science Reviews*, 273, <https://doi.org/10.1016/j.quascirev.2021.107263>, 2021.
- Baxter, A. J., Verschuren, D., Peterse, F., Miralles, D. G., Martin-Jones, C. M., Maitituerdi, A., Van der Meeren, T., Van Daele, M., Lane, C. S., Haug, G. H., Olago, D. O., and Sinninghe Damsté, J. S.: Reversed Holocene temperature–moisture relationship in the Horn of Africa, *Nature*, 620, 336–343, <https://doi.org/10.1038/s41586-023-06272-5>, 2023.
- 1175 Bechtel, A., Smittenberg, R. H., Bernasconi, S. M., and Schubert, C. J.: Distribution of branched and isoprenoid tetraether lipids in an oligotrophic and a eutrophic Swiss lake: Insights into sources and GDGT-based proxies, *Organic Geochemistry*, 41, <https://doi.org/10.1016/j.orggeochem.2010.04.022>, 2010.
- Bittner, L., De Jonge, C., Gil-Romera, G., Lamb, H. F., Russell, J. M., and Zech, M.: A Holocene temperature (brGDGT) record from Garba Guracha, a high-altitude lake in Ethiopia, *Biogeosciences*, 19, <https://doi.org/10.5194/bg-19-5357-2022>, 2022.
- 1180 Blaauw, M. and Christen, J. A.: Flexible paleoclimate age-depth models using an autoregressive gamma process, *Bayesian Analysis*, 6, <https://doi.org/10.1214/11-BA618>, 2011.
- Blaga, C. I., Reichart, G. J., Heiri, O., and Damsté, J. S. S.: Tetraether membrane lipid distributions in water-column particulate matter and sediments: A study of 47 European lakes along a north-south transect, *Journal of Paleolimnology*, 41, <https://doi.org/10.1007/s10933-008-9242-2>, 2009.
- 1185 Blaga, C. I., Reichart, G. J., Lotter, A. F., Anselmetti, F. S., and Damsté, J. S. S.: A TEX<sub>86</sub> lake record suggests simultaneous shifts in temperature in Central Europe and Greenland during the last deglaciation, *Geophysical Research Letters*, 40, <https://doi.org/10.1002/grl.50181>, 2013.
- Blome, M. W., Cohen, A. S., Tryon, C. A., Brooks, A. S., and Russell, J.: The environmental context for the origins of modern human diversity: A synthesis of regional variability in African climate 150,000-30,000 years ago, *Journal of Human Evolution*, 62, 563–592, <https://doi.org/10.1016/j.jhevol.2012.01.011>, 2012.
- 1190

- Bodé, S., De Wispelaere, L., Hemp, A., Verschuren, D., and Boeckx, P.: Water-isotope ecohydrology of Mount Kilimanjaro, *Ecohydrology*, 13, <https://doi.org/10.1002/eco.2171>, 2020.
- 1195 van Bree, L. G., Peterse, F., Baxter, A. J., De Crop, W., Van Grinsven, S., Villanueva, L., Verschuren, D., and Damsté, J. S. S.: Seasonal variability and sources of in situ brGDGT production in a permanently stratified African crater lake, *Biogeosciences*, 17, <https://doi.org/10.5194/bg-17-5443-2020>, 2020.
- 1200 van Bree, L. G., Peterse, F., van der Meer, M. T., Middelburg, J. J., Negash, A. M., Crop, W. D., Cocquyt, C., Wieringa, J. J., Verschuren, D., and Sinninghe Damsté, J. S.: Seasonal variability in the abundance and stable carbon-isotopic composition of lipid biomarkers in suspended particulate matter from a stratified equatorial lake (Lake Chala, Kenya/Tanzania): Implications for the sedimentary record, *Quaternary Science Reviews*, <https://doi.org/10.1016/j.quascirev.2018.05.023>, 2018.
- Buckles, L. K., Villanueva, L., Weijers, J. W., Verschuren, D., and Damsté, J. S.: Linking isoprenoidal GDGT membrane lipid distributions with gene abundances of ammonia-oxidizing Thaumarchaeota and uncultured crenarchaeotal groups in the water column of a tropical lake (Lake Challa, East Africa), *Environmental Microbiology*, 15, 2445–2462, <https://doi.org/10.1111/1462-2920.12118>, 2013.
- 1205 Buckles, L. K., Weijers, J. W. H., Verschuren, D., and Damsté, J. S. S.: Sources of core and intact branched tetraether membrane lipids in the lacustrine environment: Anatomy of Lake Challa and its catchment, equatorial East Africa, *Geochimica et Cosmochimica Acta*, <https://doi.org/10.1016/j.gca.2014.04.042>, 2014.
- Buckles, L. K., Verschuren, D., Weijers, J. W., Cocquyt, C., Blaauw, M., and Damsté, J. S.: Interannual and (multi-)decadal variability in the sedimentary BIT index of Lake Challa, East Africa, over the past 2200 years: Assessment of the precipitation proxy, *Climate of the Past*, 12, 1243–1262, <https://doi.org/10.5194/cp-12-1243-2016>, 2016.
- 1210 Cao, M., Rivas-Ruiz, P., del Carmen Trapote, M., Vegas-Vilarrúbia, T., Rull, V., and Rosell-Melé, A.: Seasonal effects of water temperature and dissolved oxygen on the isoGDGT proxy (TEX<sub>86</sub>) in a Mediterranean oligotrophic lake, *Chemical Geology*, 551, <https://doi.org/10.1016/j.chemgeo.2020.119759>, 2020.
- 1215 Chen, Y., Zheng, F., Yang, H., Yang, W., Wu, R., Liu, X., Liang, H., Chen, H., Pei, H., Zhang, C., Pancost, R. D., and Zeng, Z.: The production of diverse brGDGTs by an Acidobacterium providing a physiological basis for paleoclimate proxies, *Geochimica et Cosmochimica Acta*, 337, 155–165, 2022.
- Cheng, H., Edwards, R. L., Sinha, A., Spötl, C., Yi, L., Chen, S., Kelly, M., Kathayat, G., Wang, X., Li, X., Kong, X., Wang, Y., Ning, Y., and Zhang, H.: The Asian monsoon over the past 640,000 years and ice age terminations, *Nature*, 534, <https://doi.org/10.1038/nature18591>, 2016.
- Cohen, A. S.: *Paleolimnology: the history and evolution of lake systems*, Oxford university press, 2003.
- 1220 Cohen, A. S., Stone, J. R., Beuning, K. R. M., Park, L. E., Reinthal, P. N., Dettman, D., Scholz, C. A., Johnson, T. C., King, J. W., Talbot, M. R., Brown, E. T., and Ivory, S. J.: Ecological consequences of early Late Pleistocene megadroughts in tropical Africa, *Proceedings of the National Academy of Sciences*, <https://doi.org/10.1073/pnas.0703873104>, 2007.
- Dang, X., Yang, H., Naafs, B. D. A., Pancost, R. D., and Xie, S.: Evidence of moisture control on the methylation of branched glycerol dialkyl glycerol tetraethers in semi-arid and arid soils, *Geochimica et Cosmochimica Acta*, 189, <https://doi.org/10.1016/j.gca.2016.06.004>, 2016.
- 1225 De Crop, W. and Verschuren, D.: Determining patterns of stratification and mixing in tropical crater lakes through intermittent water-column profiling: A case study in western Uganda, *Journal of African Earth Sciences*, 153, <https://doi.org/10.1016/j.jafrearsci.2019.02.019>, 2019.
- De Crop, W. and Verschuren, D.: Mixing regimes in the equatorial crater lakes of western Uganda, *Limnologia*, 90, <https://doi.org/10.1016/j.limno.2021.125891>, 2021.

- De Jonge, C., Hopmans, E. C., Stadnitskaia, A., Rijpstra, W. I. C., Hofland, R., Tegelaar, E., and Damsté, J. S. S.: Identification of novel  
1230 penta- and hexamethylated branched glycerol dialkyl glycerol tetraethers in peat using HPLC-MS2, GC-MS and GC-SMB-MS, *Organic Geochemistry*, <https://doi.org/10.1016/j.orggeochem.2012.10.004>, 2013.
- De Jonge, C., Hopmans, E. C., Zell, C. I., Kim, J. H., Schouten, S., and Damsté, J. S. S.: Occurrence and abundance of 6-methyl  
branched glycerol dialkyl glycerol tetraethers in soils: Implications for palaeoclimate reconstruction, *Geochimica et Cosmochimica Acta*,  
<https://doi.org/10.1016/j.gca.2014.06.013>, 2014.
- 1235 De Jonge, C., Stadnitskaia, A., Hopmans, E. C., Cherkashov, G., Fedotov, A., Streletskaia, I. D., Vasiliev, A. A., and Damsté, J. S. S.:  
Drastic changes in the distribution of branched tetraether lipids in suspended matter and sediments from the Yenisei River and Kara  
Sea (Siberia): Implications for the use of brGDGT-based proxies in coastal marine sediments, *Geochimica et Cosmochimica Acta*, 165,  
<https://doi.org/10.1016/j.gca.2015.05.044>, 2015.
- De Jonge, C., Radujković, D., Sigurdsson, B. D., Weedon, J. T., Janssens, I., and Peterse, F.: Lipid biomarker temperature proxy  
1240 responds to abrupt shift in the bacterial community composition in geothermally heated soils, *Organic Geochemistry*, 137,  
<https://doi.org/10.1016/j.orggeochem.2019.07.006>, 2019.
- De Rosa, M. and Gambacorta, A.: The lipids of archaeobacteria, *Progress in Lipid Research*, 27, [https://doi.org/10.1016/0163-7827\(88\)90011-2](https://doi.org/10.1016/0163-7827(88)90011-2), 1988.
- De Wispelaere, L., Bodé, S., Hervé-Fernández, P., Hemp, A., Verschuren, D., and Boeckx, P.: Plant water resource partitioning and isotopic  
1245 fractionation during transpiration in a seasonally dry tropical climate, *Biogeosciences*, 14, <https://doi.org/10.5194/bg-14-73-2017>, 2017.
- Elling, F. J., Könneke, M., Nicol, G. W., Stieglmeier, M., Bayer, B., Spieck, E., de la Torre, J. R., Becker, K. W., Thomm, M., Prosser,  
J. I., Herndl, G. J., Schleper, C., and Hinrichs, K. U.: Chemotaxonomic characterisation of the thaumarchaeal lipidome, *Environmental  
Microbiology*, 19, <https://doi.org/10.1111/1462-2920.13759>, 2017.
- Feakins, S. J., Wu, M. S., Ponton, C., and Tierney, J. E.: Biomarkers reveal abrupt switches in hydroclimate during the last glacial in southern  
1250 California, *Earth and Planetary Science Letters*, 515, <https://doi.org/10.1016/j.epsl.2019.03.024>, 2019.
- Garelick, S., Russell, J. M., Dee, S., Verschuren, D., and Olago, D. O.: Atmospheric controls on precipitation isotopes and hydro-  
climate in high-elevation regions in Eastern Africa since the Last Glacial Maximum, *Earth and Planetary Science Letters*, 567,  
<https://doi.org/10.1016/j.epsl.2021.116984>, 2021.
- Griepentrog, M., De Wispelaere, L., Bauters, M., Bodé, S., Hemp, A., Verschuren, D., and Boeckx, P.: Influence of plant growth form,  
1255 habitat and season on leaf-wax n-alkane hydrogen-isotopic signatures in equatorial East Africa, *Geochimica et Cosmochimica Acta*, 263,  
<https://doi.org/10.1016/j.gca.2019.08.004>, 2019.
- Halamka, T. A., Raberg, J. H., McFarlin, J. M., Younkin, A. D., Mulligan, C., Liu, X. L., and Kopf, S. H.: Production of diverse brGDGTs  
by *Acidobacterium Solibacter usitatus* in response to temperature, pH, and O<sub>2</sub> provides a culturing perspective on brGDGT proxies and  
biosynthesis, *Geobiology*, 21, <https://doi.org/10.1111/gbi.12525>, 2023.
- 1260 Hemp, A.: Continuum or zonation? Altitudinal gradients in the forest vegetation of Mt. Kilimanjaro, *Plant Ecology*, 184,  
<https://doi.org/10.1007/s11258-005-9049-4>, 2006.
- Holzheimer, M., Damsté, J. S. S., Schouten, S., Havenith, R. W., Cunha, A. V., and Minnaard, A. J.: Total Synthesis of the Alleged Structure  
of Crenarchaeol Enables Structure Revision, *Angewandte Chemie - International Edition*, 60, <https://doi.org/10.1002/anie.202105384>,  
2021.



- 1265 Hopmans, E. C., Weijers, J. W., Schefuß, E., Herfort, L., Damsté, J. S. S., and Schouten, S.: A novel proxy for terrestrial organic matter in sediments based on branched and isoprenoid tetraether lipids, *Earth and Planetary Science Letters*, 224, 107–116, <https://doi.org/10.1016/j.epsl.2004.05.012>, 2004.
- Hopmans, E. C., Schouten, S., and Damsté, J. S. S.: The effect of improved chromatography on GDGT-based palaeoproxies, *Organic Geochemistry*, <https://doi.org/10.1016/j.orggeochem.2015.12.006>, 2016.
- 1270 Horak, R. E., Qin, W., Bertagnolli, A. D., Nelson, A., Heal, K. R., Han, H., Heller, M., Schauer, A. J., Jeffrey, W. H., Armbrust, E. V., Moffett, J. W., Ingalls, A. E., Stahl, D. A., and Devol, A. H.: Relative impacts of light, temperature, and reactive oxygen on thaumarchaeal ammonia oxidation in the North Pacific Ocean, *Limnology and Oceanography*, 63, <https://doi.org/10.1002/lno.10665>, 2018.
- Huguet, C., Hopmans, E. C., Febo-Ayala, W., Thompson, D. H., Damsté, J. S. S., and Schouten, S.: An improved method to determine the absolute abundance of glycerol dibiphytanyl glycerol tetraether lipids, <https://doi.org/10.1016/j.orggeochem.2006.05.008>, 2006.
- 1275 Hutchinson, G. E.: A Contribution to the Limnology of Arid Regions, *Transactions of the Connecticut Academy of Arts and Sciences*, 33, 47–132, 1937.
- Håkanson, L. and Jansson, M.: Principles of Lake Sedimentology, <https://doi.org/10.1007/978-3-642-69274-1>, 1983.
- Johnson, T. C., Werne, J. P., Brown, E. T., Abbott, A., Berke, M., Steinman, B. A., Halbur, J., Contreras, S., Grosshuesch, S., Deino, A., Scholz, C. A., Lyons, R. P., Schouten, S., and Damsté, J. S. S.: A progressively wetter climate in southern East Africa over the past 1.3 million years, *Nature*, <https://doi.org/10.1038/nature19065>, 2016.
- 1280 Jones, R. N., McMahon, T. A., and Bowler, J. M.: Modelling historical lake levels and recent climate change at three closed lakes, Western Victoria, Australia (c.1840-1990), *Journal of Hydrology*, 246, [https://doi.org/10.1016/S0022-1694\(01\)00369-9](https://doi.org/10.1016/S0022-1694(01)00369-9), 2001.
- Katsev, S., Crowe, S. A., Mucci, A., Sundby, B., Nomosatryo, S., Douglas Haffner, G., and Fowle, D. A.: Mixing and its effects on biogeochemistry in the persistently stratified, deep, tropical Lake Matano, Indonesia, *Limnology and Oceanography*, 55, 763–776, 2010.
- 1285 Kim, J. G., Jung, M. Y., Park, S. J., Rijpstra, W. I. C., Damsté, J. S. S., Madsen, E. L., Min, D., Kim, J. S., Kim, G. J., and Rhee, S. K.: Cultivation of a highly enriched ammonia-oxidizing archaeon of thaumarchaeotal group I.1b from an agricultural soil, *Environmental Microbiology*, 14, <https://doi.org/10.1111/j.1462-2920.2012.02740.x>, 2012.
- Kim, J. H., van der Meer, J., Schouten, S., Helmke, P., Willmott, V., Sangiorgi, F., Koç, N., Hopmans, E. C., and Damsté, J. S. S.: New indices and calibrations derived from the distribution of crenarchaeal isoprenoid tetraether lipids: Implications for past sea surface temperature reconstructions, *Geochimica et Cosmochimica Acta*, 74, 4639–4654, <https://doi.org/10.1016/j.gca.2010.05.027>, 2010.
- 1290 Lewis, W. M.: A Revised Classification of Lakes Based on Mixing, *Canadian Journal of Fisheries and Aquatic Sciences*, 40, <https://doi.org/10.1139/f83-207>, 1983.
- Lewis, W. M.: Tropical limnology, *Annual review of ecology and systematics*, 18, <https://doi.org/10.1146/annurev.es.18.110187.001111>, 1987.
- 1295 Li, M., Hinnov, L., and Kump, L.: Acycle: Time-series analysis software for paleoclimate research and education, *Computers and Geosciences*, 127, <https://doi.org/10.1016/j.cageo.2019.02.011>, 2019.
- Lisiecki, L. E. and Raymo, M. E.: A Pliocene-Pleistocene stack of 57 globally distributed benthic  $\delta^{18}\text{O}$  records, *Paleoceanography*, 20, <https://doi.org/10.1029/2004PA001071>, 2005.
- Loomis, S. E., Russell, J. M., Ladd, B., Street-Perrott, F. A., and Damsté, J. S. S.: Calibration and application of the branched GDGT temperature proxy on East African lake sediments, *Earth and Planetary Science Letters*, 357-358, 277–288, <https://doi.org/10.1016/j.epsl.2012.09.031>, 2012.
- 1300

- Loomis, S. E., Russell, J. M., Eggermont, H., Verschuren, D., and Damsté, J. S. S.: Effects of temperature, pH and nutrient concentration on branched GDGT distributions in East African lakes: Implications for paleoenvironmental reconstruction, *Organic Geochemistry*, 66, <https://doi.org/10.1016/j.orggeochem.2013.10.012>, 2014a.
- 1305 Loomis, S. E., Russell, J. M., Heurreux, A. M., D'Andrea, W. J., and Damsté, J. S. S.: Seasonal variability of branched glycerol dialkyl glycerol tetraethers (brGDGTs) in a temperate lake system, *Geochimica et Cosmochimica Acta*, 144, 173–187, 2014b.
- Lê, S., Josse, J., and Husson, F.: FactoMineR: An R package for multivariate analysis, *Journal of Statistical Software*, 25, <https://doi.org/10.18637/jss.v025.i01>, 2008.
- Maitituerdi, A.: Depositional history of Lake Chala (Mt. Kilimanjaro, equatorial east Africa): reference frame for a high-resolution, 250 kyr  
1310 paleoenvironmental archive, Unpublished Doctoral thesis, University of Haifa, Israel, 2023.
- Maitituerdi, A., Daele, M. V., Verschuren, D., Batist, M. D., and Waldmann, N.: Depositional history of Lake Chala (Mt. Kilimanjaro, equatorial East Africa) from high-resolution seismic stratigraphy, *Journal of African Earth Sciences*, 189, <https://doi.org/10.1016/j.jafrearsci.2022.104499>, 2022.
- Martin-Jones, C., Lane, C., Daele, M. V., Van Der Meeren, T., Wolff, C., Moorhouse, H., Tomlinson, E., and Verschuren, D.: History of  
1315 scoria-cone eruptions on the eastern shoulder of the Kenya–Tanzania Rift revealed in the 250-ka sediment record of Lake Chala near Mount Kilimanjaro, *Journal of Quaternary Science*, <https://doi.org/10.1002/jqs.3140>, 2020.
- Martínez-Sosa, P. and Tierney, J. E.: Lacustrine brGDGT response to microcosm and mesocosm incubations, *Organic Geochemistry*, 127, <https://doi.org/10.1016/j.orggeochem.2018.10.011>, 2019.
- Martínez-Sosa, P., Tierney, J. E., and Meredith, L. K.: Controlled lacustrine microcosms show a brGDGT response to environmental pertur-  
1320 bations, *Organic Geochemistry*, 145, 104–111, 2020.
- Martínez-Sosa, P., Tierney, J. E., Stefanescu, I. C., Dearing Crampton-Flood, E., Shuman, B. N., and Routson, C.: A global Bayesian temperature calibration for lacustrine brGDGTs, *Geochimica et Cosmochimica Acta*, 305, <https://doi.org/10.1016/j.gca.2021.04.038>, 2021.
- Melles, M., Brigham-Grette, J., Minyuk, P. S., Nowaczyk, N. R., Wennrich, V., DeConto, R. M., Anderson, P. M., Andreev, A. A., Coletti, A., Cook, T. L., et al.: 2.8 million years of Arctic climate change from Lake El'gygytgyn, NE Russia, *Science*, 337, 315–320, 2012.
- 1325 Merbt, S. N., Stahl, D. A., Casamayor, E. O., Martí, E., Nicol, G. W., and Prosser, J. I.: Differential photoinhibition of bacterial and archaeal ammonia oxidation, *FEMS Microbiology Letters*, 327, <https://doi.org/10.1111/j.1574-6968.2011.02457.x>, 2012.
- Miller, C. S., Gosling, W. D., Kemp, D. B., Coe, A. L., and Gilmour, I.: Drivers of ecosystem and climate change in tropical West Africa over the past ~540 000 years, *Journal of Quaternary Science*, <https://doi.org/10.1002/jqs.2893>, 2016.
- Miller, D. R., Habicht, M. H., Keisling, B. A., Castañeda, I. S., and Bradley, R. S.: A 900-year New England temperature reconstruction from  
1330 in situ seasonally produced branched glycerol dialkyl glycerol tetraethers (brGDGTs), *Climate of the Past*, 14, <https://doi.org/10.5194/cp-14-1653-2018>, 2018.
- Moernaut, J., Verschuren, D., Charlet, F., Kristen, I., Fagot, M., and Batist, M. D.: The seismic-stratigraphic record of lake-level fluctuations in Lake Challa: Hydrological stability and change in equatorial East Africa over the last 140 kyr, *Earth and Planetary Science Letters*, 290, <https://doi.org/10.1016/j.epsl.2009.12.023>, 2010.
- 1335 Naafs, B., Gallego-Sala, A., Inglis, G., and Pancost, R.: Refining the global branched glycerol dialkyl glycerol tetraether (brGDGT) soil temperature calibration, *Organic Geochemistry*, 106, 48–56, 2017a.
- Naafs, B., Oliveira, A., and Mulholland, A.: Molecular dynamics simulations support the hypothesis that the brGDGT paleothermometer is based on homeoviscous adaptation, *Geochimica et Cosmochimica Acta*, 312, <https://doi.org/10.1016/j.gca.2021.07.034>, 2021.

- Naafs, B. D., Inglis, G. N., Zheng, Y., Amesbury, M. J., Biester, H., Bindler, R., Blewett, J., Burrows, M. A., del Castillo Torres, D., Chambers, F. M., Cohen, A. D., Evershed, R. P., Feakins, S. J., Galka, M., Gallego-Sala, A., Gandois, L., Gray, D. M., Hatcher, P. G., Coronado, E. N. H., Hughes, P. D., Huguet, A., Könönen, M., Laggoun-Défarge, F., Lähteenoja, O., Lamentowicz, M., Marchant, R., McClymont, E., Pontevedra-Pombal, X., Ponton, C., Pourmand, A., Rizzuti, A. M., Rochefort, L., Schellekens, J., Vleeschouwer, F. D., and Pancost, R. D.: Introducing global peat-specific temperature and pH calibrations based on brGDGT bacterial lipids, *Geochimica et Cosmochimica Acta*, 208, <https://doi.org/10.1016/j.gca.2017.01.038>, 2017b.
- 1345 Naeher, S., Peterse, F., Smittenberg, R. H., Niemann, H., Zigah, P. K., and Schubert, C. J.: Sources of glycerol dialkyl glycerol tetraethers (GDGTs) in catchment soils, water column and sediments of Lake Rotsee (Switzerland) - Implications for the application of GDGT-based proxies for lakes, *Organic Geochemistry*, 66, <https://doi.org/10.1016/j.orggeochem.2013.10.017>, 2014.
- Niemann, H., Stadnitskaia, A., Wirth, S. B., Gilli, A., Anselmetti, F. S., Sinninghe Damsté, J. S., Schouten, S., Hopmans, E. C., and Lehmann, M. F.: Bacterial GDGTs in Holocene sediments and catchment soils of a high Alpine lake: Application of the MBT/CBT-paleothermometer, *Climate of the Past*, 8, <https://doi.org/10.5194/cp-8-889-2012>, 2012.
- 1350 Pancost, R. D., Hopmans, E. C., and Sinninghe Damsté, J. S.: Archaeal lipids in mediterranean cold seeps: Molecular proxies for anaerobic methane oxidation, *Geochimica et Cosmochimica Acta*, 65, [https://doi.org/10.1016/S0016-7037\(00\)00562-7](https://doi.org/10.1016/S0016-7037(00)00562-7), 2001.
- Parish, M., Du, X., Bijaksana, S., and Russell, J.: A brGDGT-Based Reconstruction of Terrestrial Temperature From the Maritime Continent Spanning the Last Glacial Maximum, *Paleoceanography and Paleoclimatology*, 38, e2022PA004 501, 2023.
- 1355 Payne, B. R.: Water balance of Lake Chala and its relation to groundwater from tritium and stable isotope data, *Journal of Hydrology*, 11, [https://doi.org/10.1016/0022-1694\(70\)90114-9](https://doi.org/10.1016/0022-1694(70)90114-9), 1970.
- Pearson, E. J., Juggins, S., Talbot, H. M., Weckström, J., Rosén, P., Ryves, D. B., Roberts, S. J., and Schmidt, R.: A lacustrine GDGT-temperature calibration from the Scandinavian Arctic to Antarctic: Renewed potential for the application of GDGT-paleothermometry in lakes, *Geochimica et Cosmochimica Acta*, 75, 6225–6238, <https://doi.org/10.1016/j.gca.2011.07.042>, 2011.
- 1360 Peterse, F., Nicol, G. W., Schouten, S., and Damsté, J. S. S.: Influence of soil pH on the abundance and distribution of core and intact polar lipid-derived branched GDGTs in soil, *Organic Geochemistry*, 41, <https://doi.org/10.1016/j.orggeochem.2010.07.004>, 2010.
- Peterse, F., van der Meer, J., Schouten, S., Weijers, J. W. H., Fierer, N., Jackson, R. B., Kim, J. H., and Damsté, J. S. S.: Revised calibration of the MBT-CBT paleotemperature proxy based on branched tetraether membrane lipids in surface soils, *Geochimica et Cosmochimica Acta*, 96, 215–229, <https://doi.org/10.1016/j.gca.2012.08.011>, 2012.
- 1365 Petit, J. R., Raynaud, D., Basile, I., Chappellaz, J., Davisk, M., Ritz, C., Delmotte, M., Legrand, M., Lorius, C., Pe, L., and Saltzman, E.: Climate and atmospheric history of the past 420, 000 years from the Vostok ice core, *Antarctica, Nature*, 399, 1999.
- Pitcher, A., Rychlik, N., Hopmans, E. C., Spieck, E., Rijpstra, W. I. C., Ossebaar, J., Schouten, S., Wagner, M., and Damsté, J. S. S.: Crenarchaeol dominates the membrane lipids of *Candidatus Nitrososphaera gargensis*, a thermophilic Group I.1b Archaeon, *ISME Journal*, 4, <https://doi.org/10.1038/ismej.2009.138>, 2010.
- 1370 Pitcher, A., Hopmans, E. C., Mosier, A. C., Park, S. J., Rhee, S. K., Francis, C. A., Schouten, S., and Damsté, J. S. S.: Core and intact polar glycerol dibiphytanyl glycerol tetraether lipids of ammonia-oxidizing Archaea enriched from marine and estuarine sediments, *Applied and Environmental Microbiology*, 77, <https://doi.org/10.1128/AEM.02758-10>, 2011.
- Powers, L., Werne, J. P., Vanderwoude, A. J., Damsté, J. S. S., Hopmans, E. C., and Schouten, S.: Applicability and calibration of the TEX<sub>86</sub> paleothermometer in lakes, *Organic Geochemistry*, <https://doi.org/10.1016/j.orggeochem.2009.11.009>, 2010.
- 1375 Powers, L. A., Werne, J. P., Johnson, T. C., Hopmans, E. C., Damsté, J. S. S., and Schouten, S.: Crenarchaeotal membrane lipids in lake sediments: A new paleotemperature proxy continental paleoclimate reconstruction?, *Geology*, <https://doi.org/10.1130/G20434.1>, 2004.

- Powers, L. A., Johnson, T. C., Werne, J. P., Castañeda, I. S., Hopmans, E. C., Damsté, J. S. S., and Schouten, S.: Large temperature variability in the southern African tropics since the Last Glacial Maximum, *Geophysical Research Letters*, 32, <https://doi.org/10.1029/2004GL020214>, 2005.
- 1380 Powers, L. A., Johnson, T. C., Werne, J. P., Castañeda, I. S., Hopmans, E. C., Damsté, J. S. S., and Schouten, S.: Organic geochemical records of environmental variability in Lake Malawi during the last 700 years, Part I: The TEX<sub>86</sub> temperature record, *Palaeogeography, Palaeoclimatology, Palaeoecology*, 303, <https://doi.org/10.1016/j.palaeo.2010.09.006>, 2011.
- Raberg, J. H., Harning, D. J., Crump, S. E., Wet, G. D., Blumm, A., Kopf, S., Áslaug Geirsdóttir, Miller, G. H., and Sepúlveda, J.: Revised fractional abundances and warm-season temperatures substantially improve brGDGT calibrations in lake sediments, *Biogeosciences*, 18, <https://doi.org/10.5194/bg-18-3579-2021>, 2021.
- 1385 Raberg, J. H., Miller, G. H., Áslaug Geirsdóttir, and Sepúlveda, J.: Near-universal trends in brGDGT lipid distributions in nature, *Science Advances*, 8, <https://doi.org/10.1126/sciadv.abm7625>, 2022.
- Ramos-Roman, M. J., De Jonge, C., Magyari, E., Veres, D., Ilvonen, L., Develle, A.-L., and Seppä, H.: Lipid biomarker (brGDGT)-and pollen-based reconstruction of temperature change during the Middle to Late Holocene transition in the Carpathians, *Global and Planetary Change*, 215, 103 859, 2022.
- 1390 Russell, J. M., Hopmans, E. C., Loomis, S. E., Liang, J., and Damsté, J. S. S.: Distributions of 5- and 6-methyl branched glycerol dialkyl glycerol tetraethers (brGDGTs) in East African lake sediment: Effects of temperature, pH, and new lacustrine paleotemperature calibrations, *Organic Geochemistry*, <https://doi.org/10.1016/j.orggeochem.2017.12.003>, 2018.
- Sahonero-Canavesi, D. X., Siliakus, M. F., Abdala Asbun, A., Koenen, M., von Meijenfheldt, F. B., Boeren, S., Bale, N. J., Engelman, J. C., Fiege, K., Strack van Schijndel, L., et al.: Disentangling the lipid divide: Identification of key enzymes for the biosynthesis of membrane-spanning and ether lipids in Bacteria, *Science advances*, 8, eabq8652, 2022.
- 1395 Scholz, C. A., Johnson, T. C., Cohen, A. S., King, J. W., Peck, J. A., Overpeck, J. T., Talbot, M. R., Brown, E. T., Kalinidekafe, L., Amoako, P. Y. O., Lyons, R. P., Shanahan, T. M., Castañeda, I. S., Heil, C. W., Forman, S. L., McHargue, L. R., Beuning, K. R., Gomez, J., and Pierson, J.: East African megadroughts between 135 and 75 thousand years ago and bearing on early-modern human origins, *Proceedings of the National Academy of Sciences*, 104, 16 416–16 421, <https://doi.org/10.1073/pnas.0703874104>, 2007.
- 1400 Schouten, S., Wakeham, S. G., and Damsté, J. S. S.: Evidence for anaerobic methane oxidation by archaea in euxinic waters of the Black Sea, vol. 32, [https://doi.org/10.1016/S0146-6380\(01\)00110-3](https://doi.org/10.1016/S0146-6380(01)00110-3), 2001.
- Schouten, S., Hopmans, E. C., Schefuß, E., and Damsté, J. S. S.: Distributional variations in marine crenarchaeotal membrane lipids: a new tool for reconstructing ancient sea water temperatures?, *Earth and Planetary Science Letters*, 204, 265–274, 2002.
- 1405 Schouten, S., Forster, A., Panoto, F. E., and Damsté, J. S. S.: Towards calibration of the TEX<sub>86</sub> palaeothermometer for tropical sea surface temperatures in ancient greenhouse worlds, *Organic Geochemistry*, 38, <https://doi.org/10.1016/j.orggeochem.2007.05.014>, 2007.
- Schouten, S., Hopmans, E. C., and Damsté, J. S. S.: The organic geochemistry of glycerol dialkyl glycerol tetraether lipids: A review, *Organic Geochemistry*, 54, 19–61, <https://doi.org/10.1016/j.orggeochem.2012.09.006>, 2013.
- Sepulchre, P., Ramstein, G., Fluteau, F., Schuster, M., Tiercelin, J. J., and Brunet, M.: Tectonic uplift and Eastern Africa aridification, *Science*, 313, <https://doi.org/10.1126/science.1129158>, 2006.
- 1410 Shanahan, T. M., Hughen, K. A., and Mooy, B. A. V.: Temperature sensitivity of branched and isoprenoid GDGTs in Arctic lakes, *Organic Geochemistry*, 64, <https://doi.org/10.1016/j.orggeochem.2013.09.010>, 2013.
- Singarayer, J. S. and Burrough, S. L.: Interhemispheric dynamics of the African rainbelt during the late Quaternary, *Quaternary Science Reviews*, 124, <https://doi.org/10.1016/j.quascirev.2015.06.021>, 2015.

- 1415 Sinninghe Damsté, J. S.: Spatial heterogeneity of sources of branched tetraethers in shelf systems: The geochemistry of tetraethers in the Berau River delta (Kalimantan, Indonesia), *Geochimica et Cosmochimica Acta*, 186, 13–31, 2016.
- Sinninghe Damsté, J. S., Schouten, S., Hopmans, E. C., Duin, A. C. V., and Geenevasen, J. A.: Crenarchaeol: The characteristic core glycerol dibiphytanyl glycerol tetraether membrane lipid of cosmopolitan pelagic crenarchaeota, *Journal of Lipid Research*, 43, <https://doi.org/10.1194/jlr.M200148-JLR200>, 2002.
- 1420 Sinninghe Damsté, J. S., Ossebaar, J., Abbas, B., Schouten, S., and Verschuren, D.: Fluxes and distribution of tetraether lipids in an equatorial African lake: Constraints on the application of the TEX<sub>86</sub> palaeothermometer and BIT index in lacustrine settings, *Geochimica et Cosmochimica Acta*, 73, 4232–4249, <https://doi.org/10.1016/j.gca.2009.04.022>, 2009.
- Sinninghe Damsté, J. S., Ossebaar, J., Schouten, S., and Verschuren, D.: Distribution of tetraether lipids in the 25-ka sedimentary record of Lake Challa: Extracting reliable TEX<sub>86</sub> and MBT/CBT palaeotemperatures from an equatorial African lake, *Quaternary Science Reviews*, 50, 43–54, <https://doi.org/10.1016/j.quascirev.2012.07.001>, 2012a.
- 1425 Sinninghe Damsté, J. S., Rijpstra, W. I. C., Hopmans, E. C., Jung, M.-Y., Kim, J.-G., Rhee, S.-K., Stieglmeier, M., and Schleper, C.: Intact polar and core glycerol dibiphytanyl glycerol tetraether lipids of group I.1a and I.1b Thaumarchaeota in soil, *Applied and Environmental Microbiology*, 78, <https://doi.org/10.1128/AEM.01681-12>, 2012b.
- Sinninghe Damsté, J. S., Hopmans, E. C., Pancost, R. D., Schouten, S., and Geenevasen, J. A.: Newly discovered non-isoprenoid glycerol dialkyl glycerol tetraether lipids in sediments, *Chemical Communications*, <https://doi.org/10.1039/b004517i>, 2000.
- 1430 Sinninghe Damsté, J. S., Ossebaar, J., Schouten, S., and Verschuren, D.: Altitudinal shifts in the branched tetraether lipid distribution in soil from Mt. Kilimanjaro (Tanzania): Implications for the MBT/CBT continental palaeothermometer, *Organic Geochemistry*, 39, 1072–1076, <https://doi.org/10.1016/j.orggeochem.2007.11.011>, 2008.
- Sinninghe Damsté, J. S., Rijpstra, W. I. C., Hopmans, E. C., Weijers, J. W., Foesel, B. U., Overmann, J., and Dedysh, S. N.: 13,16-Dimethyl octacosanedioic acid (iso-Diabolic Acid), a common membrane-spanning lipid of Acidobacteria subdivisions 1 and 3, *Applied and Environmental Microbiology*, 77, <https://doi.org/10.1128/AEM.00466-11>, 2011.
- 1435 Sinninghe Damsté, J. S., Rijpstra, W. I. C., Hopmans, E. C., Foesel, B. U., Wüst, P. K., Overmann, J., Tank, M., Bryant, D. A., Dunfield, P. F., Houghton, K., and Stott, M. B.: Ether- and ester-bound iso-diabolic acid and other lipids in members of Acidobacteria subdivision 4, *Applied and Environmental Microbiology*, 80, <https://doi.org/10.1128/AEM.01066-14>, 2014.
- 1440 Sinninghe Damsté, J. S., Rijpstra, W. I. C., Foesel, B. U., Huber, K. J., Overmann, J., Nakagawa, S., Kim, J. J., Dunfield, P. F., Dedysh, S. N., and Villanueva, L.: An overview of the occurrence of ether- and ester-linked iso-diabolic acid membrane lipids in microbial cultures of the Acidobacteria: Implications for brGDGT paleoproxies for temperature and pH, *Organic Geochemistry*, 124, <https://doi.org/10.1016/j.orggeochem.2018.07.006>, 2018.
- Sinninghe Damsté, J. S., Weber, Y., Zopfi, J., Lehmann, M. F., and Niemann, H.: Distributions and sources of isoprenoidal GDGTs in Lake Lugano and other central European (peri-)alpine lakes: Lessons for their use as paleotemperature proxies, *Quaternary Science Reviews*, 277, <https://doi.org/10.1016/j.quascirev.2021.107352>, 2022.
- 1445 Stager, J. C., Cocquyt, C., Bonnefille, R., Weyhenmeyer, C., and Bowerman, N.: A late Holocene paleoclimatic history of Lake Tanganyika, East Africa, *Quaternary Research*, 72, <https://doi.org/10.1016/j.yqres.2009.04.003>, 2009.
- Stockhecke, M., Bechtel, A., Peterse, F., Guillemot, T., and Schubert, C. J.: Temperature, precipitation, and vegetation changes in the Eastern Mediterranean over the last deglaciation and Dansgaard-Oeschger events, *Palaeogeography, Palaeoclimatology, Palaeoecology*, 577, <https://doi.org/10.1016/j.palaeo.2021.110535>, 2021.
- 1450

- Stone, J. R., Westover, K. S., and Cohen, A. S.: Late Pleistocene paleohydrography and diatom paleoecology of the central basin of Lake Malawi, Africa, *Palaeogeography, Palaeoclimatology, Palaeoecology*, 303, <https://doi.org/10.1016/j.palaeo.2010.01.012>, 2011.
- 1455 Sun, W., Zhang, E., Chang, J., Shulmeister, J., Bird, M. I., Zhao, C., Jiang, Q., and Shen, J.: Archaeal lipid-inferred paleohydrology and paleotemperature of Lake Chenghai during the Pleistocene-Holocene transition, *Climate of the Past*, 16, <https://doi.org/10.5194/cp-16-833-2020>, 2020.
- Swai, V.: Lake Chala stratigraphy: Developing a method to identify and quantify surficial slope sediment remobilization, Unpublished Masters thesis, Ghent University, Belgium, 2018.
- 1460 Tantu, H.: 250,000 years of diatom community dynamics in Lake Chala, a meromictic crater lake in equatorial East Africa, in: Past and present phytoplankton communities in East-African crater lakes: Paleolimnology and biomonitoring, unpublished Doctoral thesis, Ghent University, Belgium, 2021.
- Tierney, J. E. and Russell, J. M.: Distributions of branched GDGTs in a tropical lake system: Implications for lacustrine application of the MBT/CBT paleoproxy, *Organic Geochemistry*, 40, 1032–1036, <https://doi.org/10.1016/j.orggeochem.2009.04.014>, 2009.
- 1465 Tierney, J. E., Russell, J. M., Huang, Y., Damsté, J. S. S., Hopmans, E. C., and Cohen, A. S.: Northern hemisphere controls on tropical southeast African climate during the past 60,000 years, *Science*, 322, <https://doi.org/10.1126/science.1160485>, 2008.
- Tierney, J. E., Mayes, M. T., Meyer, N., Johnson, C., Swarzenski, P. W., Cohen, A. S., and Russell, J. M.: Late-twentieth-century warming in Lake Tanganyika unprecedented since AD 500, *Nature Geoscience*, 3, 422–425, <https://doi.org/10.1038/ngeo865>, 2010a.
- 1470 Tierney, J. E., Russell, J. M., Eggermont, H., Hopmans, E. C., Verschuren, D., and Sinninghe Damsté, J. S.: Environmental controls on branched tetraether lipid distributions in tropical East African lake sediments, *Geochimica et Cosmochimica Acta*, 74, 4902–4918, <https://doi.org/10.1016/j.gca.2010.06.002>, 2010b.
- Tierney, J. E., Russell, J. M., and Huang, Y.: A molecular perspective on Late Quaternary climate and vegetation change in the Lake Tanganyika basin, East Africa, *Quaternary Science Reviews*, 29, <https://doi.org/10.1016/j.quascirev.2009.11.030>, 2010c.
- Tierney, J. E., Smerdon, J. E., Anchukaitis, K. J., and Seager, R.: Multidecadal variability in East African hydroclimate controlled by the Indian Ocean, *Nature*, 493, 389–392, <https://doi.org/10.1038/nature11785>, 2013.
- 1475 Tjallingii, R., Claussen, M., Stuut, J. B. W., Fohlmeister, J., Jahn, A., Bickert, T., Lamy, F., and Röhl, U.: Coherent high- and low-latitude control of the northwest African hydrological balance, *Nature Geoscience*, 1, <https://doi.org/10.1038/ngeo289>, 2008.
- Verschuren, D.: Influence of depth and mixing regime on sedimentation in a small, fluctuating tropical soda lake, *Limnology and Oceanography*, 44, <https://doi.org/10.4319/lo.1999.44.4.1103>, 1999.
- 1480 Verschuren, D.: Reconstructing fluctuations of a shallow East African lake during the past 1800 yrs from sediment stratigraphy in a submerged crater basin, *Journal of Paleolimnology*, 25, <https://doi.org/10.1023/A:1011150300252>, 2001.
- Verschuren, D.: Lake-based climate reconstruction in Africa: Progress and challenges, *Hydrobiologia*, 500, <https://doi.org/10.1023/A:1024686229778>, 2003.
- Verschuren, D., Damsté, J. S. S., Moernaut, J., Kristen, I., Blauw, M., Fagot, M., and Haug, G. H.: Half-precessional dynamics of monsoon rainfall near the East African Equator, *Nature*, 462, 637–641, <https://doi.org/10.1038/nature08520>, 2009.
- 1485 Verschuren, D., Olagod, D. O., Rucina, S. M., and Odhengo, P. O.: DeepCHALLA: Two glacial cycles of climate and ecosystem dynamics from equatorial East Africa, *Scientific Drilling*, <https://doi.org/10.2204/iodp.sd.15.09.2013>, 2013.
- Wagner, B., Vogel, H., Francke, A., Friedrich, T., Donders, T., Lacey, J. H., Leng, M. J., Regattieri, E., Sadori, L., Wilke, T., et al.: Mediterranean winter rainfall in phase with African monsoons during the past 1.36 million years, *Nature*, 573, 256–260, 2019.

- Wainwright, C. M., Marsham, J. H., Keane, R. J., Rowell, D. P., Finney, D. L., Black, E., and Allan, R. P.: 'Eastern African Paradox' rainfall decline due to shorter not less intense Long Rains, *npj Climate and Atmospheric Science*, 2, <https://doi.org/10.1038/s41612-019-0091-7>, 2019.
- Weber, Y., De Jonge, C., Rijpstra, W. I. C., Hopmans, E. C., Stadnitskaia, A., Schubert, C. J., Lehmann, M. F., Damsté, J. S. S., and Niemann, H.: Identification and carbon isotope composition of a novel branched GDGT isomer in lake sediments: Evidence for lacustrine branched GDGT production, *Geochimica et Cosmochimica Acta*, 154, 118–129, <https://doi.org/10.1016/j.gca.2015.01.032>, 2015.
- 1495 Weber, Y., Damsté, J. S. S., Zopfi, J., De Jonge, C., Gilli, A., Schubert, C. J., Lepori, F., Lehmann, M. F., and Niemann, H.: Redox-dependent niche differentiation of tetraether producing bacteria: Evidence for multiple branched GDGT sources in lakes, *Proceedings of the National Academy of Sciences of the United States of America*, <https://doi.org/10.1073/pnas.1805186115>, 2018.
- Weijers, J. W., Schouten, S., Hopmans, E. C., Geenevasen, J. A., David, O. R., Coleman, J. M., Pancost, R. D., and Damsté, J. S. S.: Membrane lipids of mesophilic anaerobic bacteria thriving in peats have typical archaeal traits, *Environmental Microbiology*, 8, <https://doi.org/10.1111/j.1462-2920.2005.00941.x>, 2006a.
- 1500 Weijers, J. W., Schouten, S., Spaargaren, O. C., and Damsté, J. S. S.: Occurrence and distribution of tetraether membrane lipids in soils: Implications for the use of the TEX<sub>86</sub> proxy and the BIT index, *Organic Geochemistry*, 37, <https://doi.org/10.1016/j.orggeochem.2006.07.018>, 2006b.
- Weijers, J. W., Schouten, S., van den Donker, J. C., Hopmans, E. C., and Damsté, J. S. S.: Environmental controls on bacterial tetraether membrane lipid distribution in soils, *Geochimica et Cosmochimica Acta*, 71, <https://doi.org/10.1016/j.gca.2006.10.003>, 2007.
- 1505 Weijers, J. W., Panoto, E., van bleijswijk, J., Schouten, S., Rijpstra, W. I. C., Balk, M., Stams, A. J., and Damsté, J. S.: Constraints on the biological source(s) of the orphan branched tetraether membrane lipids, *Geomicrobiology Journal*, 26, <https://doi.org/10.1080/01490450902937293>, 2009.
- Wolff, C., Haug, G. H., Timmermann, A., Damsté, J. S. S., Brauer, A., Sigman, D. M., Cane, M. A., and Verschuren, D.: Reduced interannual rainfall variability in East Africa during the last ice age, *Science*, 333, <https://doi.org/10.1126/science.1203724>, 2011.
- 1510 Wolff, C., Kristen-Jenny, I., Schettler, G., Plessen, B., Meyer, H., Dulski, P., Naumann, R., Brauer, A., Verschuren, D., and Haug, G. H.: Modern seasonality in Lake Challa (Kenya/Tanzania) and its sedimentary documentation in recent lake sediments, *Limnology and Oceanography*, 59, <https://doi.org/10.4319/lo.2014.59.5.1621>, 2014.
- Woltering, M., Johnson, T. C., Werne, J. P., Schouten, S., and Damsté, J. S. S.: Late Pleistocene temperature history of Southeast Africa: A TEX<sub>86</sub> temperature record from Lake Malawi, *Palaeogeography, Palaeoclimatology, Palaeoecology*, 303, <https://doi.org/10.1016/j.palaeo.2010.02.013>, 2011.
- 1515 Woltering, M., Werne, J. P., Kish, J. L., Hicks, R., Damsté, J. S. S., and Schouten, S.: Vertical and temporal variability in concentration and distribution of thaumarchaeotal tetraether lipids in Lake Superior and the implications for the application of the TEX<sub>86</sub> temperature proxy, *Geochimica et Cosmochimica Acta*, <https://doi.org/10.1016/j.gca.2012.03.024>, 2012.
- 1520 Wu, J., Yang, H., Pancost, R. D., Naafs, B. D. A., Qian, S., Dang, X., Sun, H., Pei, H., Wang, R., Zhao, S., and Xie, S.: Variations in dissolved O<sub>2</sub> in a Chinese lake drive changes in microbial communities and impact sedimentary GDGT distributions, *Chemical Geology*, 579, <https://doi.org/10.1016/j.chemgeo.2021.120348>, 2021.
- 1525 Wuchter, C., Schouten, S., Coolen, M. J., and Damsté, J. S. S.: Temperature-dependent variation in the distribution of tetraether membrane lipids of marine Crenarchaeota: Implications for TEX<sub>86</sub> paleothermometry, *Paleoceanography*, 19, <https://doi.org/10.1029/2004PA001041>, 2004.

- Xiao, W., Xu, Y., Ding, S., Wang, Y., Zhang, X., Yang, H., Wang, G., and Hou, J.: Global calibration of a novel, branched GDGT-based soil pH proxy, *Organic Geochemistry*, 89-90, <https://doi.org/10.1016/j.orggeochem.2015.10.005>, 2015.
- 1530 Yao, Y., Zhao, J., Vachula, R. S., Werne, J. P., Wu, J., Song, X., and Huang, Y.: Correlation between the ratio of 5-methyl hexamethylated to pentamethylated branched GDGTs (HP5) and water depth reflects redox variations in stratified lakes, *Organic Geochemistry*, 147, <https://doi.org/10.1016/j.orggeochem.2020.104076>, 2020.
- Zhang, C., Zhao, C., Zhou, A., Zhang, H., Liu, W., Feng, X., Sun, X., Yan, T., Leng, C., Shen, J., and Chen, F.: Quantification of temperature and precipitation changes in northern China during the “5000-year” Chinese History, *Quaternary Science Reviews*, 255, <https://doi.org/10.1016/j.quascirev.2021.106819>, 2021.
- 1535 Zhang, Z., Smittenberg, R. H., and Bradley, R. S.: GDGT distribution in a stratified lake and implications for the application of TEX<sub>86</sub> in paleoenvironmental reconstructions, *Scientific Reports*, 6, <https://doi.org/10.1038/srep34465>, 2016.
- Zhao, C., Rohling, E. J., Liu, Z., Yang, X., Zhang, E., Cheng, J., Liu, Z., An, Z., Yang, X., Feng, X., Sun, X., Zhang, C., Yan, T., Long, H., Yan, H., Yu, Z., Liu, W., Yu, S. Y., and Shen, J.: Possible obliquity-forced warmth in southern Asia during the last glacial stage, *Science Bulletin*, 66, <https://doi.org/10.1016/j.scib.2020.11.016>, 2021.
- Zolitschka, B.: Varved lake sediments.[W:] SA Elias (red.), *Encyclopedia of Quaternary Science*, 2006.



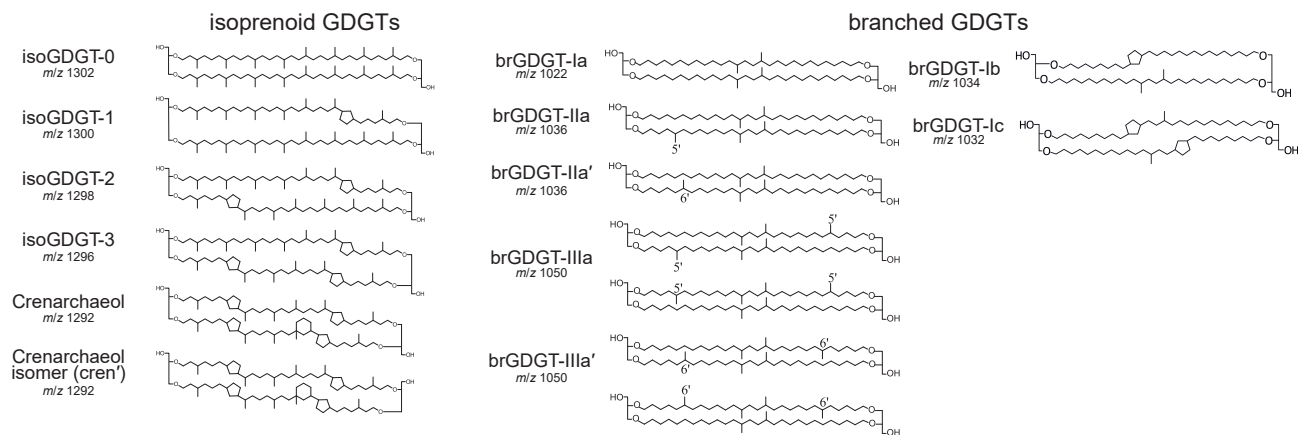


**Figure S1.** Molecular structure and names of iso- and brGDGTs used in the [GDGT indices and proxies](#) presented in this study. BrGDGTs with one (as in IIa and IIa') and two (as in IIIa and IIIa') additional methyl groups may also include one or two rings (i.e., I Ib-c, I Ib-c', I IIb-c and I IIb-c'; structures not shown).

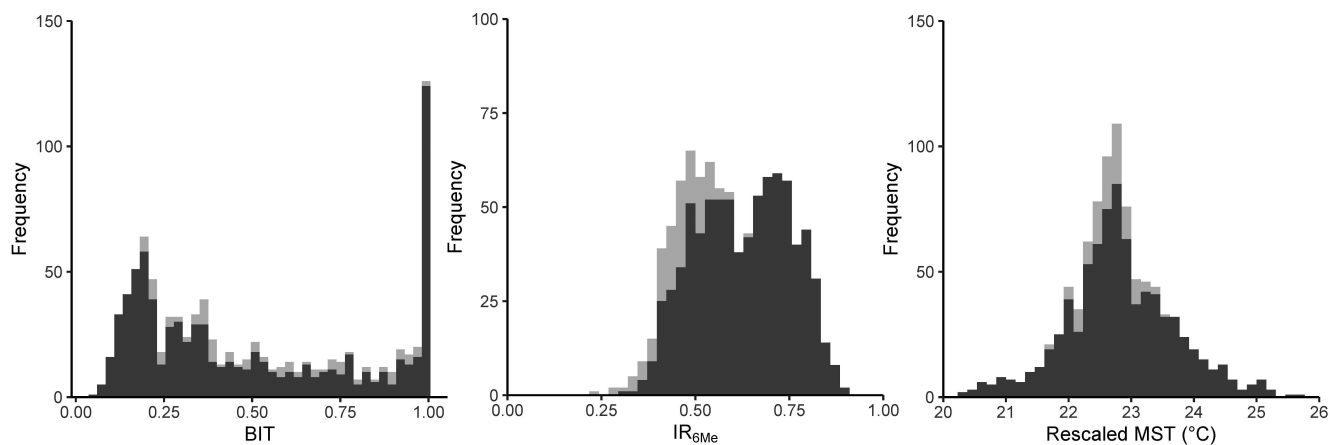


**Figure S2.** [Distribution-Frequency distribution](#) of [calculated values for](#) (a) [the BIT index](#) (b) IR<sub>6Me</sub> and (c) [rescaled MST \(mean summer temperature; Pearson et al. \(2011\); Baxter et al. \(2023\)\)](#) [Pearson et al. \(2011\), Baxter et al. \(2023\) values](#) throughout the [full 250-kyr DeepCHALLA sequence \(250–0 ka; light grey\)](#) and [during in the period-section 180 - 0 ka \(dark grey/black\)](#).

## 250 – 0 ka

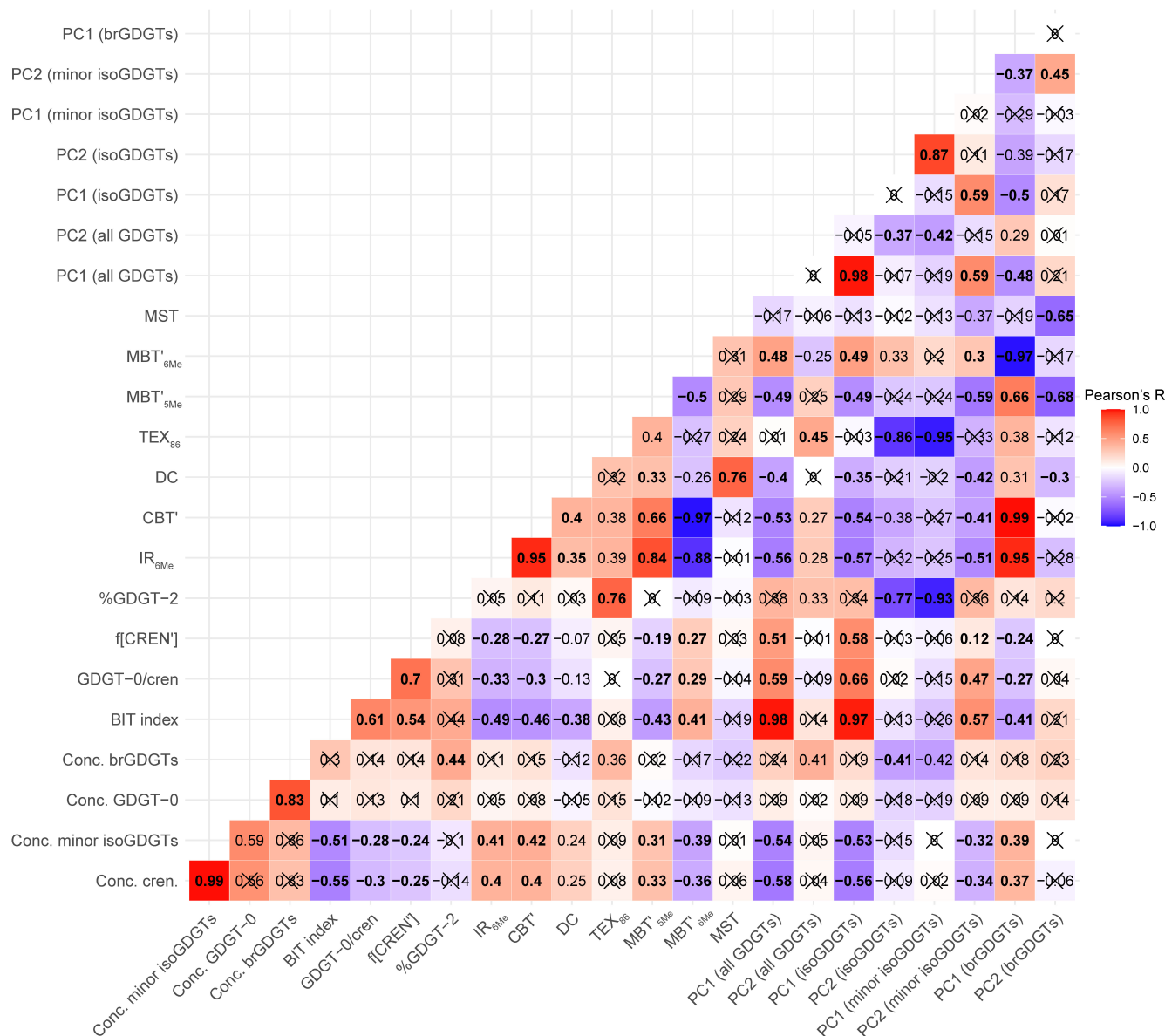


**Figure S3. Correlation-Pearson correlation (pearsonR value) matrix between time series of GDGT concentration, indices, and principal component (PC) scores for over the full complete 250-kyr DeepCHALLA sequence. Squares marked with x are not significantly correlated ( $p > 0.01$ ,  $n = 906$  samples with defined values for all variables). Correlation coefficients (R value) of significantly correlated variable values in bold are indicated with normal script used to reflect those cases where significant at  $p < 0.001$ , those in regular type at  $< 0.01$ , and bold text for where those crossed out reflect lack of significance at the  $p < 0.001$  level.**

## 250 – 180 ka

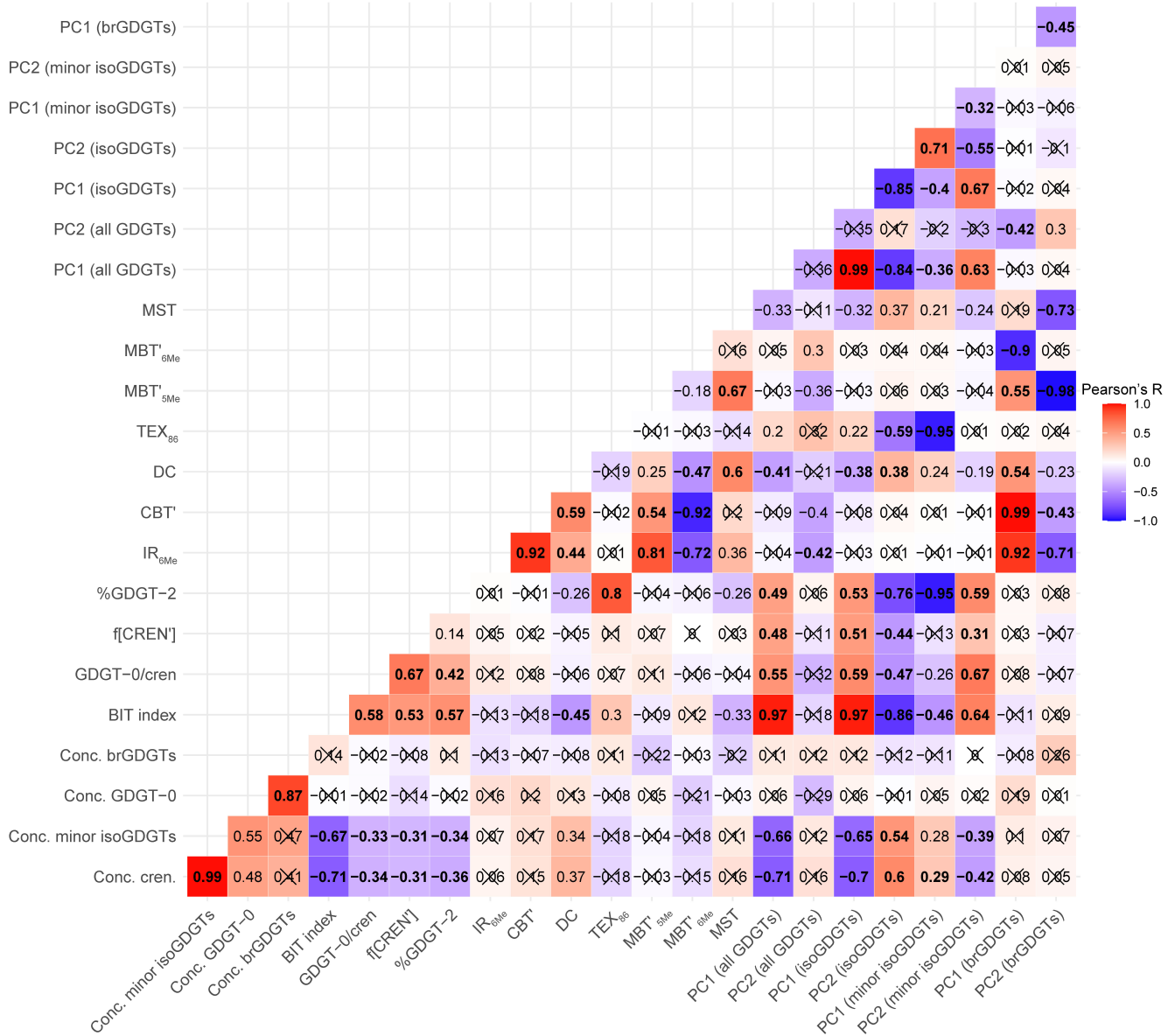


**Figure S4.** As described in Fig. S3 but for the period 250–180 ka of the DeepCHALLA sequence only ( $n = 117$ ).

## 250 – 144 ka

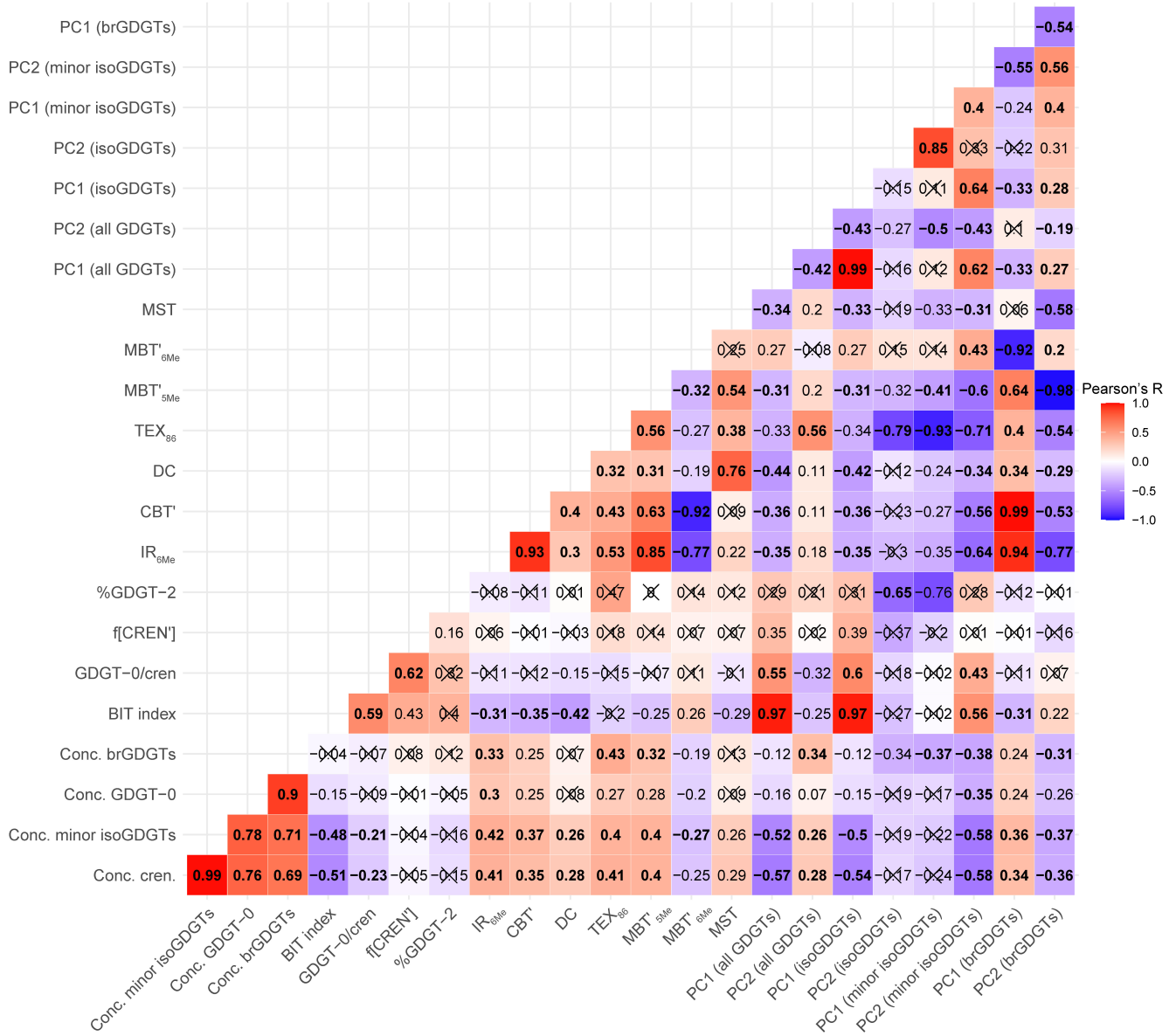


**Figure S5.** As described in Fig. S3 but for the period 250–144 ka of the DeepCHALLA sequence only ( $n = 219$ ).

# 180 – 0 ka

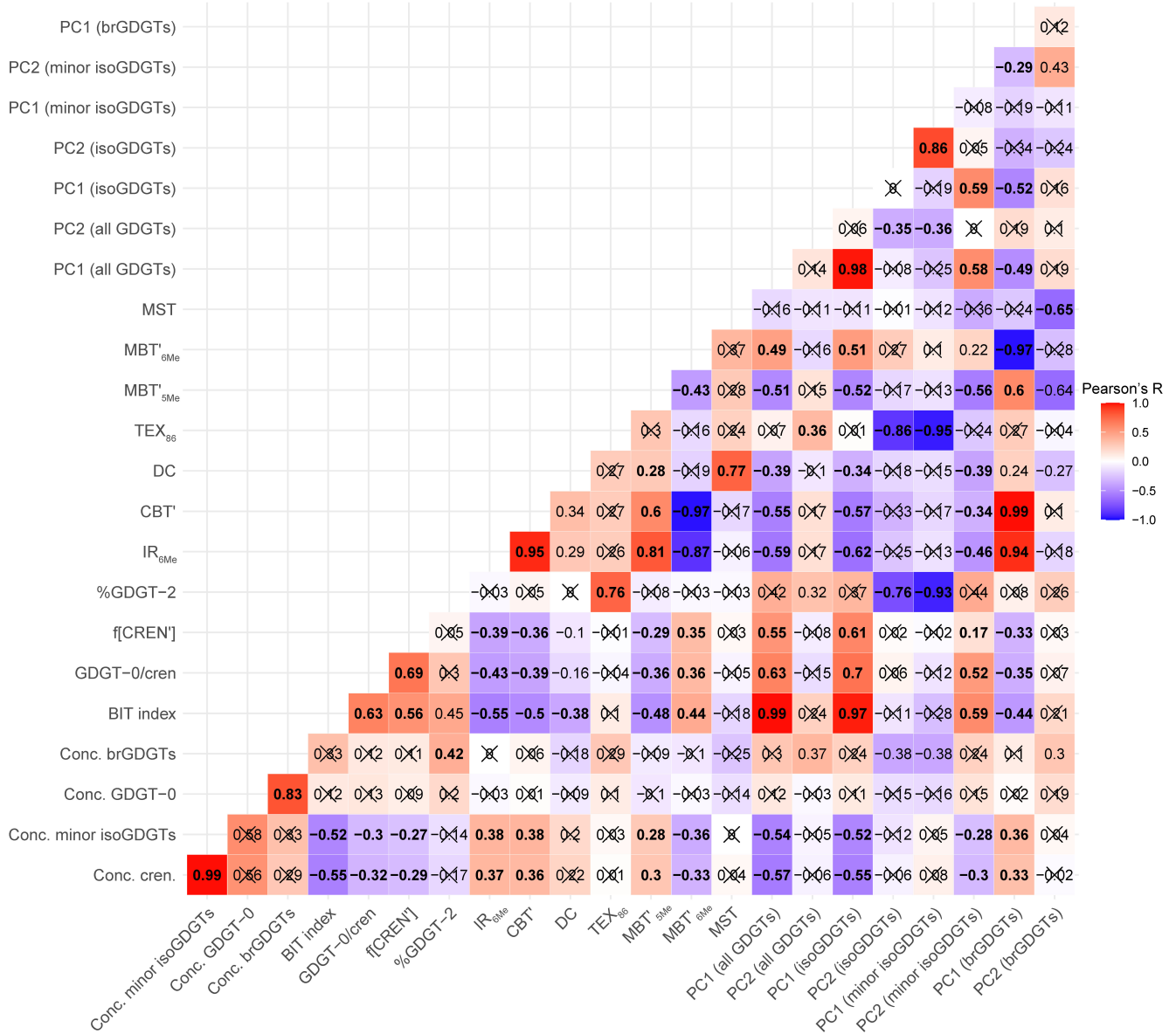


Figure S6. As described in Fig. S3 but for the period 180–0 ka of the DeepCHALLA sequence only ( $n = 789$ ).

# 144 – 0 ka

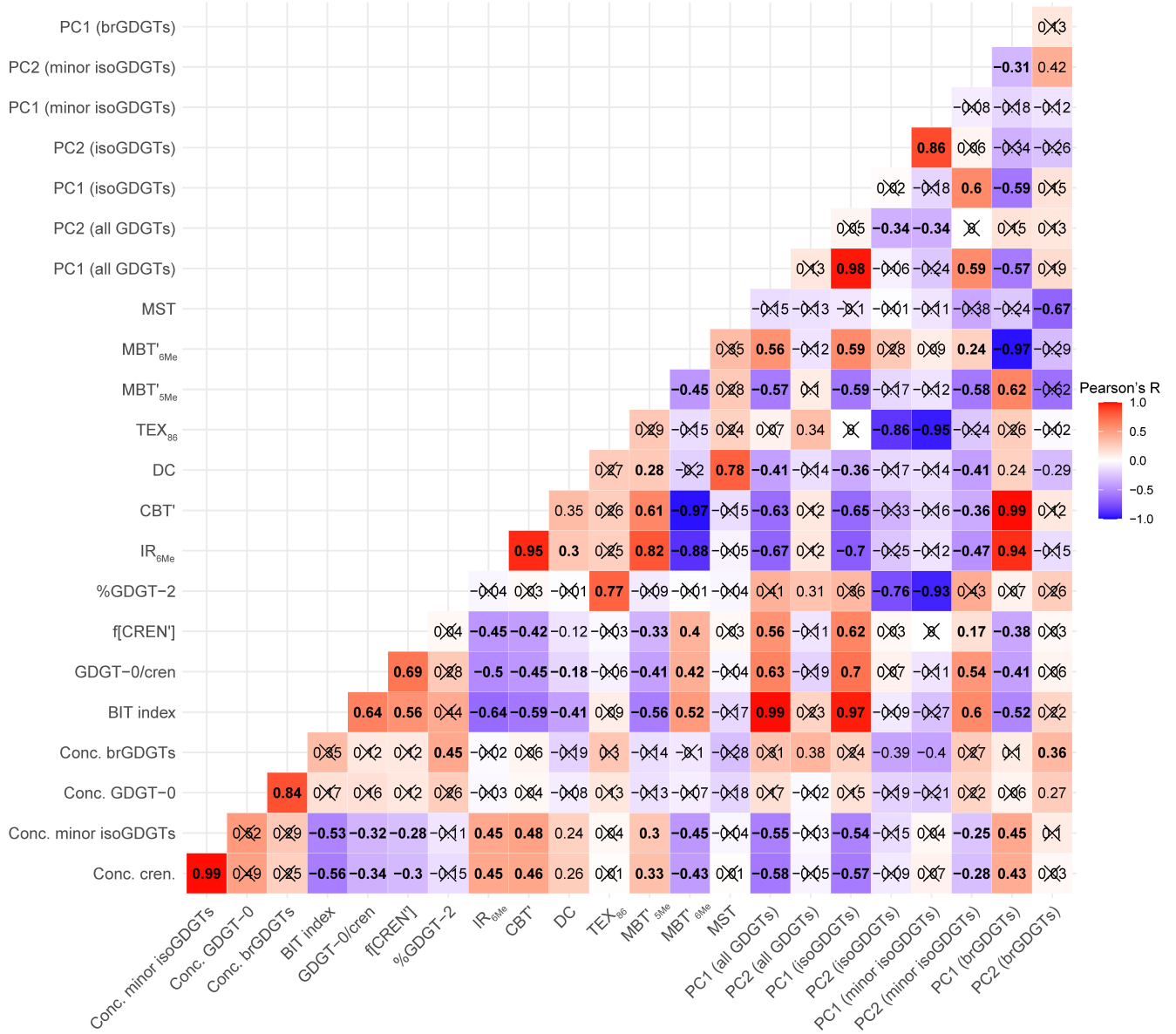
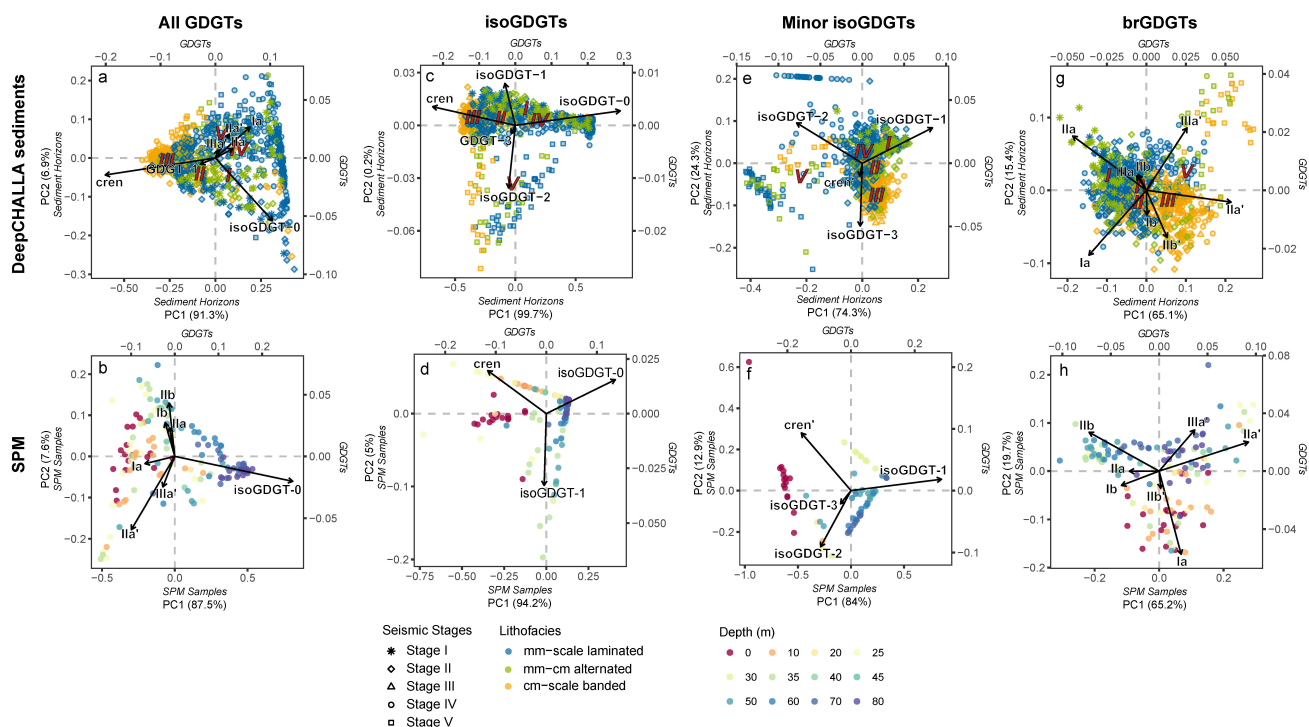
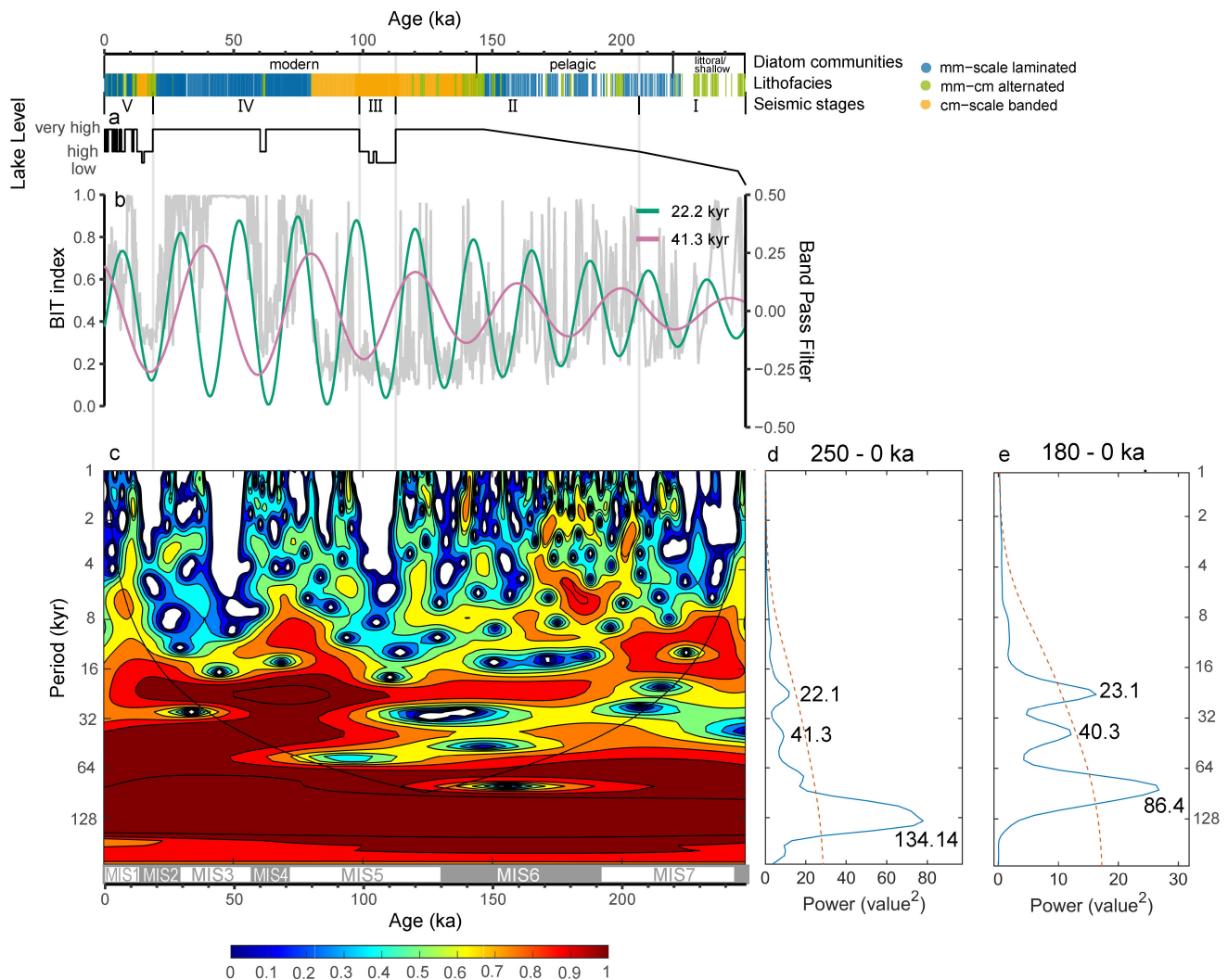


Figure S7. As described in Fig. S3 but for the period 144–0 ka of the DeepCHALLA sequence only ( $n = 687$ ).



**Figure S8.** Principal component analysis (PCA) biplots of the fractional abundances of GDGTs in the DeepCHALLA core sediment sequence and in suspended particulate matter (SPM) from modern-day Lake Chala. PCA From left to right, biplots of all GDGTs in (a) DeepCHALLA sediments and in (b) the SPM, the isoGDGTs in (c) DeepCHALLA sediments and (d) the SPM, the minor isoGDGTs (i.e., isoGDGT-1, -2, -3 and the crenarchaeol isomer) in (e) the DeepCHALLA sequence sediments and (f) the SPM, and the brGDGTs in (g) DeepCHALLA sediments and (h) the SPM. The loadings of individual GDGTs are shown in the plot with arrows. In cases where GDGTs contributed < contributing at least 1% of the to variability of the data among samples on both either PC1 and or PC2 were removed to improve readability (but their fractional abundances were still included during analysis or both) are shown as arrows. Individual scores of DeepCHALLA sediment horizons (In the top panels a, e, e, g) sediment horizons from depositional stages I-V are presented by different symbols, and colored according to lithofacies, with seismic stage indicate by different symbols. Red numerals (V-I) in panels (a, e, e, and g) I-V represent the centroid values (i.e., average PC scores) of sequence separated according to the samples from those respective depositional stages. SPM in the bottom panels (b, d, f, and h) SPM samples are colored according to sampling depth in the water column. Note that separate PC axes indicate the position different scales of the individuals PC axes for individual samples (sediment horizons or SPM) and variables (GDGT-vectors GDGTs) and that the amount of variability within the dataset predicted by PC1 and PC2 is provided as a percentage (in brackets).



**Figure S9.** Periodicity analysis of the BIT index in the 250-kyr DeepCHALLA sediment sequence. Indicated from on top to bottom, are the timing of three major phases in the diatom communities-lake ecology as registered in the DeepCHALLA sequence fossil diatom assemblages (Tanttu, 2021), the lithofacies category of each sediment horizon (colored bar), and the depositional stages (V-I) based on the seismic stratigraphy of Lake Chala, as well as Maittuerdi et al. (2022). Subsequent panels show (a) the lake level reconstruction based on the seismic reflection data stratigraphy (Maittuerdi et al., 2022), (b) The the BIT index from the DeepCHALLA sequence time series in light grey with green and pink curves representing the band-pass filtered time series after band-pass filtering with periods reflected by wavelet analysis which are comparable similar to the periods those of orbital precession and obliquity, respectively, as revealed by wavelet analysis, and (c) Wavelet visual representation of wavelet analysis using a morlet function, with warm and cold colors reflect reflecting high and low values of the power spectrum. Also shown is the timing of the marine isotope stages (MIS; Lisiecki and Raymo (2005)), respectively for reference. Panels (d) The and (e) summarize the BIT-index wavelet spectra resulting from analysis of in the full sequence complete DeepCHALLA sequence and additionally (e) 250-0 ka) wavelet spectra from analysis of and in the section 180-0 ka only, to highlight more pronounced precession and obliquity cycles in the latter. The red stippled line in panels (d) and (e) represents the 95% confidence interval; dominant frequencies are labelled at the top of the maxima.



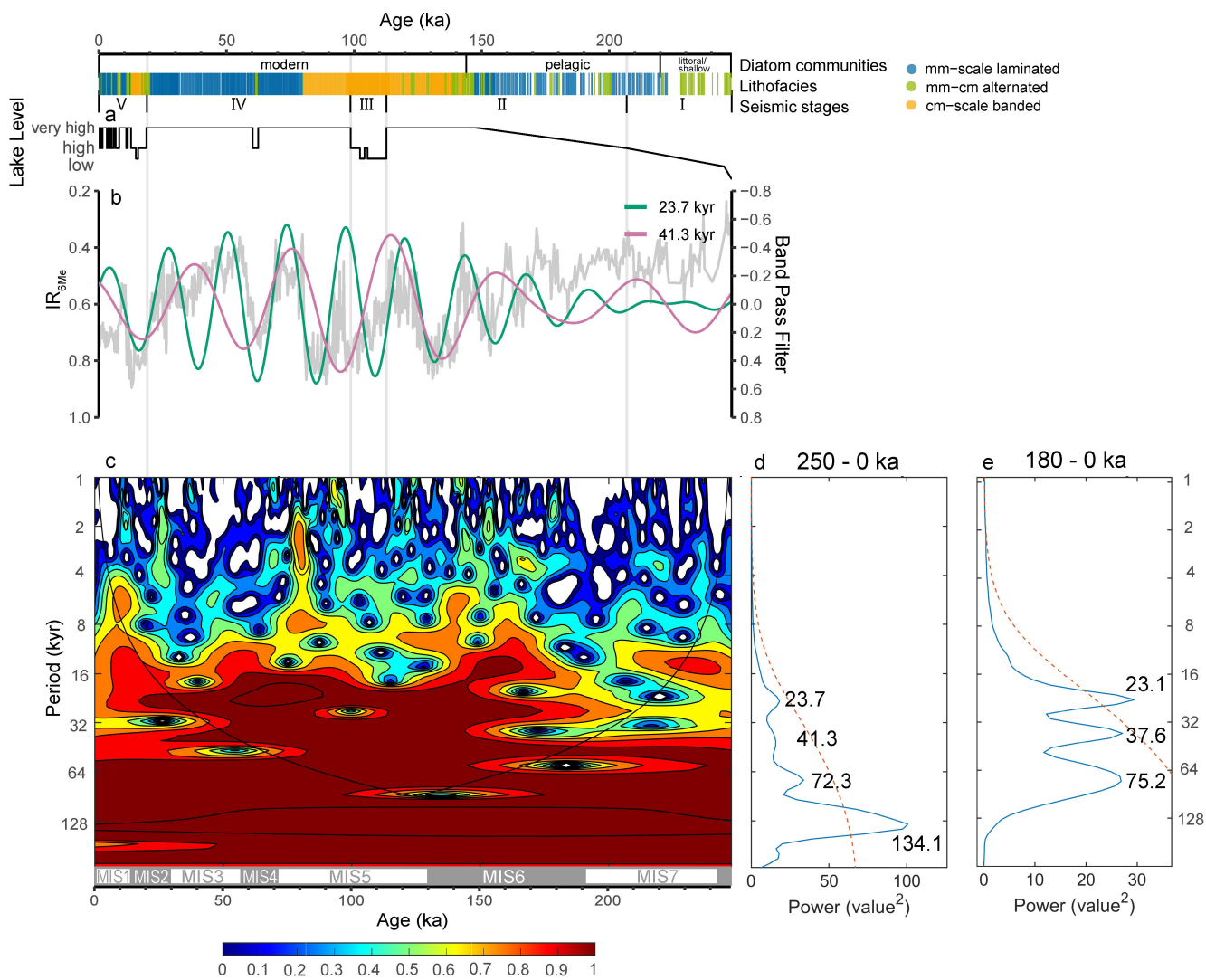


**Figure S10.** As described for Fig. S9 but for the ratio of the between 6-Me and 5-Me brGDGTs (IR<sub>6Me</sub>).

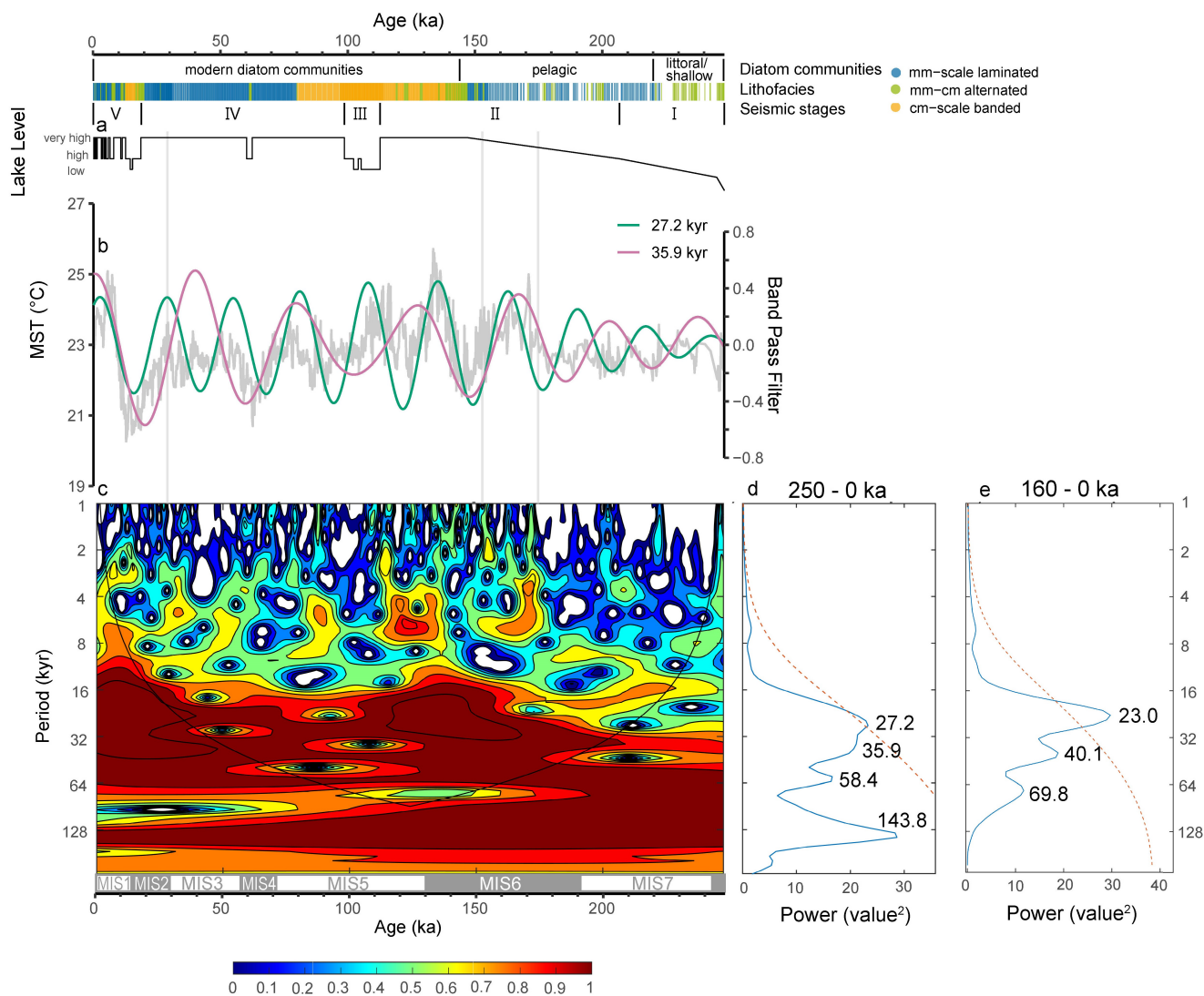


**Figure S11.** As described for Fig. S9 but for Mean Summer Temperature (MST) reconstructed based on a calibration using brGDGT abundances (the Pearson et al., 2011 calibration of brGDGTs in globally distributed lake sediments (Pearson et al., 2011), and where panel with (e) reflects representing the period 160 - 0 ka.